Magnetoencephalographic studies of neural systems associated with higher order processes in humans

Thesis

Magnetoencephalographic studies of neural systems associated with higher order processes in humans

Thesis submitted in accordance with the requirements of
The Open University for the degree of Doctor of Philosophy

by

Sven Bräutigam, Diplom-Physiker

July 1998

Declaration

I hereby declare that none of the material has been previously submitted to this or any other university. All work was carried out in the Department of Physics of The Open University and at the Low Temperature Laboratory of Helsinki University of Technology. The work was completed during the period July 1994 to June 1998 under the supervision of Dr. SJ Swithenby.

Contributions from this work are contained in the following references:

- Swithenby SJ, Bailey AJ, Bräutigam S, Josephs OE, Jousmäki V, and Tesche CD. Neural processing of human faces: a magnetoencephalographic study. Exp. Brain Res. 118:501, 1998.
- Swithenby SJ, Bräutigam S, Bailey AJ, Joumaki V, and Tesche CD. Comparison between the processing of static images of human faces in high functioning autistic subjects and normal controls. Proceedings of the 10th International Conference on Biomagnetism 1996 (in print).
- Bailey AJ, Bräutigam S, Swithenby SJ, Jousmaki V, and Hari R. An MEG study of high functioning autistic adults. Brain Topography 10:49, 1997 (abstracts of the 8th World Congress of the International Society for Brain Electromagnetic Topography).
- Bräutigam S, Swithenby SJ, and Bailey AJ. Vector time series: a numerical study with application to prestimulus brain states. Brain Topography 10:49, 1997 (abstracts of the 8th World Congress of the International Society for Brain Electromagnetic Topography).
- Bräutigam S and Swithenby SJ. Relationship between prestimulus brain states and visually evoked resonses: an MEG study employing nonlinear methods. Electroenceph. clin. Neurophysiol. 103:201, 1997 (abstracts of the 14th International Congress of EEG and Clinical Neurophysiology).

Abstract

This thesis has been concerned with the neuromagnetic fields associated with the processing of faces and sentences in humans. In four, largely independent sub-projects, results were obtained using novel methods of analysis to extract neurophysiologically relevant information from magnetoencephalographic MEG readings. Using the MEG facility of the Helsinki University of Technology, Finland, the research has led to four main suggestions: a) there are early latency face-specific neural systems in humans that are predominantly in right inferior occipito-temporal cortex, b) MEG recordings are useful in the study of autism, in that autistic subjects exhibit different responses to normal subjects following face presentation, c) phase-locked γ-band activity has a specific role in semantic processing of sentences in normal subjects, and d) the late components of responses to face images are modified by endogenous priming, which is detectable before stimulus arrival in normal subjects.

In order to pursue these neuroscience objectives, new methods for treating MEG data were developed, implemented and used. These comprise: a) an improved parameterisation of signal power over regions of interest, b) the use of re-sampling strategies to achieve statistical assessment of spectral coefficients within subjects, and c) a pre-stimulus method for the study of face processing using a tailored state-space representation approach.

Acknowledgements

I would like to thank Steve who supervised this thesis in a relaxed manner offering help whenever needed. Here is another character, Tony who can claim a lot of the credit, together with Steve, in initiating the whole scenario of commuting between England and Finland just to collect some brain data. Together, I believe, we have had much fun and achieved reasonable things so far. Thank you to the staff and colleagues at the Low Temperature Laboratory for coping with us and our peculiar experiments. There are the people in the Physics Department who treated me in a very open minded fashion, even endured my lengthy talks at one or the other occasion. There are the people at home, meaning at home in England. A thank you to the close and not so close friends, who showed an appreciation of what I have been doing; and those who were still supportive although not realising what at all was going on. At home, meaning in Germany, there are many left behind. Helga and Rolf, my parents, who have been very supportive all the time being convinced that my adventure is definitely the right thing to do; a thank you to them. A thank you to Knud, my brother, and Iris, his girlfriend, for visiting me. Last but certainly not least, a very big thank you very much to Maren my girlfriend for an enjoyable and unbroken relationship despite periods of separation.

Contents

List of Figures

List of Tables

Chapter 1

Introduction

The human brain is certainly the most complex structure known to mankind. Throughout all centuries, it has attracted a staggering range of research activities of both fundamental and clinical interest. The scale of investigations spans from the minutiae of atomic-sized ion channels in neural membranes to the macroscopic behaviour of human societies. All conceivable levels have been explored comprising the myriads of possibilities arising from combinations of biochemical, electrophysiological, and behavioural causes and effects under normal and pathological conditions.

Recently, a new technique called magnetoencephalography MEG has been added to the repertoire of investigative methods. The technique allows the detection of minute magnetic fields associated with the neuronal activity outside the skull. The MEG was discovered in 1968, when Dr. Cohen, a physicist at the Massachusetts Institute of Technology, recorded alpha waves using coils placed near the head. Since then, MEG technology has been improved, and reached a stage of considerable complexity. Whole head systems allow the simultaneous measurement of magnetic fields emanating from all parts of the brain, within sophisticated experimental settings which relate the signals to cognitive processes. The MEG opens another window into the macroscopic brain dynamics on a millisecond scale previously only accessible through electroencephalography EEG and related techniques [135].

This thesis centres on the use of MEG to study neural dynamics associated with the processing of faces and sentences in humans. Linked to this theme is the development of a number of new analysis tools.

1.1 From brains to signals

1.1.1 Basic anatomy of the human brain

MEG is most suited to the study of the cerebral cortex. This is the brain's uppermost layer of gray tissue or nerve cell tissue, which has an average thickness of 1.5 to 4.5 mm and a total surface of $\approx$2500 cm^2. It is folded in a complex way to fit into the cranial cavity forming gyri (folds) and sulci (fissures). The cortex as well as the whole brain consists of a left and a right hemisphere separated by the longitudinal fissure. Each half, in turn, is divided into lobes by deep grooves. The Sylvian fissure, which is almost horizontal, lies above the temporal lobe while the Rolandic fissure (or central sulcus) separates the frontal and parietal lobes. There are four lobes in each half of the cortex: the frontal, temporal, parietal and occipital lobe (Figure 1.1, adapted from [58]).

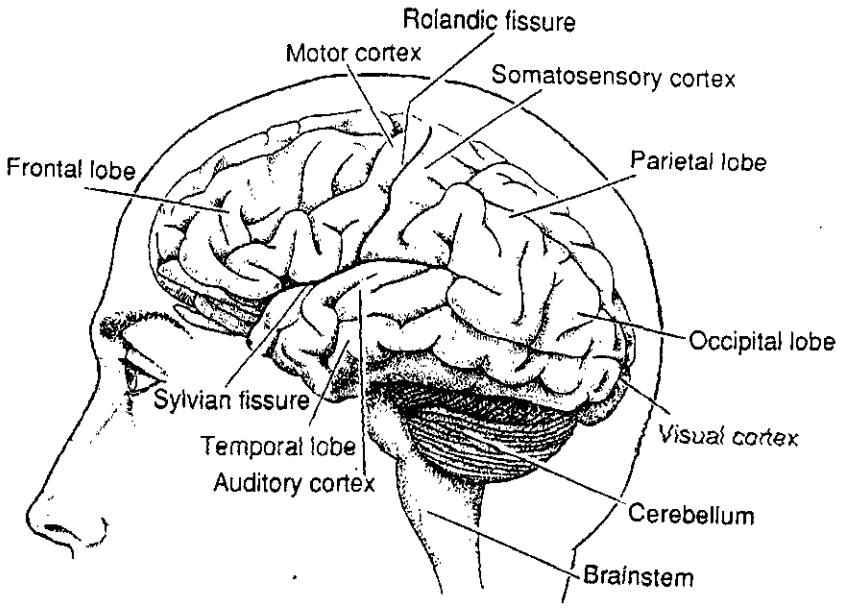

Figure 1.1: Schematic side view of the human brain

Many areas of the cortex have been mapped functionally, i.e. can be associated with projections from parts of the body's sensory system or are accompanied by circumscribed malfunctions if damaged. For example, visual information projects to an area in the occipital lobe known as the primary visual cortex, and auditory information projects to the primary auditory cortex in the temporal lobe and is buried within the depths of the Sylvian fissure. The primary somatosensory cortex receives information about touch, pressure, and joint position, and is found posterior to the central sul-

cus. Just anterior to the central sulcus is the primary motor or precentral cortex, the cortical area most concerned with the control of movement [52, 146].

1.1.2 The origin of neuromagnetic signals

The human brain contains about 10^{12} neurons, highly specialised cells forming a complicated network. The communication between the nerve cells is fundamentally linked to their electrical properties. In the resting state, a small dc voltage ($\approx$70 mv) is maintained across the cell membrane, the inside of the cell being negative. Change in this membrane potential conveys information and, at suitable locations, can make a neuron fire, i.e. emit an action potential via its axon into the network. An action potential is associated with currents of ions giving rise to fluctuating magnetic fields with a typical time scale of $\approx$1 ms and a field strength decreasing rapidly with the distance d from the locus of generation, as $1/d^3$.

When an action potential reaches a synapse, the junction to the next neuron, a biochemical neurotransmitter is released. The substance transverses the synaptic cleft and opens selectively ion channels in the postsynaptic cell membrane of the target neuron. A postsynaptic potential is generated which is accompanied by a current flow, and gives rise to fluctuating magnetic fields with a typical time scale of about 10 to 100 ms and a field strength decreasing with the distance d from the locus of generation as $1/d^2$.

It is generally agreed that the currents associated with the postsynaptic potentials constitute the principal sources of magnetic fields outside the head as well as the electrical signals measured on the scalp. The strength to distance relationship for postsynaptic potentials is more favourable than for action potentials, and the longer time scale facilitates a coherence, or summation over many thousands of neurons needed for a signal of detectable strength. Specifically, it is assumed that the main contribution to external signals stems from the pyramidal neurons in the cortex (Figure 1.2). The geometry of the cell's apical dendrites supports a spatial summation of postsynaptic currents approximately orthogonal to the cortical surface [78, 135].

1.1.3 Signal phenomenology

The coherent activity of many thousands of neurons produces signals detectable outside the skull, which reflect the ongoing activity. Typically, spontaneous activity, when measured over many seconds, is characterised by a broad frequency spectrum contain-

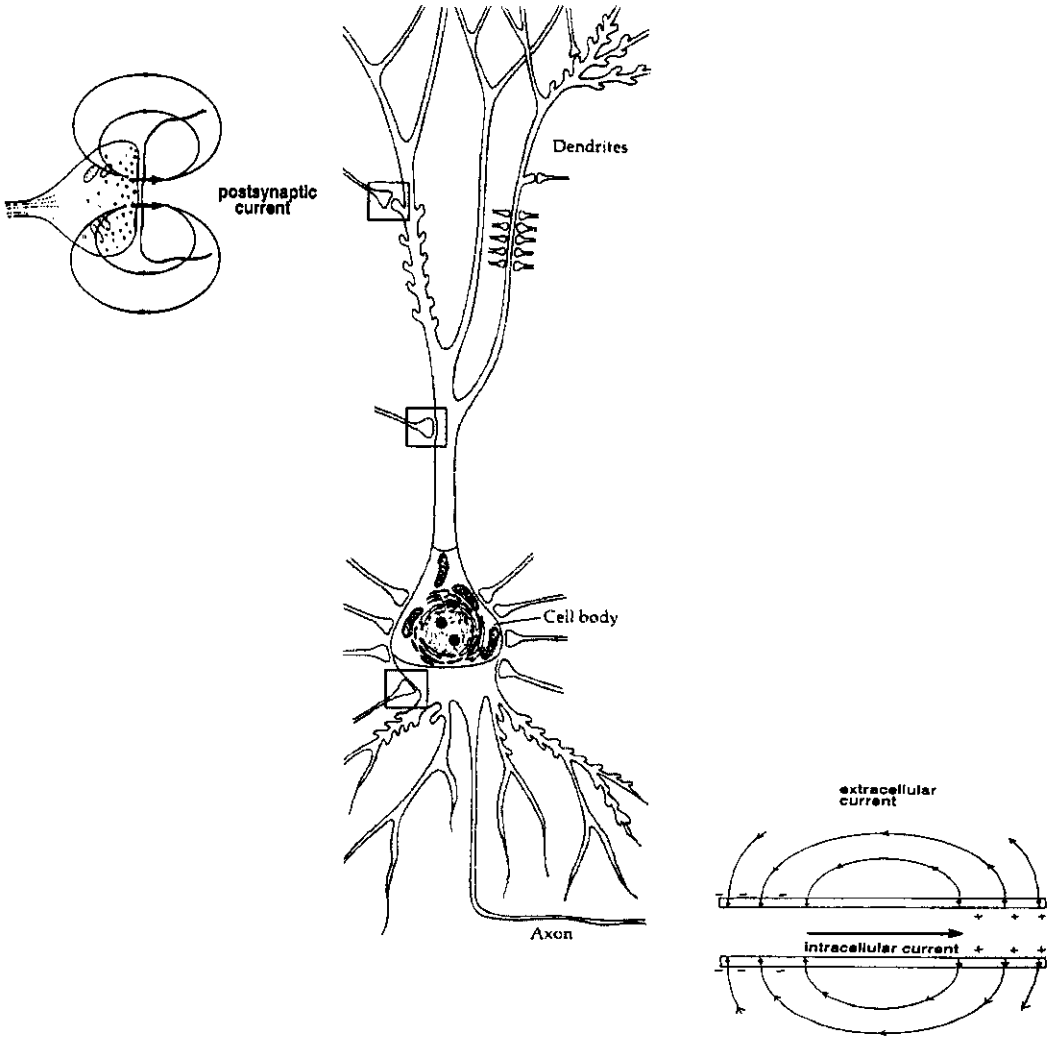

Figure 1.2: Pyramidal neuron

The insets depict the propagation of an action potential along the neuron's axon (right), and the current flow associated with a postsynaptic potential at a synapse at an apical dendrite (adapted from [135, 157]).

ing well known spectral peaks in certain bands (Figure 1.3, left). Most commonly encountered in MEG and EEG observations are the θ (4 to 7 Hz), α (8 to 13 Hz), and β-bands (13 to 30 Hz). These bands relate variously to the degree of arousal, states of pathological abnormalities, or very general aspects of visual attention etc. Higher frequencies are referred to as the γ-band, which is here defined as frequencies[1] above 20 Hz [137].

There are many ways of analysing neural activity: the so-called event-related approach is relevant in this thesis. Within some experimental setting, a stimulus is presented to a subject repeatedly. The appearance of a stimulus marks a point in

[1]There is no generally used definition of the γ-band. The range used here is common even though there is an overlap with the β-band.

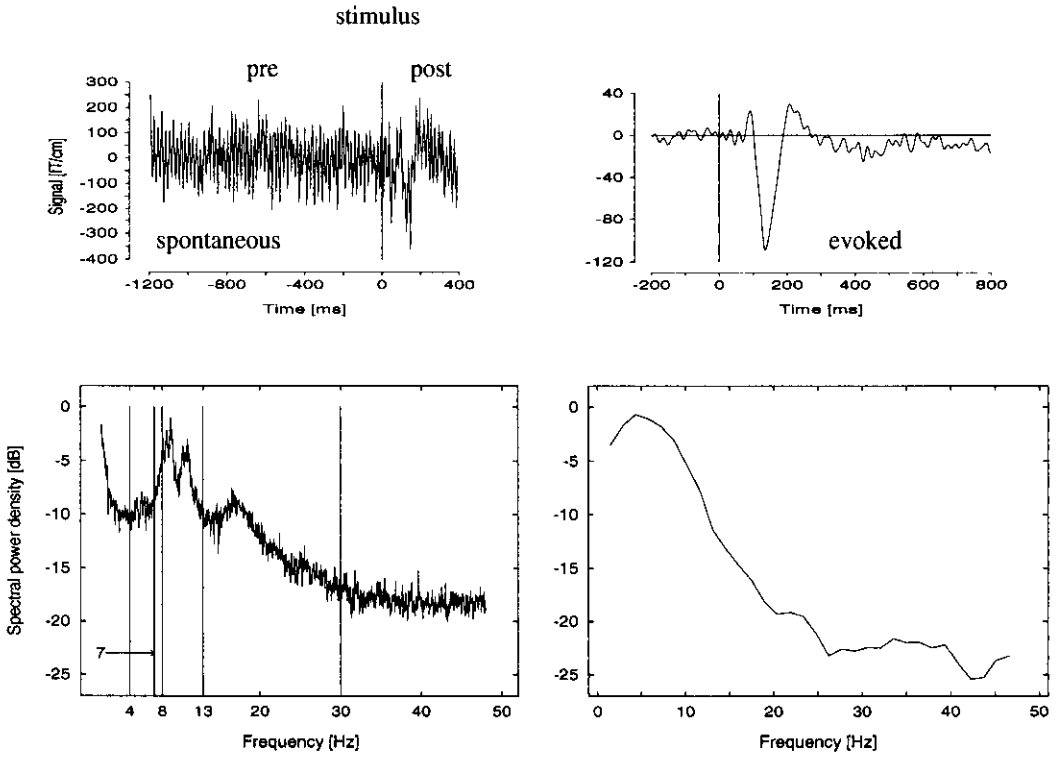

Figure 1.3: Phenomenological signal types
'Typical' spontaneous (left) and evoked (right) signals displayed as a function of time (upper) and frequency (lower).

time, usually denoted by $t = 0$, with respect to which a stretch of data is defined, denoted as an epoch. The epoch consists of two parts, the pre and post-stimulus interval. Conventionally, the signal $s(t)$ in the post-stimulus interval is viewed as a sum

$$s(t) = c(t) + \varepsilon$$

where c is assumed to be the same neural response for all stimuli under consideration, i.e. it depends only on t, and ε denotes a Gaussian random process. It is well known that, with this assumption, c can be recovered from the sum by averaging over stimuli the data corresponding to the same time t with respect to each stimulus. This reduces the noise variance proportionally to the number of stimuli N. The resultant waveform is usually called an evoked response. The process of averaging normally applies to a given site, or channel, of measurement, and a given subject. If the averaging is extended over several subjects, a grand mean waveform is obtained for a given site of measurement [49]. The spectral characteristics of an evoked response is usually dominated by low frequencies corresponding to the width of major deflections (Figure 1.3, right; data taken from the present work).

This section is concluded by a brief comment on two commonly used techniques to

measure neural activity which complement MEG and EEG methods. Results obtained with such techniques will be referenced occasionally.

Functional imaging techniques

Neural activity is necessarily accompanied by a consumption of metabolic energy. The energy demand influences the regional cerebral blood flow rCBF, where local changes in energy demand (neural activity) are tightly linked in time with changes in rCBF, because of the brain's limited capacity to maintain energy reservoirs. These changes in rCBF can be monitored with two functional imaging techniques known as:

1) positron emission tomography PET. The technique is based on the detection of γ-rays associated with the decay of radioactive positron emitting tracers whose distribution is a function of rCBF.

2) functional magnetic resonance imaging fMRI. The technique is based on the detection of changes in the magnetic resonance properties of hydrogen nuclei in mobile molecules. These properties depend on rCBF.

PET and fMRI are based on vastly different physical principles, but both allow the observation of local changes in blood flow with a high spatial resolution. However, the resolution in time is much less than is possible with MEG and EEG, being limited to of order minutes or seconds respectively [4, 76].

1.2 Outline of the thesis

The work on which this thesis is based is part of a long term project involving neuromagnetic measurements which builds towards a better understanding of the electrophysiological correlates of autism. Autism is a complex disorder, involving a number of cognitive deficits. Therefore, it was necessary for the project to encompass a large set of experimental paradigms, in keeping with the complexity of the condition. In this project, studies have been carried out involving a variety of cognitive functions; object recognition (specifically faces), processing of words and sentences, motor memory sequence learning, and attention shift processes. Despite this overall framework, this thesis is not a dissertation on autism. Instead, the author has taken the opportunity to study brain dynamics within a setting motivated by the possible clinical usefulness.

The work connects with existing paradigms and approaches, but it introduces new methods of analysis.

A total of 9 research visits were made to the Neuromag-122 facility located at the Low Temperature Laboratory of the Helsinki University of Technology (HUT) where all the experiments were performed. The visits had to be fitted into the tight time schedule of an internationally acclaimed laboratory used by many groups from all over the world. Seven high-functioning autistic subjects as well as some of the 18 control subjects were transported from England to Finland and approximately 30 Gb (giga bytes) of sampled data were collected. The time available in the laboratory was mainly consumed by collecting the data, and, as a prerequisite, making the experimental protocols operational. Analysis was done at the laboratory only up to a preliminary level and, usually, in such a way that decisions could be made as to whether one should carry on with a particular experiment under given circumstances.

Chapter 2 introduces the Neuromag-122 detector system, the tool used for magnetoencephalographic investigations, and presents the technical aspects of the specific experiments presented in the thesis. These include the stimulus protocol system as well as the stimuli themselves. Included are remarks on artefacts, and (pre-)processing as well as the transfer of data.

Chapter 3 deals with the responses involved in processing images of faces and other objects in normal subjects. A review of face processing is given followed by the presentation and discussion of results obtained from experiments designed to address questions related to image class discrimination in the context of a variety of specific tasks. The emphasis has been put on specific patterns of evoked responses at early latencies using a parameterisation scheme which extends previous work on root-mean-square averaged response classification.

Chapter 4 continues the theme of Chapter 3 in the discussion of the data from 7 autistic subjects. A short introduction to autism is followed by an analysis of the experiments presented in the previous chapter. As far as possible, the results are discussed in comparison to the normal controls.

Chapter 5 attempts to combine two directions of research interest, namely the effects of semantic violations in language processing and the stimulus specificity of oscillatory dynamics. The chapter briefly introduces both and discusses results obtained from a sentence reading paradigm, where only normal subjects were measured. The method of Gabor spectrograms was employed extended by the use of statistical bootstrapping.

Chapter 6 investigates the relationship between ongoing brain activity, as seen in pre-stimulus intervals, and the responses evoked by certain stimuli. The research on pre-stimulus states is briefly reviewed followed by an introduction to methods of nonlinear time series techniques. A classification scheme based on vector-embedding is proposed in which individual pre-stimulus epochs are viewed as instantiations of stationary, deterministic and possibly chaotic processes. The results of an experiment designed to probe for the possible influence of endogenous components are discussed. Here, only normal subjects were measured.

Chapter 7 summarises the main conclusions of the thesis and points to future research.

Finally, five appendices follow. In the first, details about the subjects are supplied. In the second, the basic numerical techniques used throughout the core part of the present work are listed. Two appendices follow in which the methods used in Chapter 3 are elaborated. In the final appendix, further details are provided of the methods used in Chapter 5.

A remark on software — The present work involved a considerable amount of software development carried out by the author. The algorithms used in this thesis were implemented using a data flow framework [2]. Details about the strategy of implementation and functionality are given in the author's first year report (Physics Department, The Open University).

Chapter 2

Instrumentation

In this chapter, a brief introduction is given to the magnetoencephalographic instrument Neuromag-122 used for the work of this thesis. The presentation is followed by a short description of the stimulus protocol system used to control the technical aspects of the experiments. This system developed at the Open University is the only instrumental contribution added to the equipment. The chapter continues with a description of the stimulus material (i.e. the images). Finally, some issues concerning the data acquisition and the control of artefacts are discussed. These issues are common to all experiments, and are not made explicitly in conjunction with a particular paradigm.

2.1 The neuromagnetic instrument Neuromag-122

SQUIDS

The signal strength associated with neural activity is extremely small, typically one part in one thousand million of the Earth's geomagnetic field. The detection of such a small field requires highly sensitive detectors. To date, the only instrument with the needed sensitivity is the Superconducting QUantum Interference Device SQUID. The device operates at the cryogenic temperature of liquid helium, where certain materials become superconductors. Two phenomena are utilised to convert tiny changes in the magnetic field into a voltage which can be further processed: a) the flux quantisation which ensures that the total flux through a loop of a superconducting wire is an integral multiple of the flux quantum $\Phi_0 = 2.07 \times 10^{-15}$ Vs, and b) the Josephson effect associated with the quantum mechanical tunnelling of electrons from one superconducting region to another separated by an insulating barrier (called a weak link or a Josephson junction).

A modern dc SQUID has two weak links (Figure 2.1). The flux is inductively coupled into the SQUID via a pickup coil which connects the device to the experiment. The device is biased with a dc current above a threshold characteristic for the SQUID. A dc voltage is developed across the junctions which is a periodic function of the flux applied through the pickup coil. Using complex electronics, this output voltage is amplified and used to generate a feedback current. This current is coupled back into the SQUID loop to null the applied signal flux. As a result, the device is locked at a single flux bias point, and the feedback current is a direct measure of changes in the flux applied to the SQUID [9, 84, 135].

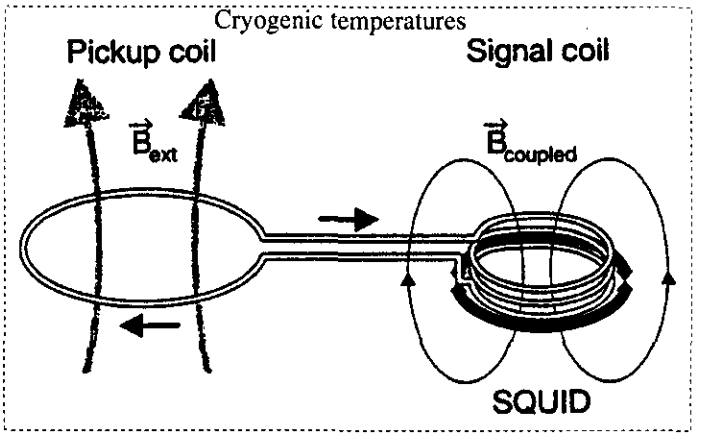

Figure 2.1: Coupled dc SQUID
The solid ring symbolises the superconducting loop with the two junctions (arrows) across which a flux modulated dc voltage develops (adapted from [3]).

Detectors

For the Neuromag system[1], each pick-up coil is figure-of-eight shaped, and pairs of such coils are mounted orthogonally on a single chip (Figure 2.2 left). With this design, each pick-up coil becomes a 1st order gradiometer, sensitive to the spatial derivative of the local z-component of the magnetic field along the axis joining the coil centres. The gradiometer is a means of noise reduction in that magnetic fields originating from sources far away from the detector usually have very small spatial variations (gradients) over the extent of the coil. Each gradiometer chip houses the pick-up and coupling coils as well as the superconducting device for two channels. Due to the orthogonality[2], independent information is provided by the two gradiometers on each chip.

[1]The main references for the system are [3, 108], on which this section is based.
[2]Strictly speaking, this holds for orthogonal lead fields in free space.

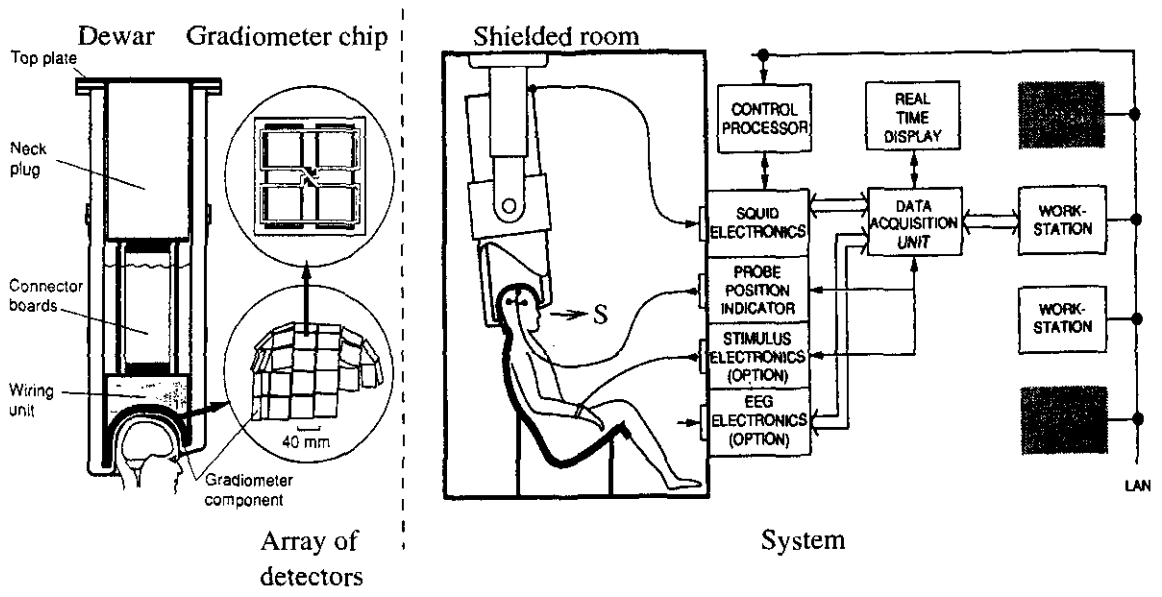

Figure 2.2: The Neuromag-122 system

Left: the magnetometer probe comprising the dewar and the modular insert structure. The zoom inserts depict the helmet shaped array of 61 dual sensors, and one of the sensors (i.e. a planar gradiometer chip). The distance between the skull and the detectors at cryogenic temperatures is about 2.5 cm. Each gradiometer defines an orthogonal local co-ordinate system, where the the x and y-axis are coincident with the plane of the chip. All measurements are with respect to the local co-ordinate systems (e.g. the solid black coil measures $\partial \vec{B}_z/\partial x$). Right: the Neuromag-122 system. S: screen, LAN: local area network (adapted from: left [58], right [108]).

System

There are 61 gradiometer chips, or detector sites, arranged into a helmet shaped array of sensors. The array is held at cryogenic temperatures (liquid helium) within a dewar (Figure 2.2 left). The dewar resides in a μ-metal shielded room (Figure 2.2 right). The shielded environment is the second provision to reduce external noise. There are a variety of connections between the inside and the outside of the shielded room, the most important of which is the link between the sensors, the SQUID electronics and the data acquisition unit DAQ. The latter constitutes the user interface and allows for technical control over an experiment.

Signals

The readout from the gradiometers is converted into a sampled time series by the data acquisition unit (DAQ). Each time series represents the local field gradient for a given channel at a sampled time t:

$$S^{\mathcal{C}}(t) = \left.\frac{\partial \vec{B}_z}{\partial \alpha}\right|_t$$

where α denotes either x or y. Calligraphic letters are used to denote either a single channel $\mathcal{C}$ or a detector site $\mathcal{D}$, in which the signal S becomes a 2-vector $S^{\mathcal{D}}$ used without vector notation. Assuming a single current dipole with parameters (q_x, q_y, q_z) located at $(0, 0, z)$, $z \neq 0$ with respect to the local co-ordinate system of a detector, the following relation holds between the (vector) reading and the parameter of the dipole:

$$\begin{pmatrix} \frac{\partial \vec{B}_z}{\partial y} \\ -\frac{\partial \vec{B}_z}{\partial x} \end{pmatrix} \sim \frac{1}{|z|^3} \begin{pmatrix} q_x \\ q_y \end{pmatrix}. \tag{2.1}$$

Strictly speaking, this equation only holds approximately because of the finite coil sizes. The quantity on the left of Equation 2.1 is referred to as the 'rotated gradient' and is readily visualised in the detector's local co-ordinate system. A plot containing the rotated gradients of all sites can be interpreted as a momentary representation of the sources directly underlying each detector. The plots are useful in the initial steps of the data analysis. They are given preference over the usual contour plots of $\vec{B}_z$ which can be calculated from the data although doing so requires certain model assumptions.

Head positioning

In order to determine the sensor positions with respect to the head of a subject, a two step procedure is applied: 1) The positions of three fiducial points on the skull are measured with respect to an arbitrary co-ordinate system outside the shielded room using a commercially available 3D localisation system ISOTRAK [116]. Additionally, the positions of 3 to 4 small coils attached to the skull are measured with respect to the same co-ordinate system. 2) Once the subject's head is under the dewar, the same coils are activated by currents making them sources of magnetic fields which are measured by the detectors. Based on the readings, the position of each coil is calculated with respect to the co-ordinate system of the dewar.

Thus, the position of the coils is known in the two co-ordinate systems, and standard linear algebra can be used to transform between these. For all experiments relevant to this thesis, the three fiducial points were chosen to be the nasion and the two pre-auricular points. These define an orthogonal head co-ordinate system given by: the line joining the two pre-auricular points (x-direction, $x > 0$ to the right), the line through the nasion perpendicular to the pre-auricular line (y-direction, $y > 0$ rostrally), and the line through the intercept orthogonal to the plane just defined (z-direction, $z > 0$ towards the vertex). This co-ordinate system is known as the PAN system from the names of the fiducial points used in its definition.

2.1.1 The array of detectors

Throughout the thesis, the data has been referenced by channel numbers whenever appropriate. Below, 4 different views of the layout of the gradiometer sites are given (Figure 2.3). These views are convenient when relating the data to the location over the skull. Occasionally, the data from subsets of the 122 channels will be presented in a 2 dimensional projection representing approximately the anatomical location of each channel (Figure 2.4).

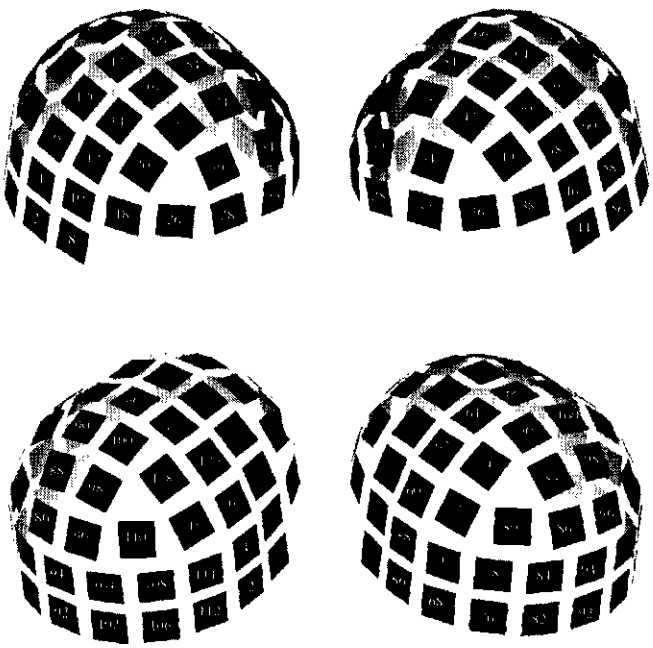

Figure 2.3: 4 views of the helmet
Each site is labelled with an even channel number. The channels are paired 1 and 2, 3 and 4 etc.

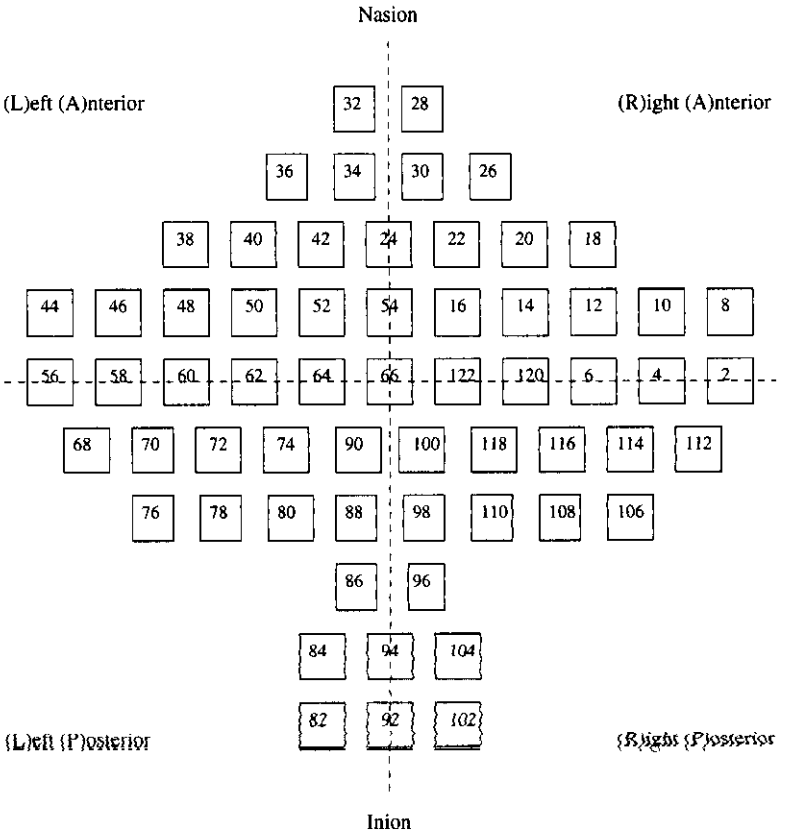

Figure 2.4: Projection into 2 dimensions

In data displays, odd numbered channels are placed in the lower half of the square and even channels in the upper. It is convenient to divide the array into four quadrants along the longitudinal fissure and approximately along the central sulcus (dashed lines).

2.2 Stimulus protocol system

The experiments were carried out using a script-based image display (SID) system developed in the department[3]. The production of a portable, tailored but still versatile system is convenient given that: a) the main preparatory work and 'dry' runs had to be carried out in the UK, as work in the Finnish laboratory was often tightly scheduled, and b) subject responses via a keypad were not supported with the HUT-based equipment when the experimentation for the project began. The keypad is an important part of the experiments as it allows the monitoring of task performance and the measurement of reaction times. The scripts control the processing of the keypad data, the various parameters involved in the presentation of the images, and the trigger mechanism needed for the synchronisation between the stimulus onset and the acquisition of data. A script file can be executed repeatedly using exactly the same parameters, thereby ensuring the technical reproducibility of an experiment.

The software uses palette swapping for image draw operations. This allows for smooth and fast transitions from background colour to image. Additionally, all image operations are synchronised with the vertical scan rate of the projection monitor to avoid flicker [145]. The software includes basic image manipulation tools like resizing, mirroring, changing of background colours, superposition of fixation points, and adjustment of mean luminosity. These tools are meant for on-site solving of minor problems under changing laboratory conditions and do not obviate the need for careful image selection or manipulation using more sophisticated software. The software produces a result file containing actual key presses made by the subject and the corresponding reaction times.

The display program resides on a standard Laptop personal computer. It communicates with the outside world via a standard Centronics printer port. This interface *provides an easy-to-use, cost effective, and sufficiently fast solution* [32]. The relationship between the SID and the Neuromag facility is shown in Figure 2.5. The images are displayed in the shielded room via a projector residing outside the room with its lens close to a hole in the wall. The light is reflected once by a mirror and then directed to a screen close to the subject. Trigger codes corresponding to the images are sent to the host facility for synchronisation purposes. Four trigger lines are used which are physically different from the lines for the keypad electronics.

[3]Software by the author; hardware by other members of the Physics Department of the Open University.

The non-magnetic keypad is located within comfortable reach of the subject[4] inside the shielded room. It is connected to the keypad electronics via optical fibres which are used instead of electrical connections to avoid disturbances. The core mechanism of the keypad consists of five simple switches, each of which interrupts a light path when the associated key is pressed. When the subject presses a key the electronics detects the interrupted light path and issues a hardware-interrupt to the Centronic port of the PC. Simultaneously, the key code is written to the port lines. The hardware interrupt mechanism is more effective than continuously interrogating the keypad electronics. For the experiments, interrupts are rare events handled within a few microseconds and this causes no timing problems.

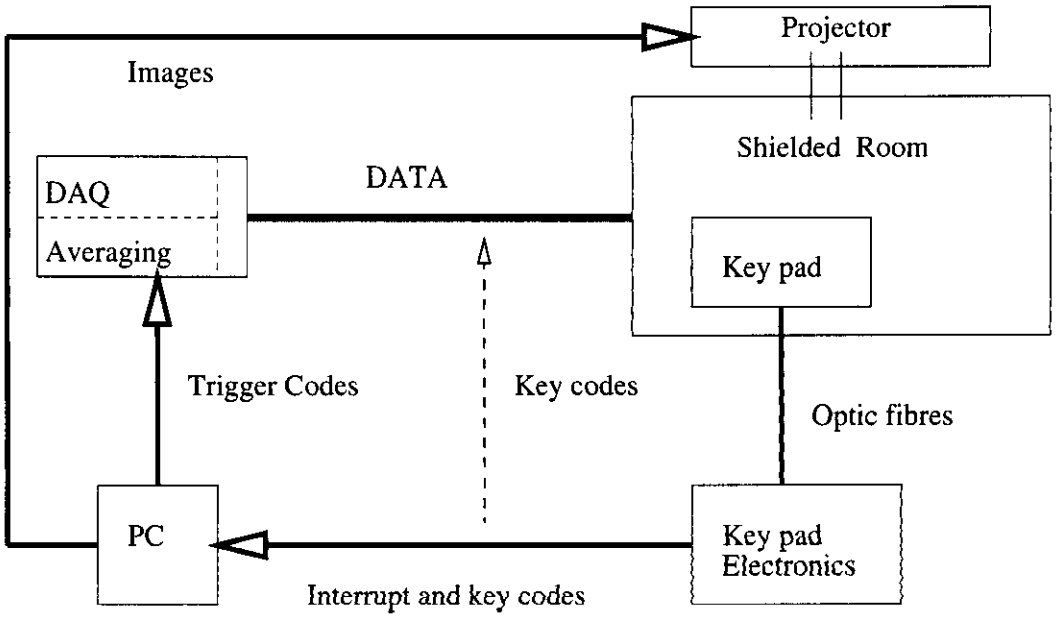

Figure 2.5: Hardware connections

As accurate timing is important in MEG experiments, it is noted that personal computers are not real-time devices per se. In order to assess the accuracy of SID, an extensive survey was carried out using a variety of scripts. Assuming that all hardware is connected properly and the SID runs on a dedicated[5] computer with sufficient memory to keep all images:

1) the duration of an image is predictable up to an accuracy of 8% for a display period between 100 and 200 ms.

[4]Only a keypad for the right hand is currently available.

[5]Here, dedicated means: a) the display program is the only active user process, b) the port used by the keypad electronics is the only active one, and c) the pointer device ('mouse') is not being used during the run of an experiment.

2) the display of the image on the screen is delayed by 22.5±2.4 ms with respect to the trigger signal. This delay is entirely due to the transmission path between the computer and the projector. The time lag was measured by detecting changes in luminance accompanying the appearance of an image, and comparing the luminance signal with the transitions of the trigger line using equipment of the Finnish laboratory (Figure 2.6). It is noted that the fluctuations of luminance during the presentation of an image are imperceptible.

Thus, the system's performance is uncritical for most experiments, however, the last point introduces a limitation in the context of the language experiment LT as explained in Chapter 5. For all of the present work, the evoked responses have been shifted by 22 ms towards earlier latencies in order to compensate for the monitor delay.

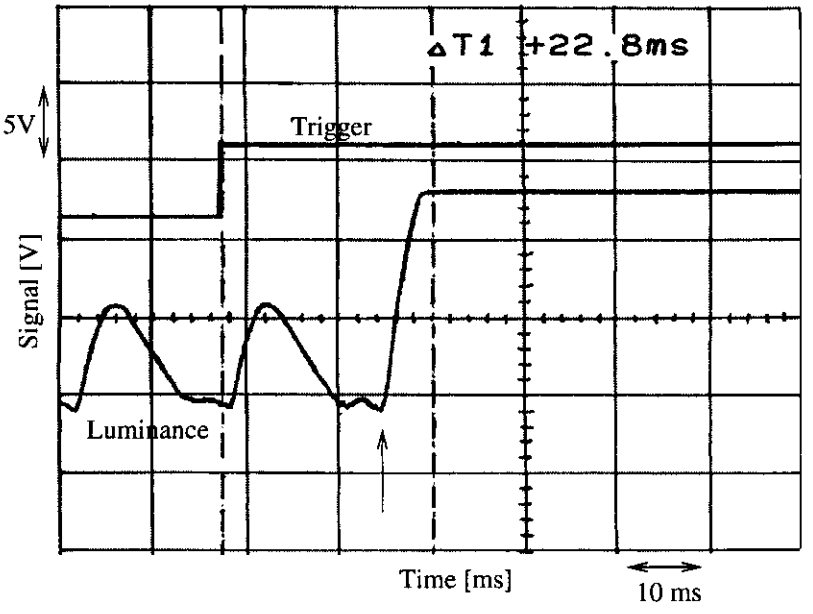

Figure 2.6: Monitor delay

Snapshot of the delay between the trigger and the change of image on screen. The graph is reproduced from the screen dump of a digital storage oscilloscope. Upper trace: signal from the trigger port. Lower trace: luminance signal at the screen centre showing fluctuations of the background (uniform gray image) due to the video rate of 70 Hz. The arrow indicates the onset of the image which reaches maximum (photo-transistor overdrive) intensity about 5 ms later. This trace has been amplified to fit conveniently on the screen together with the trigger line.

2.3 Images

All visual stimuli were presented in the form of prepared (bitmap) images[6] mapped to the screen. There were enough images in each category to run all experiments under consideration on one subject with either no or only a few repetitions of pictures. The different image categories are listed below (Figure 2.7).

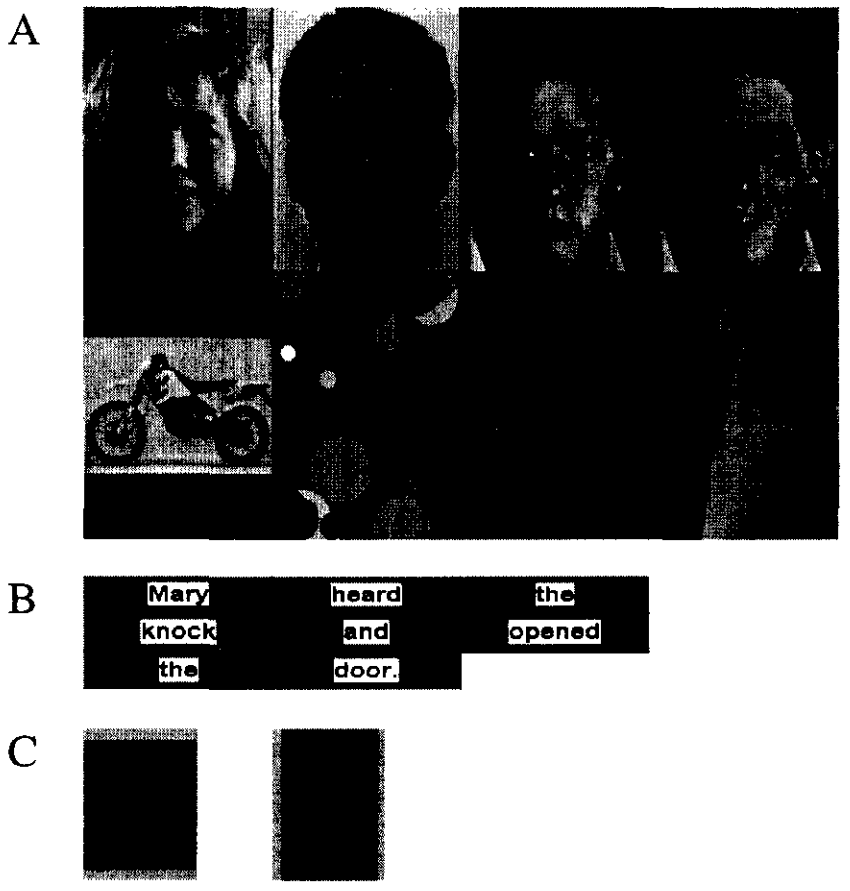

Figure 2.7: Images

A: various image types used in the face processing experiments; adult face (2x), boy's face (neutral, smiling), motor bike, dot pattern, coffee mug, and animal (left to right, upper to lower row). B: words forming a sentence. Each word is presented as a separate image. C: visual prompt signs. The black horizontal and vertical lines in A and B are drawn for clarity and are not part of the images.

Adult faces (F) Photographs of adult Caucasians viewed full face. Pictures were selected from computer databases and other sources so as to ensure homogeneity of the picture's background, absence of strongly distracting features (like skin colour, skin impairments, etc), and expression. Some photographs passed selection although the individuals wear glasses or have beards. However, in these cases, the features were

[6]Windows BMP-format

not considered as serious distractors. The pictures showed persons with a neutral or slightly smiling expression (according to subjective judgement).

Boy's faces (F) Photographs of UK-schoolboys aged 12 and 13 viewed full face. The pictures were taken by a professional photographer instructed to pay attention to visual homogeneity of the photographs. Specifically, the boys had their hair drawn back or covered by a cap (which is not obvious in the final image). Each child was asked to pose with an emotionally neutral and then a smiling expression. If clarification is needed, N or S (neutral/smiling) will be used in describing the images in this class.

Animals (A) Photographs of various animals selected from similar sources as for the adult faces. Images were chosen to be naturalistic, thus showing different backgrounds (usually part of the animal's habitat). Although the pictures show either predominantly the whole animal or the animal's head/face, a clear distinction between animal and animal face is not possible.

Motor bikes (m-bike, B) Photographs of common motor bikes selected from a catalogue. The pictures show a variety of motor bike types from various manufacturers in their standard, unrendered form (side view) without licence plates.

Dot patterns (D) Computer generated images of randomly positioned filled circles with varying radius and grey shade. In contrast to all other image classes, only a restricted number of grey shades was used ($\approx$16). This provision became necessary to allow for a reasonably easy distinction between images in one of the experiments.

Coffee mugs (M) Photographs of standard coffee mugs of about the same size. Mugs were mounted[7] against a homogeneous background (support invisible) with the mug's handle to the right. Not selected were mugs picturing words, or letter and symbol strings, or faces and persons in any form. However, some mugs show drawings of animals or clearly identifiable objects like buildings or common household commodities.

Words (W) Computer generated images of words (articles, nouns, verbs, etc) presented in sentences. Images are painted black on white within a grey background. They do not appear together with any of the above image classes.

[7]The photographs were taken by the author of this thesis.

Signs Computer generated horizontal and vertical bars (light grey on dark grey background). Only two bitmaps are used signalling 'get ready'/'experiment done' (horizontal bars) and 'press key' (vertical bars).

Each image is 180 pixels wide and 225 high (words: 180 and 30) using a grey scale of 256 uniformly distributed shades. Under usual conditions, the images subtend visual angles of approximately 6° and 8° (words: 6° and 1.2°) horizontally and vertically at the eye. Each image was histogram adjusted to restrict grey shades to the range between 5% and 95% of the whole scale. Additionally, histograms were globally scaled to maintain a mean luminance of 40 cdm^{-2} within a narrow range (±10%). Further attempts to balance images according to their grey shades was not possible without destroying the naturalistic character. Thus, distributions of grey values vary considerably across image classes (and even within a subset).

To further assess possible inhomogeneities across the images (apart from the content), a spatial frequency analysis was performed for a representative sample of each image category (Appendix B, [N-8]). The power density is very similar for all non-word image classes in the low frequency range (Figure 2.8). Frequency components higher than 20 c/i have relative powers of -35 dB or less and are unlikely to cause any neurophysiological effects. In general, motor bike images have greater spectral power compared to other images at higher frequencies, reflecting the richness of object details.

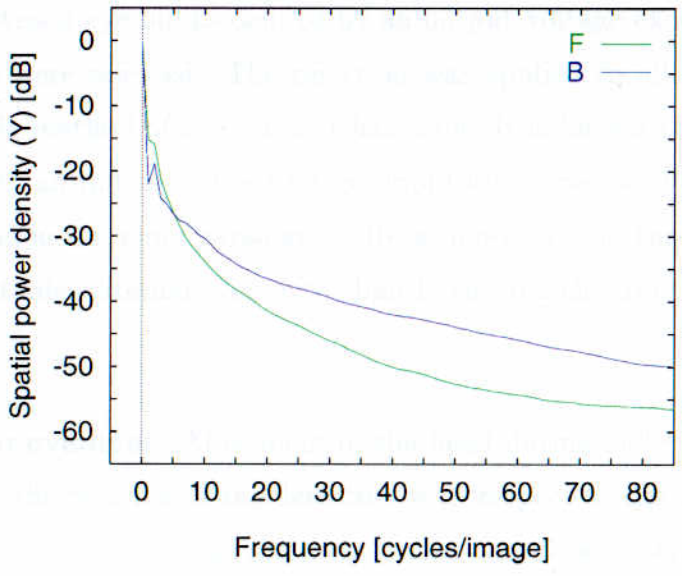

Figure 2.8: Spatial spectral power: faces and motor bikes

Spectral power in y-direction (f_y) for face and motor bike images. Each curve represents an average over 20 images.

2.4 Data acquisition and data handling

All data was acquired using the DAQ-program belonging to the HUT facility. The program allows for the setting of various control parameters and writes the data to mass storage devices in a format proprietary to Neuromag. This format, functional-image-format fif, is used by the various software packages on site, but has not been made public to external researchers. For data analysis outside HUT, software is available to convert unidirectionally fif-files into either standard ASCII or suitable binary[8] files. The software on site as well as the conversion programs allow access to the data from a certain level of pre-processing onwards. In this sense, the term 'raw' data refers to the output of the SQUID electronics, bandpass filtered (analog anti-aliasing) and digitised. For this work, all data was filtered between 0.01 and 130 Hz before digitisation at a sampling rate of 373 Hz.

2.5 Artefacts

Artefacts: electro-oculogram EOG The moving eye generates strong time varying magnetic fields due to the electric charge disparity between the corneal and retinal areas. It follows that eye-blinks can create strong artefacts[9]. Vertical eye movement was monitored in all experiments with two electrodes. The impedance between electrodes was always lower than 10 kΩ using the same equipment for all subjects. Stretches of data indicating strong eye blinks defined by an output voltage exceeding 120 μV in absolute amplitude were rejected. The rejection was applied to all channels, and is the simplest possible method of eye-artefact handling. It is known that differences in electrode placement can influence the EOG's amplitude as well as its waveform [54], a fact to be considered for some paradigms. Here, however, the threshold of 120 μV was found to be a stable criterion even with slightly varying electrode positions across subjects.

Artefacts: head movement Movement of the head during or between runs of an experiment changes the position of the detectors with respect to the anatomical areas and can cause signal artefacts due to motor as well as muscle activity. The Neuromag facility allows head positioning only prior to the data acquisition making it difficult

[8] ASCII files are written in the '%g'-format of the C-programming language providing 6-digit precision [83]. Binary files reflect the output of the anolog-to-digital converter, and can only be used in conjunction with ASCII files specifying channel conversion factors.

[9] Much of this section is considered common knowledge. A good general reference is [49].

to determine when precisely a movement occurred. Despite possible problems due to movements, most experiments had to be split into two parts (runs) with a break in order to achieve a bearable run time or to change control conditions. If the shift of head position (with respect to the dewar system) did not exceed 5 mm, these two runs were merged, and viewed as resulting from one continuous acquisition. This criterion is compatible with the Neuromag software[10] requesting the user to restart the head positioning if distances between coils differ by more than 5 mm as measured by the ISOTRAK and the MEG system respectively [108].

Artefacts: other The laboratory environment itself might give rise to various artefacts[11]. These were removed, usually with the help of the technical staff of the laboratory. The measurements were not begun or resumed until a satisfactory status had been reached. Attention was paid to avoid metal objects attached to the body or clothes[12].

The beating heart is another source of magnetic activity (measured with techniques similar to the MEG and known as magnetocardiography, MCG) which might interfere with the brain's magnetic fields. Visual inspection only was employed to detect the well known traces of the heart activity within the readings of the brain signals. For this reason, one subject's data[13] had to be excluded altogether from the analysis due to strong overlap of MEG and MCG signals. Only weak and intermittent evidence for data corruption by MCG signals was found in all other subjects.

Drift correction and channel variance (noise) Despite the high quality of the equipment, some changes (drifts) of the detectors' characteristics are unavoidable during the run of an experiment. In this thesis, the common technique of (adaptive) mean value correction has been chosen (the simple algorithm is explained in Appendix B, [N-3]). The method, which establishes a common 'zero' across signals, originated in EEG analysis[14] where it is usually called baseline correction. However, the term baseline is reserved for a different context in this thesis, and drift correction is used instead.

[10]This seems to reflect the ISOTRAK's maximal static accuracy of 2.4 mm (rms, [116])

[11]On one occasion, hours of measurement time were lost because the electronics for the keypad caused distortions, although it was at its usual place within the stimulus cabinet (Faraday cage) outside the shielded room. By trial and error, a new location was eventually found solving the problem.

[12]Volunteers as well as autistic patients were occasionally asked to change clothes.

[13]Subject S19 participated in some of the experiments, but his data has not been taken into consideration for this thesis.

[14]Normally, baselines play a more profound role in EEG. This is because the electrical signals can only be measured with respect to some reference level.

There are no strict rules regarding where and how to apply the method for a given strategy of analysis, and the details are stated for each of the following chapters.

For the purpose of this thesis, noise estimation is based on two data sets supplied by the staff of the laboratory corresponding to the dewar being 25% and 80% full, each comprising 40 seconds of an 'empty' (no subject) measurement under average experimental conditions (i.e. with visual or auditory stimulus presentation). From these sets, a mean channel variance was computed according to

$$\overline{\mathrm{cvar}} = \frac{1}{N_t N_C} \sum_{i=1}^{N_t} \sum_{C=1}^{N_C} \left(S_i^C - \bar{S}^C \right)^2, \text{ with } \bar{S}^C = \frac{1}{N_t} \sum_{i=1}^{N_t} S_i^C \tag{2.2}$$

with $N_t = 16000$ (40 s at 400 Hz digitisation rate) and $N_C = 122$. The channel variance is almost constant for these two sets ($\overline{\mathrm{cvar}}_{25\%} = 4654.1\,(\mathrm{fT/cm})^2$ and $\overline{\mathrm{cvar}}_{80\%} = 4646.5\,(\mathrm{fT/cm})^2$).

Chapter 3

Face processing

This chapter reports on a study of the neural responses associated with the processing of images of faces and other objects. The design of the experiments follows established paradigms widely used in electrophysiological investigations of face processing, which have identified responses specific to faces at early latency. The aim of the present work is to provide some further evidence on how this differential activity is modulated by the nature of the face processing task. The quantification of the responses is achieved by a parameterisation of signal power which extends approaches using signal latencies and amplitudes.

In what follows, a brief review of relevant neurophysiological studies of face processing is given, followed by a description of the experiments employed. The chapter continues with a presentation of the results. The method used for power parameterisation has been developed after unsuccessful initial attempts at signal quantification using standard methods. It is introduced at the appropriate position within the results section. The chapter finishes with a discussion of the results.

3.1 Background on face processing

The face holds a special place among visual objects. Any social animal must possess the aptitude to distinguish and recognise members of its group. In humans, the face is the most characteristic attribute for indexing identity reliably. A widespread interdisciplinary research interest has concerned the issue as to whether face processing is 'special', compared to the processing of other objects, in that it is accomplished using a dedicated and separate system. This dedicated system might be given in terms of dissociation by anatomical location as well as by the characteristics of neural

activation [45]. Typically, research has pursued two, partially overlapping approaches: the neuropsychological and the neurophysiological. The former emphasises the possibly unique status face of processing and its functional segregation into different stages. The latter emphasises neural substrate, where evidence is sought for localised neural systems specifically related to the processing of faces.

Often cited observations which fall into the first category include: the preference to gaze at faces rather than other objects which may be developed by newborns at just 30 minutes of age [105]; or the face inversion effect, which suggests that the recognition of a face turned upside down is significantly more difficult than the recognition of a general object turned upside down [45, 159]. Also often cited in this context is a rare disorder called prosopagnosia: the impaired recognition of previously known faces after brain damage. The disorder usually implies a difficulty in recognising objects other than faces, but the deficit can appear highly selective for faces [29, 141]. Several studies on prosopagnosia suggest that the right hemisphere might play the more crucial role [25, 127].

Following the lines of neuropsychological studies, a functional model of face recognition was introduced in 1986 and named after its inventors as the Bruce and Young model. Ever since than, the model has remained influential in guiding the interpretation of results of face processing studies [23, 24]. The model is based on an extensive survey of mainly psychological and neurological observations suggesting that the process of face recognition can be partially decomposed into a number of functionally related modules processing different kinds of information carried by faces. The model assumes a principal processing pathway, aimed at detecting the personal identity. This pathway is paralleled by a number of independent satellite modules designed to elicit other kinds of information about faces. It it suggested that the information from these satellite modules remains available even when later stages of identification pathway are not accessible due to some neuropathology [25].

A simplified version of the model is shown in Figure 3.1. Modules are shown as boxes together with their functional specification. A simple arrow indicates information transfer necessary for the target module to be operational. A double arrow indicates an interaction which is usually linked to mutual gain of efficiency. Even the full version is only an approximation to reality in that it ignores an unspecified cognitive system interacting with the later stages of the identification pathway and the satellite modules.

The neurophysiological approach has gained momentum over the last decade, during which time the whole palette of modern methods has been employed to study

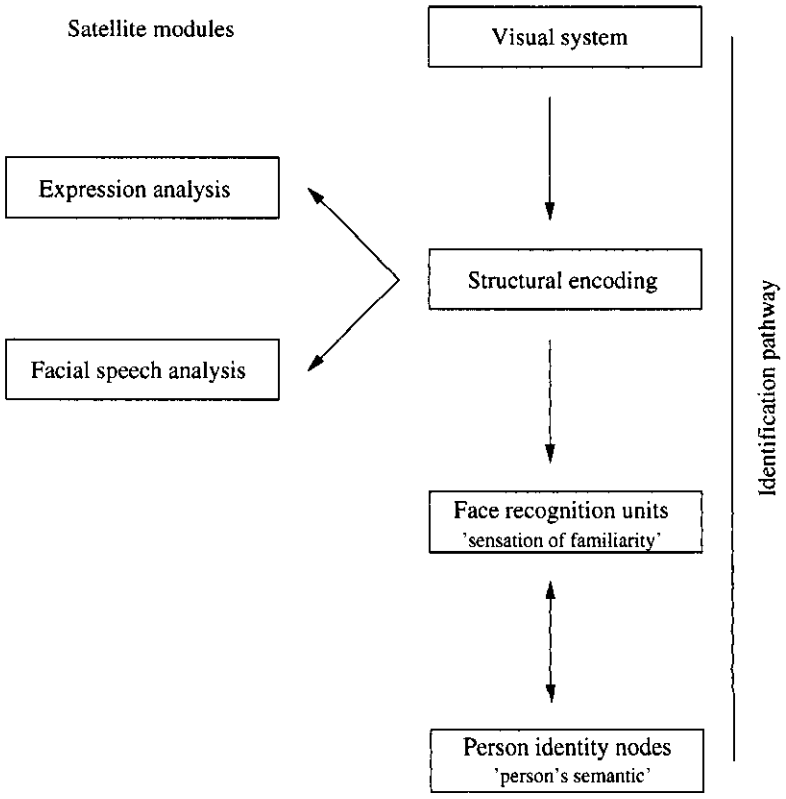

Figure 3.1: A functional model of face recognition
The graph shows a simplified version of the original Bruce and Young model. The person's semantic refers to information such as the person's occupation, or other context related information (adopted from [23, 25]).

face processing in humans. Although many individual aspects of face processing have been addressed, no systematic account is available as yet and the picture is very patchy. In the remainder of this section a brief review of relevant studies is given according to the technique used. The notion of face specificity refers to a stronger response or activation of some kind following face presentation compared to the presentation of a non-face object.

MEG

The first MEG study of face processing was carried in 1991 [94]. Responses in normal subjects to face and bird images were compared. An early latency component at 150 ms was identified only in association with face stimuli. It was detected bilaterally over inferior occipito-temporal cortex. This observation of an early latency component has been confirmed in a recent study [133], however the face specific component appeared to be predominantly over the right hemisphere.

Two linked studies have compared the responses to faces, scrambled (unrecognis-

able) faces and other images [57, 97]. In the first study, a strong face specific equivalent dipole source was located in the right posterior fusiform gyrus or the fundus of the sulcus between the fusiform and inferior temporal gyri. This dipole had maximum activity at 166 ms and 256 ms after the face presentation. The face specificity was verified by a subtraction method with scrambled faces as control images. The result was confirmed in the second study using a different method of analysis. It was found that the source in the right occipito-temporal region corresponding to the response at 166 ms was strongest for photographs of human faces and that there was no effect of image colour, gender or expression. Schematic and scrambled faces gave a reduced response, and other non-face images gave little if any response. In both studies, a similar if less clear pattern was observed at 166 ms in the left-occipito-temporal region.

EEG

Several scalp electrodes studies have demonstrated activity that is specific to faces compared with other object stimuli [14, 18, 19, 74, 139]. Dependent on the number of electrodes used, face specificity of varying degrees was found at the vertex (weak), and at posterior temporal electrode sites (strong). The latencies at which face specificity was observable ranged from ≈150 ms to 180 ms. The face specificity seen at the vertex was shown to be robust when using a variety of face images ranging from photographs to schematic line drawings. Only a few attempts have been made to localise possible neural generators underlying the face responses, suggesting sequential activation of occipital, lateral temporal, and mesio-temporal brain structures. If evaluated, face specificity seemed to be stronger over the right hemisphere.

Recent preliminary work has suggested that responses following face presentation can be specifically modified in tasks requiring the matching of face identity or facial expression [107].

Intracranial electrodes

Subdural recordings on group of epilepsy patients indicated that face specific responses are most strongly found bilaterally in central regions of the fusiform gyrus [6]. The face-specific electrode sites were partially overlapping with those associated with colour perception, which were concentrated in the posterior fusiform gyrus. The responses to faces were maximal at a latency of approximately 200 ms. The face specificity was verified through control images depicting other objects.

Widespread activity following face presentation was found in a study on a similar

group of subjects [55, 56], with the most prominent post-primary signals in the occipito-temporal cortex at latencies of 130, 180 and 240 ms. Although this study lacked the control stimuli needed to provide unambiguous evidence of face-specific processing, the authors argued for such specificity in the fusiform gyrus, and noted the possibility of processing of face stimuli at longer latency.

Functional imaging

Using PET, a variety of cortical and subcortical areas have been found to be activated during face processing in normal subjects. The involvement of the ventral occipito-temporal cortex has been found most consistently [28, 38, 60, 140, 141]. Other activated areas included the anterior temporal cortex and the right lateral occipital cortex. These studies have also reported activity linked with the performance of specific tasks (i.e. face recognition or recognition of facial emotion) in several other areas, notably the prefrontal and anterior cingulate cortices.

Using functional MRI, areas selectivity for both faces and scrambled faces has been identified in several areas including the ventral occipito-temporal cortex, the middle occipital gyri, and the superior temporal sulcus [26, 123]. No significant lateralisation was seen in these studies and face specific activity was only evident in some subjects.

In summary, these various studies suggest directly and indirectly that there are neural systems in humans that are specialised for processing face stimuli and that these systems are, to some degree, localised. However, the degree of face specificity, the lateralisation and timing of the responses, the effects of level of attention and the complexity and nature of the face processing tasks have not been established unambiguously.

3.2 The experiments

Three experimental tasks were designed in order to provide some further evidence on the issues raised above with a particular emphasis on the nature of the early latency face-specific responses (Table 3.1 and Figure 3.2). Apart from the rationale to study possible face specificity under a variety of conditions, the design of tasks has been guided in part by the Bruce and Young model of face processing. The subjects had not seen any of the images before the experiments were carried out.

Task	Description	Numbers of images	Cycles
FT1	Identification of image class	F:25, B:20, D:25, A:20	90
FT2	Identification of identity	F:23, D:20, M:20 pairs	63
FT3	Identification of emotion	N:23, S:23	46

Table 3.1: Tasks

The table shows an overview of all tasks denoted as FT1 to FT3 (face task 1 to 3). The tabulated number of cycles refers to one run. Each task was carried out twice. Images of adult Caucasians (F) were used in task FT1. Non-face objects were motor bikes (B), dots (D), animals (A), and mugs (M). Images of boys faces (also shown as F) were used in all other tasks. Only neutral expressions were used for FT2. For FT3, two emotional expressions were used, denoted by N(eutral) and S(miling). See Figure 2.7 for some examples.

FT1 Four different classes of images were presented in a randomised order in two runs. Dot images were specified as the targets in the first run and images of adult faces as targets in the second run. Face responses were compared to responses following images of common objects with fine structured features (motor bikes), objects with simple geometric shapes (dot patterns), and animals. Animals were chosen because they are entities linked with human characteristics. The task has been designed as a simple object identification problem (i.e. is the image a dot pattern or a face?).

FT2 Three different types of images were presented in a randomised sequence of pairs of images. Each pair either contained two identical or two different images of the same type. Matching and non-matching pairs were of equal probability. The type of images were boys' faces, dots and mugs. The boys were $\approx$12 years old with no major distracting features. Two identical runs were performed with pairs containing identical images of the same class as the target. Boys' faces were selected because, at that age, their faces are blander than those of adults, preventing the use of detailed facial clues. The task has been designed to extend FT1 towards object recognition in the sense of identifying images within a class.

FT3 Images of boys' faces expressing either a neutral or a smiling expression (Table 3.1) were presented in a randomised order in two runs. Neutral images were specified as the targets in the first run and smiling images in the second run. The smiling countenance was chosen as an easily recognisable, non-offending positive emotional expression. The task has been designed to extend FT1 towards the identification of facial

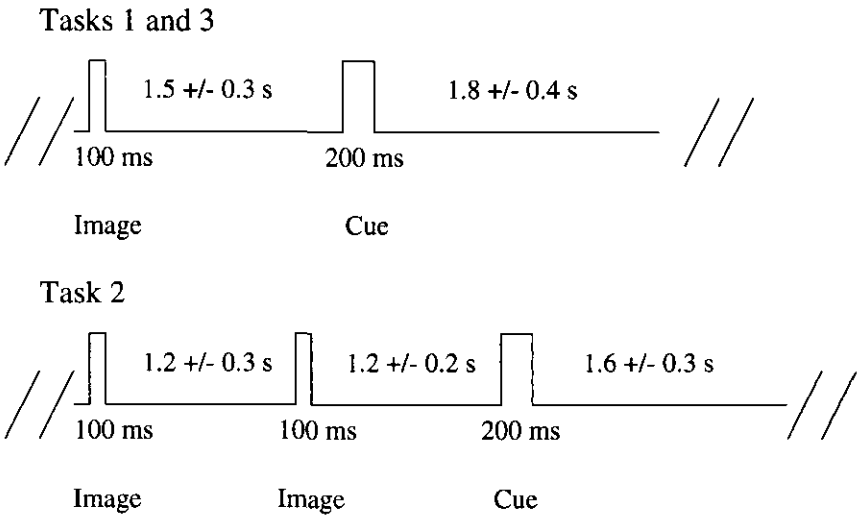

Figure 3.2: Timings

Shown are the two types of cycles used for the three tasks. Presentation periods of both the image stimuli and the visual cue (two vertical bars) were standardised. The cue was displayed for twice as long to differentiate it visually from the images.

expression.

The subjects were required to press a key once in each presentation cycle. Only two keys were used under the index and middle fingers of the right hand. The subjects either confirmed (index finger) or denied (middle finger) the appearance of a specified target image or target condition in the cycle. In each presentation cycle, the key press was explicitly requested by a visual cue appearing after the last visual stimulus. This served to separate the processes following the stimuli from the motor activity preceding the key press.

Grey scale images were chosen to minimise possible interpretation problems linked with colour-processing in posterior fusiform gyrus [7]. All visual stimuli images were presented for 100 ms. This comparatively short period was chosen to prevent saccade scanning of image features through physical eye movement. A typical scanning latency is 250 to 300 ms [137]. The short exposure does not eliminate the persistent retinal image; the effects of this process are not known. The period of 100 ms is about 3 to 4 times longer than the threshold needed for recognition of emotional expression [98].

3.2.1 Subjects

A total of 15 subjects participated overall in these tasks, with 11 completing all three experiments (Table A.1). If necessary, subjects were introduced to the laboratory

environment. They were briefed about the tasks to come and image types were named for each task. Target conditions were pointed out and the subjects were reminded to press a key only after the visual prompt.

3.3 Results

All subjects participated with the appropriate attention and dedication needed for these kinds of experiments. No problems were reported concerning the duration of the image, the use of the keypad, or the clarity of the instructions. Usually, volunteers felt reasonably comfortable within the environment of the shielded room and considered the experiments interesting. Only one subject was noticeably nervous before the first measurement. A truncated test run followed by an extended pause eased the nervousness and/or anxiety. No specific strategies were reported in coping with the tasks, although mouth and eye clues seemed to play a predominant role for FT3.

The accuracy of performance of a given task is here defined in terms of the ratio between the number of correct key presses and the number of cycles (score). All subjects accomplished FT1 with negligibly few errors yielding a score of 0.97 ± 0.01 (cohort mean). The average performance was slightly lower in FT2 and FT3 with scores of 0.93 ± 0.01 and 0.91 ± 0.01 respectively. Failure to reach the maximum score of 1 is due to wrong rather than absent key presses, and is not correlated with a particular images class.

Reaction times, in these experiments, serve as an indicator for overall vigilance and task attendance. They are given as the time elapsing between the visual cue and the button press. All subjects responded homogeneously across all tasks by pressing a key about 330 ms after the visual cue. No particular modulation of the response time as a function of the task duration was noticed.

All runs produced 'clean' data in that the subjects maintained a constant head position. If present, eye blinks followed the appearance of the visual cue. Unless stated otherwise, all results apply to the individuals evoked responses averaged over the two runs of each tasks, band-filtered between 0.8 (0.4 roll-off) and 48 (0.5 roll-off) Hz, and drift corrected between -200 and 0 ms with respect to stimulus onset (see Appendix B, [N-2] and Appendix B, [N-3]). In the case of FT2, the averages for the second image in a pair were calculated without making a distinction between matching and non-matching second images.

3.3.1 Visual inspection: all tasks

Average evoked field patterns for all subjects and across all tasks show that the processing of the image information is widespread. Typically, the stimulus is followed by strong activity in sensors located over the occipital cortex at about 100 ms. Later activity is seen in occipito-temporal (inferior-temporal), temporal, parietal, frontal and somatomotor regions.

Focusing on the posterior regions and early latencies, most salient are the average evoked response patterns over the right occipito-temporal region in the range 120–160 ms with a typical peak value between 135 and 155 ms. Here, in certain channels (varying only slightly across subjects) the responses in FT1 and FT2 to face images are distinguishable from all other responses (Figure 3.3 A). The difference is clear in at least 8 subjects, and is marginal in a further 3 subjects. In one subject the same differential pattern of responses is present but the dominant face specific response is over the left hemisphere.

Within this latency span, the signals' morphologies are complex for all stimulus classes, as suggested by the rotated gradient plots (Figure 3.3 B). Despite this complexity, the same plots show that the bulk of the signal power is confined to a relatively small number of channels over right occipito-temporal regions.

In all subjects widespread evoked activity is observed rostrally with regional peaks in power at latencies as early as 150 ms. In a few subjects, there appears to be a large magnitude response in FT3 at about 150 ms, mainly over the right anterior-temporal region. However, the signals from the anterior brain show a much greater dependence on the precise nature of the task, and the current analysis was not able to establish systematic behaviour across subjects.

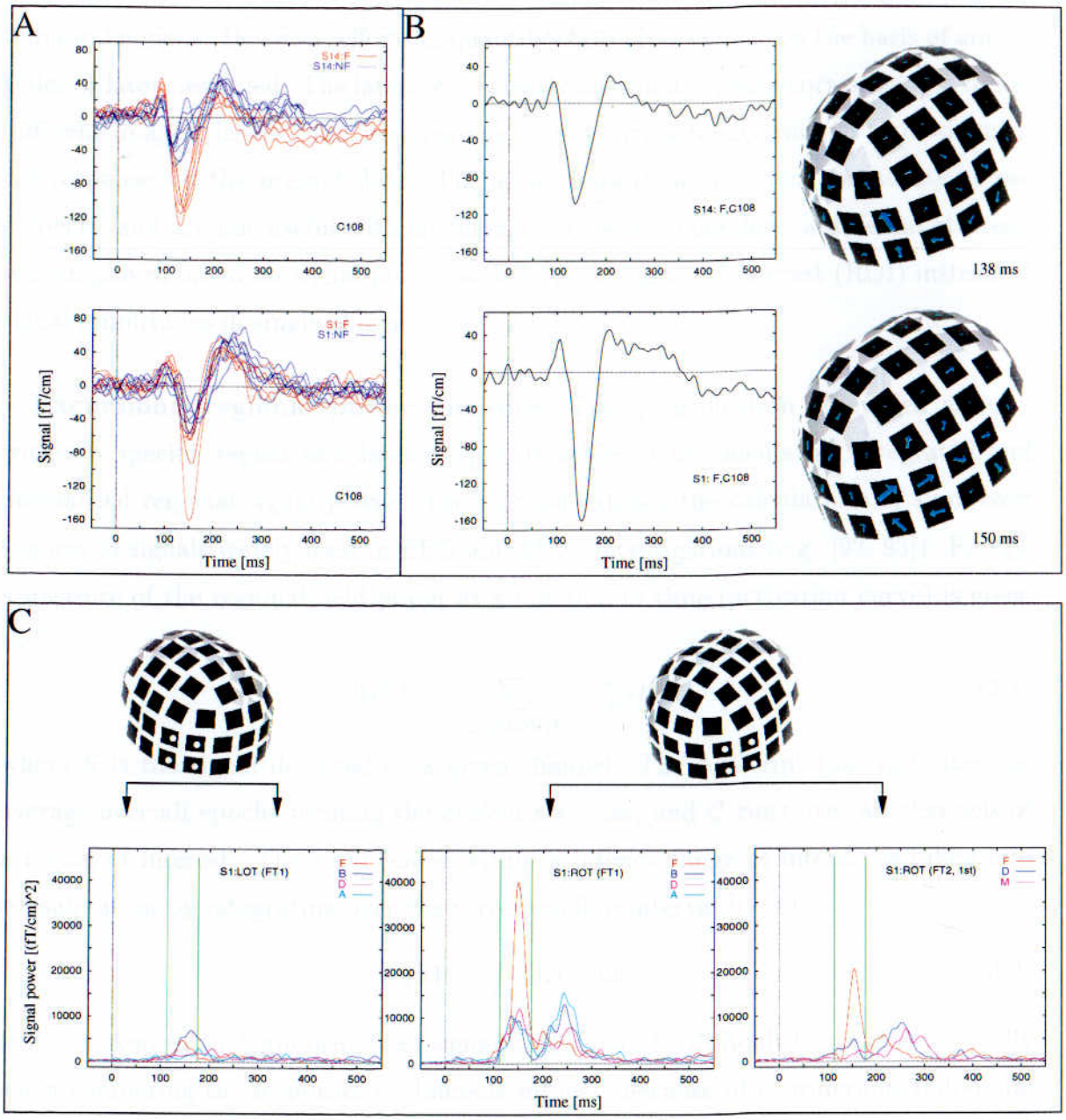

Figure 3.3: Face tasks: evoked responses

A: face (red) versus non-face (blue) responses for two subjects, superimposed for all tasks. B: face responses in FT1 for the same subjects together with corresponding rotated gradient plots at peak latency. C: channel groups used for NIRP calculations: left occipito-temporal LOT, and right occipito-temporal ROT. Examples of activation curves corresponding to these groups are given for one subject for experiments FT1 and the first images in FT2. The keys show the relevant image types. The vertical lines denote the interval of integration between 115 and 175 ms.

3.3.2 Regional power

As outlined above, visual inspection of the data suggests some differences between the face and non-face responses at latencies around 140 ms over mainly right occipito-temporal regions. However, efforts to quantify these observations on the basis of amplitudes or latencies failed. The latencies of clearly identifiable peaks corresponding to the different images classes over these regions do not vary strongly enough to distinguish the responses in the present data. The amplitudes show too much variability across subjects, and are not useful without further provision. Therefore, a different strategy was employed based on signal power pooled over a region of interest (ROI) instead of signal amplitudes in single channels.

▷ **Excursion: regional power measure** The quantification of evoked activity within a specific region and latency span is achieved by calculating integrated and normalised regional signal power. The method extends the calculations of sums over squares of signals widely used in EEG and MEG investigations (e.g. [92, 93]). Firstly, a measure of the regional field power as a function of time (activation curve) is given as:

$$\mathrm{RP}(t) = \sum_{c \in \{\mathrm{group}\}} \left(S^{c}_{av}(t)\right)^2 \tag{3.1}$$

where S is the signal detected by a given channel. The subscript (av) indicates the average over all epochs forming the evoked response, and C runs over all channels of a region of interest. The total power within a latency range of interest is taken into consideration by integrating over the corresponding interval $[t_1, t_2]$

$$\mathrm{IRP} = \int_{t_1}^{t_2} \mathrm{RP}(t)dt \tag{3.2}$$

It is well known that unnormalised signal powers can be difficult to treat statistically when comparing the responses of different subjects because of considerable individual variability. This problem can be partially accounted for by fixing a time range of length $b > 0$ in the pre-stimulus interval, usually chosen as $[-b, 0]$, and introducing a normalised, dimensionless measure of integrated regional power:

$$\mathrm{NIRP} = \frac{\mathrm{IRP}(t_1, t_2)}{\mathrm{IRP}(-b, 0)}. \tag{3.3}$$

Assuming uncorrelated, zero-mean signals across channels for each $t \in [-b, 0]$, the denominator in Definition 3.3 estimates the (integrated) ROI variance. Therefore, NIRP is analogous to the commonly used z-score. The issue concerning the baseline is further discussed in Appendix D together with other technical aspects associated with

this measure.◁

The quantification of signals was achieved by calculating normalised regional powers for a group of 8 channels and a latency range between 115 and 175 ms (Figure 3.3 C), denoted as as ROT for the right occipito-temporal group. This latency span and region[1] were chosen to include the majority of the significant power peaks for all subjects. Additionally, a second group of channels was chosen symmetrically with respect to ROT and with the same interval of integration, and denoted as LOT for the left occipito-temporal group.

These two regions constitute a compromise made to pool the activity measured over occipito-temporal cortex across subjects. An extensive preliminary survey of regions and latency spans was carried out using this methods. The final choice yielded the most consistent results using the same detector sites for all tasks. The groups reflect the main results obtained from the visual inspection, and each group extends over an area of $\approx 70\,cm^2$. The choice does not preclude the existence of some clearly identifiable signal over regions outside these channel groups at similar latency.

Attempts were made to parametrise differential signals over more anterior regions as well as at longer latency. Despite considerable efforts the attempts failed. At early latency, signals powers over the anterior brain are too variable and, essentially, too weak to establish systematic behaviour across subjects. This observation is consistent with a recent study using the same MEG facility [133]. At longer latency ($>200\,ms$), differential responses are seen in some subjects. They are widespread though particularly evident over right temporal regions. However, the variability across subjects is such that the significance of differences between responses at longer latency can only be achieved within a small subgroup (≈ 5) of subjects selectively taken out of the full group. Thus, in what follows, only the groups LOT and ROT are considered.

Analysis-of-variance ANOVA (Appendix B, [N-11]) was used to assess the significance of differences between NIRP values of responses to different stimulus classes. Initially, the main emphasis is on within-task and within-channel group comparisons of NIRP values.

3.3.3 NIRP analysis of separate face tasks

The main observation is a significantly differential activation between responses following face and non-face images over the right occipito-temporal region, in that faces

[1]The baseline for the NIRP calculation was set to -200 to 0 ms, the interval used for drift correction.

evoke greater signal power than all other images. The effect is consistently seen in FT1 and FT2. No such effect is evident over left occipito-temporal regions. The responses in task FT3 are not influenced by the facial expressions according to the NIRP values. In what follows, the results of the statistical calculations are given for each task.

Face Task 1

Face responses are strongest in both the LOT and ROT groups, where significant differences are seen in region ROT (Figure 3.4). The face responses separate from motor bike and animal responses, and weakly separate from dot responses ($HSD_{10\%}$=2.2).

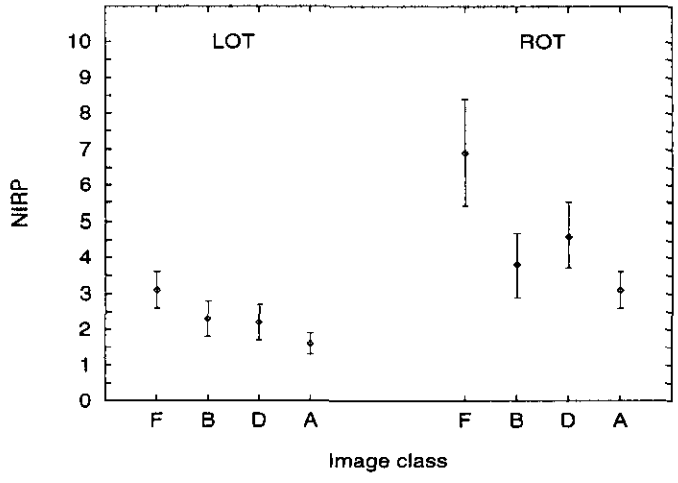

	F	B	D	A		F	B	D	A
	3.1	2.3	2.2	1.6		6.9	3.8	4.6	3.1
F		0.8	0.9	1.5			3.1	2.3	3.8
B			0.1	0.7				0.8	0.7
D				0.6					1.5

Figure 3.4: FT1: NIRP

Upper: graphical representation of the cohort means and standard deviations of NIRP values for the two channel groups LOT and ROT for the image classes of task FT1. Lower: numerical values of the cohort means together with the matrix of moduli of the differences between the mean values corresponding to the image classes. The statistical evaluation of the differences gives $F_{3,52} = 1.5$, $p \leq 0.2$ for LOT and $F_{3,52} = 2.7$, $p \leq 0.05$, $hsd_{0.05} = 2.5$ for ROT.

Face Task 2

The differential activation in group ROT is present for both the first and the second image presentation in a pair (Figure 3.5). In both cases, face responses separate weakly

from dot responses, with ($HSD_{10\%}$=2.0) and ($HSD_{10\%}$=1.0) for first and second images respectively. The NIRP values were evaluated separately for first and second images in a pair, disregarding in the latter case the distinction between matching and non-matching images. The qualitative patterns are unaltered when taking into account this distinction.

In group ROT there are differences in the latencies of the peaks of the power between responses following the first and second presentations face images within a pair. The 2nd face peaks are shifted with respect to the 1st face peaks towards lower latencies in the 9 subjects with clearly identifiable maxima in the activation curves. For these 9 subjects, the mean latencies are 149.3±3.5 ms and 143.0±3.6 ms for 1st and 2nd faces images respectively. The difference of about 6 ms is significant (T_8 = 5.2, p $\leq$ 0.001).

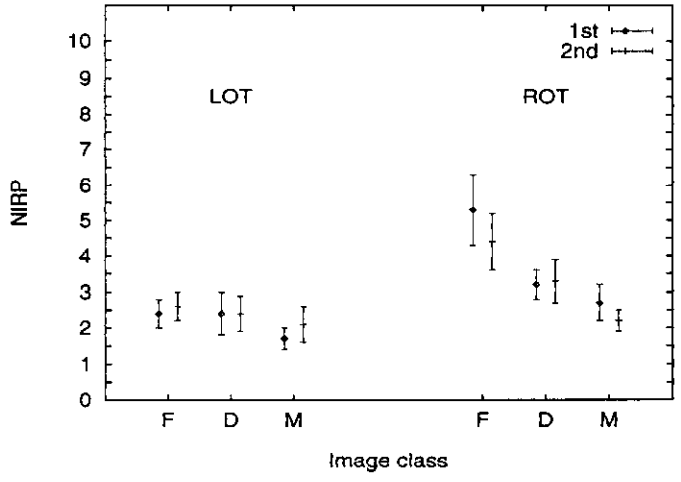

		F	D	M		F	D	M
		2.4	2.4	1.7	1st image	5.3	3.2	2.7
F			0.0	0.7			2.1	2.6
D				0.7				0.5
		2.6	2.4	2.1	2nd image	4.4	3.3	2.2
F			0.2	0.5			1.1	2.2
D				0.3				1.1

Figure 3.5: FT2: NIRP

The NIRP calculation were carried out separately for first and second images. The statistical evaluation of the differences gives: for first images $F_{2,36}$ = 1.1, p $\leq$ 0.4 for LOT and $F_{2,36}$ = 3.6, p $\leq$ 0.05, $hsd_{0.05}$ = 2.3 for ROT; and for second images $F_{2,36}$ = 0.29, p $\leq$ 0.8 for LOT and $F_{2,36}$ = 3.5, p $\leq$ 0.05, $hsd_{0.05}$ = 1.2 for ROT.

Face Task 3

Neutral faces evoke slightly stronger responses than smiling faces in both regions LOT and ROT, but the difference fell well short of statistical significance (Figure 3.6).

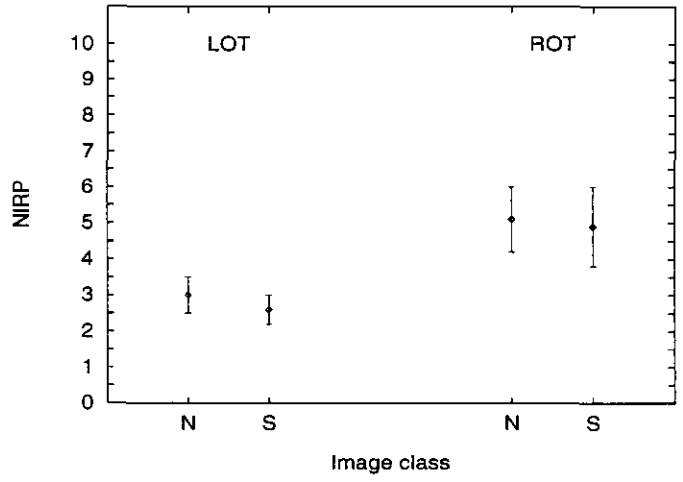

	N	S	N	S
	3.0	2.6	5.1	4.9
N		0.4		0.2

Figure 3.6: FT3: NIRP
The statistical evaluation of the differences gives $F_{1,24} = 0.34$, $p \leq 0.6$ for LOT and $F_{1,24} = 0.027$, $p \leq 0.9$ for ROT.

3.3.4 NIRP analysis comparing LOT and ROT responses

In all tasks, the responses associated with a given stimulus are stronger in group ROT than in LOT according to the NIRP values. However, the differences are only significant in the case of all face stimuli, and the dot and animal images in FT1.

3.3.5 The influence of target conditions on NIRP values

In order to assess the impact of different target conditions on the results obtained for FT1 (targets are dots and faces) and FT3 (targets are neutral and smiling faces), the power analysis was repeated separately for the individual runs in each case. In these calculations, the NIRP values obtained are smaller mainly because of the reduced number of averages. However, the qualitative assessments stated above are exactly the same with respect to the significance or lack of significance between cohort means and the NIRP correlations. This holds true for both tasks.

3.3.6 Comparisons of NIRP values across tasks

So far, consideration has been restricted to comparisons between the responses within a single task. The restriction makes the results less susceptible to artefact and more transparent. However, the consistency of the observations suggests that some inter-task comparisons are meaningful. To facilitate such comparisons, ratios of unnormalised regional power (IRP) were calculated for each subject and image class for the right channel group ROT (Table 3.2) using, in each case, both runs. It can be seen that the ratio of the responses to faces and dots is essentially the same in Tasks 1 and 2, even though the face images are different in the two cases. The ratio of the face response in Task 1 to that in Task 2 is the same as in the ratio of Task 1 to Task 3. There is some evidence that face responses are stronger in the first task than in the second and third according to this analysis.

Comparison	Mean power ratio
FT1 F/FT1 D	1.7±0.3
FT2 F 1st/FT2 D 1st	1.6±0.2
FT1 F/FT2 1st	1.4±0.2
FT1 F/FT3 N	1.5±0.2
FT1 F/FT3 S	1.5±0.3

Table 3.2: ROT: inter-task comparisons

3.3.7 Reproducibility of NIRP values

In four subjects, FT1 was repeated several times both on the same day and over several months with exactly the same image set. For one subject the luminosity was also varied systematically over a ±30% range. These additional experiments confirmed that the data were consistent and insensitive to the parameter levels (for all reasonable variations in those parameters) to within the random noise.

3.3.8 Source localisation using task FT1 data

For each data set in task FT1, the optimum (best fit) equivalent dipole was sought within the latency span between 115 and 175 ms using the procedure[2] described in Appendix C. The analysis was restricted to FT1 because here the face responses are strongest.

[2]For the calculations, two channel groups were chosen each covering the two hemispheres, excluding the anterior-frontal, vertex, and medial occipital channels.

For the different image classes, the criteria set for an acceptable fit were met for only 8 (face), 5 (motor bike, dots), and 3 (animals) data sets in the case of the signals over the right hemisphere (Table 3.3). In the case of the subject with a dominant left hemispherical face response, a reliable dipole was found for the subject's face response over the left side. Acceptable fits show a goodness-of-fit (gof) of about 0.8 with an error bound of about 4 mm. In two instances, a very good fit is suggested with a gof >0.95 and a confidence radius <2 mm. The rejected fits failed by a large margin to meet the criteria despite an adequate signal to noise ratio. The 5 motor bike, the 5 dot, and 5 out of the 8 face dipoles refer to the same 5 subjects.

Category	#	Latency [ms]	Strength [nAm]
F	8	142 ± 4	32 ± 5
F (left)	1	146	37
B	5	142 ± 7	24 ± 8
D	5	149 ± 4	21 ± 4
A	3	151 ± 6	25 ± 7

Table 3.3: Mean source parameters

The mean source parameters are for the equivalent dipoles corresponding to the signals over the right hemisphere. The one dipole obtained for the subject with a dominant left hemispherical face response has been added for comparison. All values refer to FT1, and have been rounded to the nearest integer value.

For these five subjects, there are no significant difference between the source location[3] and the latency of best fit for the different image classes. The face dipoles are significantly stronger than dot dipoles. The anatomical location of face dipoles in most cases is approximately described as the inferior temporal lobe, as suggested by the superposition of the dipole location on the individual's MRI scan (Figure 3.7).

[3]In [148], a weakly significant result suggested that face dipoles were located anterior to motor bikes. That result did not include the use of an optimised sphere fitted to an MRI scan. With this refinement, the significance of the difference of positions disappears.

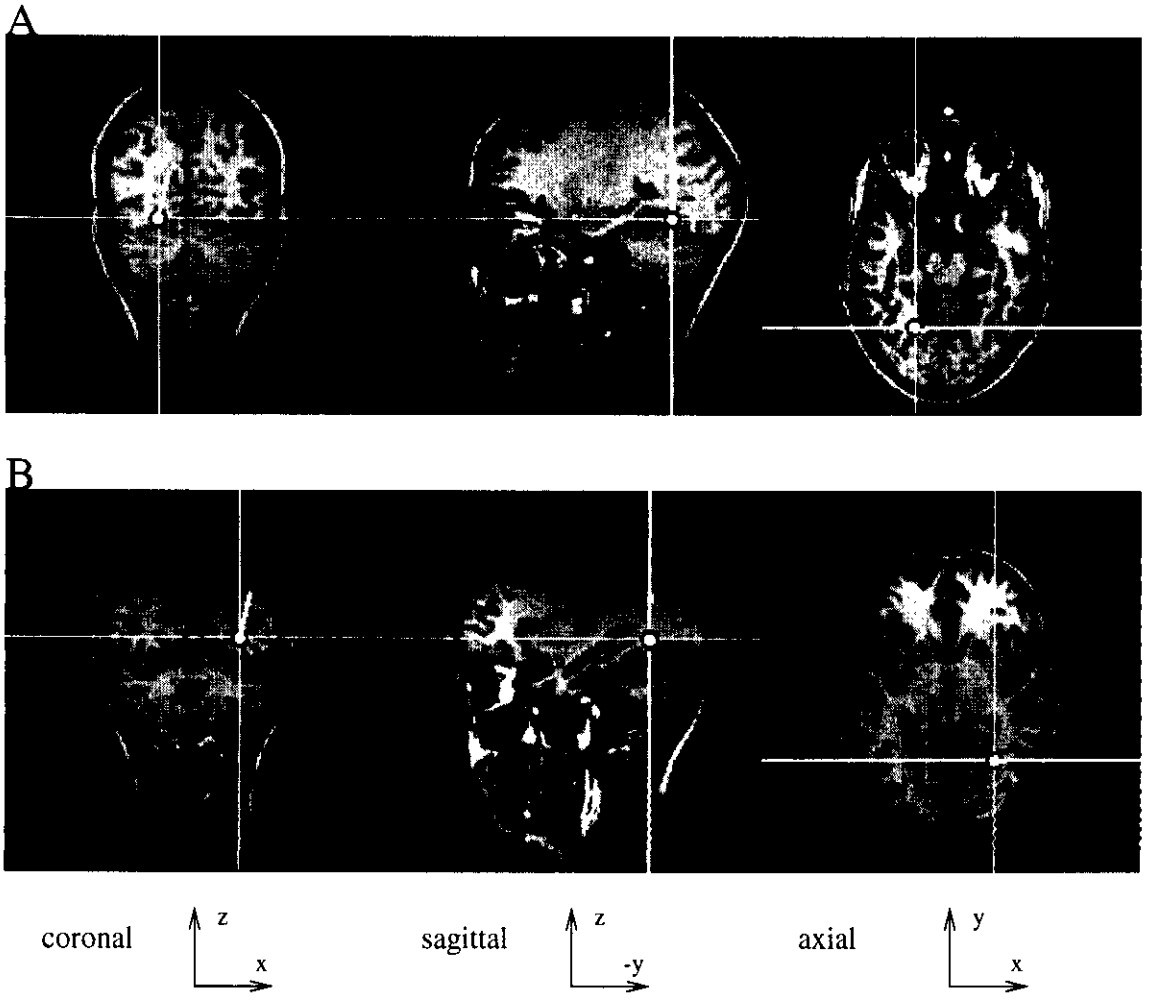

Figure 3.7: MRI Projection: face dipoles

Shown are source estimates corresponding to face dipoles. A: the subject (S5) with the dominant face response over the left hemisphere, and B: a subject (S10) with the dominant face response over the right hemisphere. The two sources at $x = -23, y = -36, z = 39$, and $x = 36, y = -28, z = 48$ for A and B respectively (in PAN co-ordinates; units in mm).

3.3.9 Correlation based analysis

The above analysis was taken further by considering rank correlations between pairs of NIRP values across subjects (Table 3.4, see Appendix B, [N-12]). The correlation is a measure of the consistency of the mapping of neural source systems onto signals. A high correlation implies that there are similar mechanisms operating across the subjects. A change in correlation implies a change in the source system linkage and therefore a change in the characteristics of the underlying generators. When this occurs across tasks, a modification of mechanisms by the varied conditions is suggested. The patterns which emerges from the analysis are complex. Currently, no more information is extracted than stating that the analysis suggests an influence of the task on the underlying mechanisms.

		LOT			ROT		
FT1		B	D	A	B	D	A
	F	---	0.61	0.74	0.54	---	---
	B		0.63	0.67		0.74	0.60
	D			0.66			0.80
FT2 1st			D	M		D	M
	F		---	---		0.68	---
	D			---			---
FT2 2nd			D	M		D	M
	F		0.70	0.62		0.68	0.57
	D			0.77			0.82
FT3				S			S
	N			0.81			0.88

Table 3.4: NIRP correlations, all tasks

The table shows the rank correlations coefficients (ϱ) corresponding to pairs of response in FT1 to FT3. Each value specifies a significant positive correlation of at least $p < 0.05$ significance. Each entry is based on n = 14 (FT1) or 13 (FT2, FT3) pairs of NIRP values corresponding to the number of subjects participating in the tasks.

3.4 Discussion

The main observation of the present study is the face-specific processing at early latencies in channels over the right occipito-temporal region. The specificity of responses following face presentation is identified as an increase in signal power compared to the responses following other stimuli. The increase in power is identified consistently across subjects by an analysis covering a time span of 60 ms centred around 145 ms. This latency will be used to label the face responses disregarding the variation in the individual peak latencies, which have a typical delay of ≈50 ms from the first major occipital component.

The face-specific processing is reasonably consistent across tasks FT1 and FT2 including the sub-tasks of the former and the image sub-categorisation of the latter. This suggests that the response is, to a first approximation, automatic, i.e. it is unlikely to be under conscious control. However, some task dependence is suggested by the observations that a) the strength of response varies appreciably between the two tasks, b) there is a latency shift between 1st and 2nd-faces in the majority of subjects in FT2, and c) the correlations of individual powers between face and non-face responses are influenced by the task. The shift in latency in FT2 is consistent with previous face studies (see [73]).

In the case of FT3, the responses following neutral and smiling faces at 145 ms are indistinguishable with the methods used, as suggested by the same regional powers and a high correlation between the two response types. The signals measured in this task are compatible in shape and latency with the face responses in FT1. The relative strengths of the responses in the two tasks are independent of the facial expression and are comparable to the relationship between FT1 and FT2 (1st image).

It is not known why the responses to face images are greater in FT1 than in FT2 or FT3, even though the latter tasks are more demanding (as judged by the scores) and arguably require the subject to scrutinise the images more closely. The difference may be because of additional activity that produces fields cancelling partially those generated in FT1 or be the result of inhibition of some part of the FT1 activity.

In general, the latency of 145 ms is broadly consistent but somewhat earlier than the face-specific activity identified from other experiments. It is not known what causes the discrepancy, which could relate to different sensitivity characteristics of other techniques, or to the tasks parameters used here, specifically the brief exposure to the face stimuli which might involve a different range of processes.

The face-specific processing is predominantly seen over the right hemisphere. Indeed, the measure used here provides no statistically significant evidence for left hemisphere face-specific involvement across the subject group as a whole. The right hemisphere dominance of the face specificity effect is consistent with previous lesion and electrode studies. However, both the normalised powers and inspection of the evoked responses does provide clear indications of activity related to face and other objects at similar latencies over the left occipito-temporal region, although less in signal power for all image classes. Additionally, the pattern of correlations varies with the task condition suggesting a differential left hemispherical involvement in the processing besides a suggested right hemispheric specialisation for complex visual stimuli.

The dipole sources identified for the face responses in FT1 are consistent with activity in the ventral occipito-temporal cortex and with sources oriented along the ventral-dorsal axis in most subjects. Both location and orientation are consistent with fusiform gyrus activation. However, the modeling issue is complicated by the probable coexistence of other sources within neighbouring cortical regions, and the individual variability and structural complexity of the brain geometry. This is indicated by the relatively modest success in fitting the data achieved by single equivalent dipole fits despite acceptable signal-to-noise ratios.

The absence of significant differences between the source locations corresponding to faces and other objects is broadly consistent with a previous EEG study on face processing [19]. It is unclear whether the sources here reflect segregated cortical areas, as seen in a recent depth electrode study suggesting that the fusiform gyrus supports areas with a gradual change in dominant function [7]. Most probably, the regional power method opens a window into the general processing of complex objects in occipito-temporal cortex, where unspecific mechanisms co-exist with processes specific to some degree to faces and possibly other objects as well. Tentatively, in this data, the dot pattern might be a candidate for such additional specificity. With regard to signal power, the dot responses are closest to faces on average, and strongest in 4 out of 6 subjects in whom faces do not elicit the strongest responses in task FT1. The underlying mechanism seems to be independent of the richness of spatial features of an image, otherwise one might expect the motor-bikes, which are richer in spatial features[4] than dots, to be closest to faces.

The activation induced by non-face objects within the same latency span over same the areas seen in the present data is consistent with previous EEG, MEG, and

[4]See Figure 2.8.

depth electrode studies [6, 14, 133]. The most sparse explanation for the present data is that the activity at 145ms is a form of spatial encoding that depends on the nature of the image and partially at least on the visual demands of the task (a similar conclusion was reached recently [14]). The responses to faces are specific in that these images engender greater responses than other images. This might reflect a greater value of coherent cortical activity, or a different distribution of activity.

The face-specific responses observed here could relate to the face-specific activity representing the second structural encoding stage of the model of Bruce and Young (Figure 3.1), acting as preparatory stages for the expression analysis or the face recognition units. The latter are presumably addressed indirectly in FT2. This assumption might explain the slight variations of the pattern of face specificity observed in the different tasks, without introducing dramatic changes.

Conclusion

It is suggested that a careful analysis of evoked signal power can efficiently probe responses associated with the processing of face and other objects. The results support the notion of face specificity in terms of increased coherent activity manifest as an increase in signal power over right occipito-temporal regions of the human brain at early latency. The early face specificity is approximately independent of the nature of the task, and indicates a right hemispherical preponderance of face processing networks.

Chapter 4

Face processing – a note on the case of autism

This chapter reports on a study of face processing in autistic subjects using MEG[1]. Seven autistic individuals were studied using the face processing tasks FT1 to FT3, with a particular interest on the regions and early latencies where face-specific activity had been identified previously in the normal subject group.

In what follows, a brief introduction to autism is given, followed by some remarks about behavioural face processing studies into that disorder. The chapter continues with a presentation of the results and a discussion.

4.1 Background on autism

4.1.1 General

The first acknowledged scientific account[2] of the disorder dates back to the year 1943. At that time, Dr. Kanner, a psychiatrist at Johns Hopkins University, wrote the first publication using the term 'autism' to describe a group of children who had severe social, communication, and behavioural problems [79]. The term derives from Greek *autos = self* and the suffix *ism = indicating a state or condition*, and carries the connotation of being absorbed in oneself. The syndrome is rare, affecting approximately four children in 10000 and is about three times more likely to affect males than females.

Since the original account, the disorder has spurred an ever growing research

[1]To the author's knowledge, this is first study of its kind.

[2]Unless referenced explicitly, the remarks in this section have been assembled from [11, 130]. A review of EEG studies in autism unrelated to the present study can be found in [27, Chapter 16].

interest into autism in mainly the behavioural and medical sciences. Over the decades, this has led to a degree of consensus on a very complex disorder succinctly characterised as:

> ... autism is a neurodevelopmental disorder, involving basic cognitive deficits, with genetic factors strongly predominant in etiology[3] ... [132]

To date, there is no physiological test to determine whether a person has autism, and the diagnosis of autism is based on behavioural characteristics. The diagnosis requires expert knowledge, and is only made if some behavioural features in each of three groups of symptoms co-occur before the age of 3 years. It is the number, severity and persistence of these features, given the age of the child, which may lead an expert, usually a psychologist or psychiatrist, to describe a child as autistic. The features are categorised into three groups[4]:

Difficulties in social interaction Such as apparent unawareness of other people's feelings, or lack of understanding of the social conventions underlying friendship.

Difficulties with language and non-verbal communication Such as telegraphic speech, or unusual eye contact during conversation.

Restricted range of activities and interests Such as preoccupation with touching a particular object, or unusual insistence on preserving the sameness of the environment, e.g. by keeping an object always in the same place.

Despite a consistent catalogue of diagnostic criteria, there is no single adjective which could be used to describe every type of person with autism. Each autistic individual has his or her own signature of needs, skills, and medical conditions. Many autistic individuals are intellectually impaired, some have exceptional skills, termed islets of ability, in one particular area such as music. Some develop epileptic seizures. In most cases autism is a life-long condition, where the pattern of difficulties may change or become less in adult life.

Autism is a complex and severe disorder of development. The understanding of its nature has made advances. However, much has yet to be resolved:

[3]developmental = affecting the development; etiology = the study of the causes of a disease or disorder; in similar definitions, 'neuro' + 'genetic factors' are alternatively specified as 'biological basis' [59].

[4]a detailed exposition of the diagnostic criteria can be found in [8, 164].

> ... it is also evident that the basic pathophysiology of autism remains unclear, the mode of inheritance is not known, and our ability to provide effective treatment is distinctly limited [132].

4.1.2 Face processing studies

The issue of face processing capacities in autism has been addressed systematically over the last two decades in behavioural studies. Intuitively, it has been suspected that a relationship exists between those capacities and the deficits that affect the autistics' social relations [34]. The following is a short summary[5] of the linkage:

It is generally agreed that autistic individuals are impaired on certain aspects of face perception. However, it is still unclear how specific this impairment is. Whereas, some studies have reported on a selective impairment in the recognition and production of facial expressions [63, 96, 112], others have found a more general deficit in perceptual abilities [33]. Other aspects of face perception have also been reported to be affected in autistic individuals, such as the memory for faces [34], specifically in the context of identifying recently seen, previously unfamiliar, faces [20]. Furthermore, autistics seem to pay relatively more attention to the lower part of the face [90], and a good performance has been found on tasks with photographs of faces turned up-side down [64, 90, 153].

The latter findings have led to the suggestion that autistic individuals might make use of abnormal face processing strategies, in that they might perceive faces in terms of their component properties alone (i.e. piecemeal processing), rather than viewing the face as a whole (i.e. holistic processing; [103]). This could account for peculiarities in perception of both facial expression and identity. So far, no comprehensive theoretical framework exists to cover the observations, the detailed nature of which often depends on the chronological age, the severity of the syndrome, and the matching condition, i.e. the choice of what is considered as 'normal' for comparison [33].

The present study has been motivated by previous work on face processing in autism, but should be seen as an independent approach, addressing the signal features of evoked responses at early latency. MEG experiments have their own requirements, often vastly different from behavioural studies. In terms of behavioural studies, the subject groups are not matched here. Nevertheless, the normal subjects studied in Chapter 3 will be referred to as the control group.

[5]The account is based on a paper from the Proceedings of the 5th Conference on autism, Spain 1997: Face processing strategies in autistic individuals, J. Pieter.

4.2 The experiments

The face processing tasks FT1, FT2, and FT3 were used as discussed in Chapter 3. The first task FT1 requires only the identification of an object as a face or non-face, and should be neutral with respect to possible impairments in face processing. FT2 relates to a possible impairment in the recognition of recently seen, but previously unknown faces, and FT3 relates to a possible impairment in the recognition of facial expression. Implicitly, if selective impairments are present in these autistic subjects, tasks FT2 and FT3 should be more difficult to cope with than FT1.

In order to preclude the use of unusual face processing strategies, as far as this can be controlled by the parameters of the experiment, a brief presentation time has been chosen making serial scanning of the image virtually impossible. The use of boys' faces with fewer prominent facial features than adult faces in FT2 and FT3 serves the same purpose in that it encourages subjects to use the face as a whole rather than a particular part of it in coping with the tasks.

4.2.1 Subjects

The subjects were seven high-functioning adult autistic individuals of British nationality. The profiles of the autistic subjects are given in Appendix A.

4.3 Results

All autistic subjects participated with reasonable attention and dedication. However, in contrast to the smooth experimentation seen in normal subjects, a variety of problems occurred in the case of this subject group. The obstacles were never insurmountable, but reruns of one or more tasks were required in some cases[6]. Once initial difficulties had been overcome, the experiments were carried out in a relaxed atmosphere where even some enjoyment was perceptible. No session had to terminated prematurely. In one case, the wish to continue with the experiments without breaks exceeded the zeal of the investigators.

The autistic subjects accomplished both FT1 and FT2 with few errors, yielding scores of 0.95 ± 0.03 and 0.90 ± 0.02 respectively, insignificantly different from the normal

[6]It is understood that all results refer to the 'stable' runs obtained for each autistic subject avoiding problems due to the first few epochs during which task confusion was fairly common. In the stable runs, the autistic subjects maintained constant head positions and avoided eye blinks. The averaging, filtering, and drift correction were the same as for the analysis of normal subjects' data.

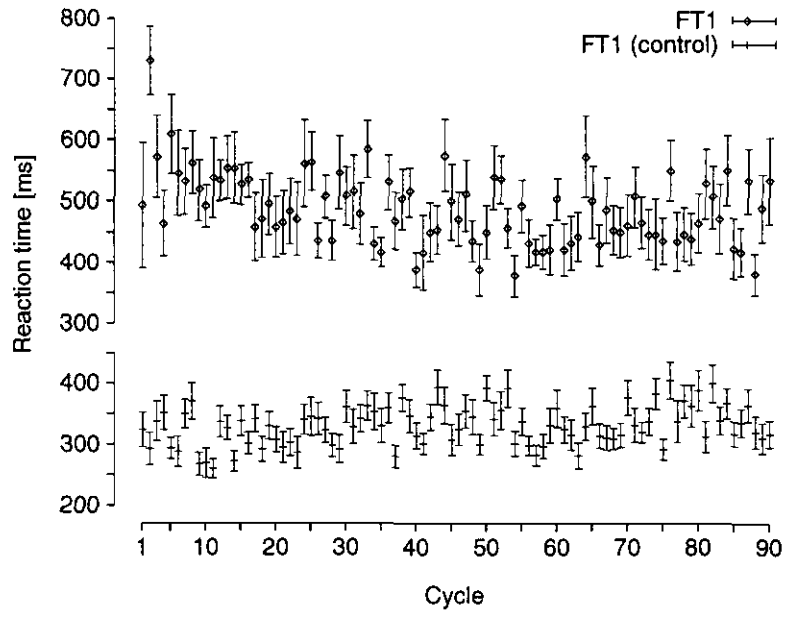

Figure 4.1: Reaction times versus task cycle

Each point is the mean and standard deviation for the relevant subject group. The graphs demonstrate the near constancy of reaction time as a function of the cycle number for the autistic subjects in FT1 (FT2 and FT3 similar). The data of the control group is shown for comparison. Normal subjects show a faster response.

group. The incorrect key presses did not correlate with the image class in either task. In FT3, however, significantly more errors were made (0.81 ± 0.03). It is noted that a neutral expression was more often mistaken for a smiling expression than vice-versa, independent of the target condition.

The profile of reaction times is very similar to the control group, and the qualitative remarks stated earlier apply here as well. However, the response times are consistently slower across all tasks compared with the control group (Figure 4.1).

4.3.1 Visual inspection: all tasks

From the earliest stages at which signals are visible up to a latency of about 200 ms, many of the comments made in the case of normal subjects hold true here as well. The stimulus is followed by strong activity in detectors over the occipital cortex at about 100 ms spreading to sites over the occipito-temporal, temporal, parietal, and somatomotor regions at later latency.

At latencies around 145 ms, evoked responses, clearly distinguished from noise, are visible in the signals of all autistic subjects over the right occipito-temporal regions (Figure 4.2 A). The consistency of signals is high across tasks and image classes within a subject, but varied across subjects. The inter-subject variability seems to be of the

same order as is observed in the control group. Indeed, the local signal waveforms can be matched between chosen pairs of autistic and normal subjects within the same channel (Figure 4.2 B). The morphology of signals around 145 ms, as indicated by rotated gradient plots, is about the same as in most normal subjects (typically similar to that of S1 in Figure 3.3 A, lower plot).

In summary, there is a considerable similarity between the signals of the autistic and control subjects with one important exception: for these autistic subjects there is no clear evidence for the differential effect between signal amplitudes following face and non-face stimuli that is readily identifiable in the data of most normal subjects.

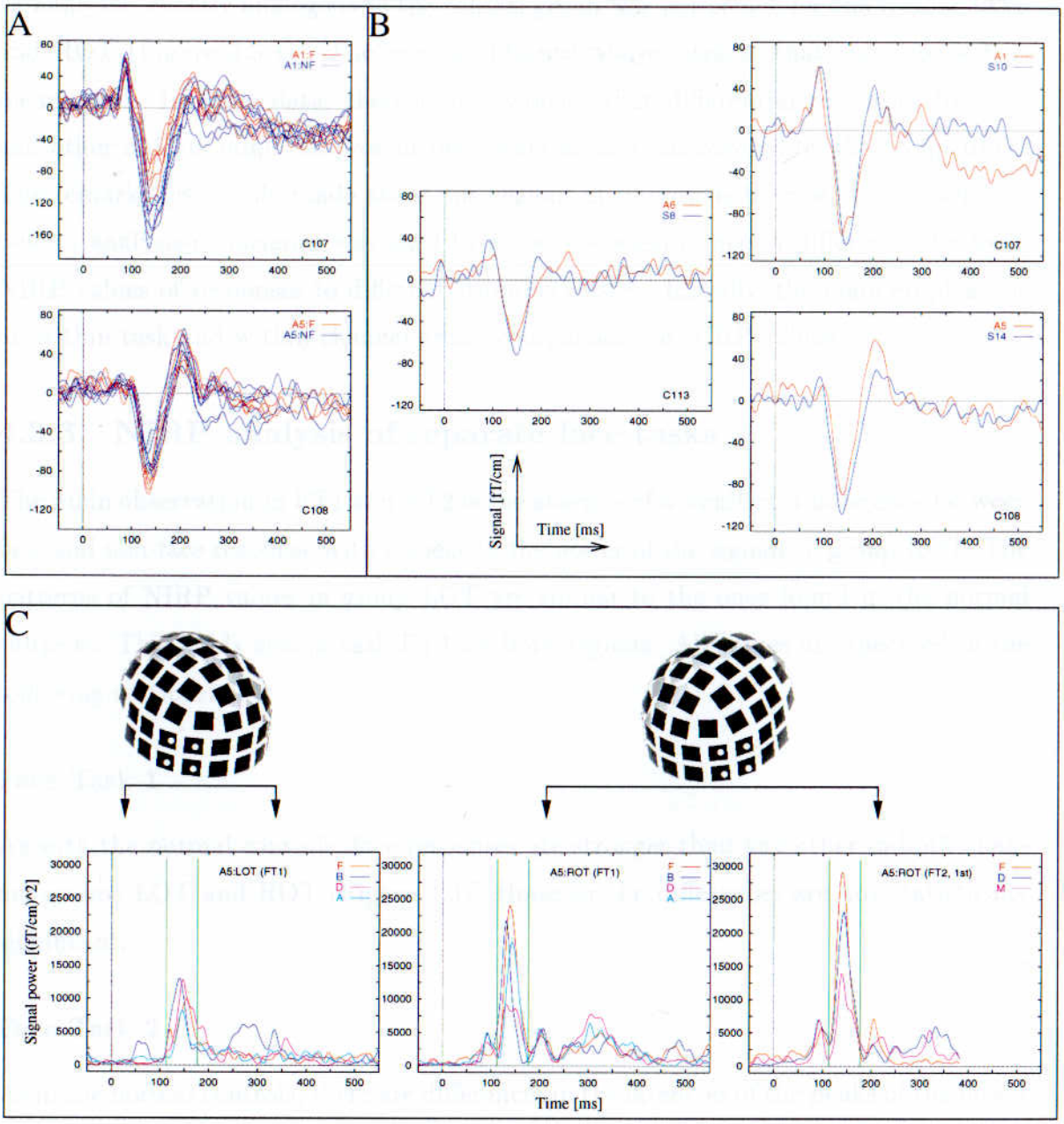

Figure 4.2: Face tasks: evoked responses (autistic subjects)

A: face (red) versus non-face (blue) responses for two autistic subjects, superimposed for all tasks. B: evoked responses from three autistic subjects shown together with signals from three control subjects matched for visual similarity of signals at latencies around 145 ms over the right occipito-temporal region. For each pair of individuals, the data applies to the same channel (denoted by C) in group ROT. The similarity often extends to much higher latencies. C: channel groups LOT and ROT. An example of the summed power is given for A5 and tasks FT1 and FT2. The integration range used in the NIRP calculations is denoted by the two vertical lines.

4.3.2 Regional power

In order to quantify the power content of signals within the latency span of interest, an analysis[7] exactly analogous to the control group was performed for the regions LOT and ROT (Figure 3.3 C). The results obtained above suggest that the approach is meaningful. In these data, there is no evidence that differential responses to faces and other objects might be present over other areas than covered by the group ROT. The remarks previously made about the regions of interest hold true here as well. As before, analysis-of-variance was used to assess the significance of differences between NIRP values of responses to different stimulus classes. Initially, the main emphasis is on within-task and within-channel group comparisons of NIRP values.

4.3.3 NIRP analysis of separate face tasks

The main observation in FT1 and FT2 is the absence of a significant difference between face and non-face response with respect to the power of the signals in group ROT. The patterns of NIRP values in group LOT are similar to the ones found in the normal subjects. This holds also in task FT3 for both regions. All values are specified in the following sections.

Face Task 1

As with the normal controls, face responses are stronger than any other in both channel groups LOT and ROT (Figure 4.3). However the differences are not statistically significant.

Face Task 2

As in the normal controls, there are differences in the latencies of the peaks of the power curves in group ROT between responses following the first and second presentations of a face image within a pair. The 2nd face peaks are shifted with respect to the 1st face peaks towards lower latencies in the 5 autistic subjects with clearly identifiable maxima in the activation curves. Restricted to these 5 subjects, mean latencies are 149.4±5.5 ms and 143.2±5.2 ms for 1st and 2nd faces images respectively. The difference of about 6 ms is significant ($T_4 = 5.6$, $p \leq 0.01$). These mean values almost exactly match the ones obtained in the control group.

[7] See also Appendix D.

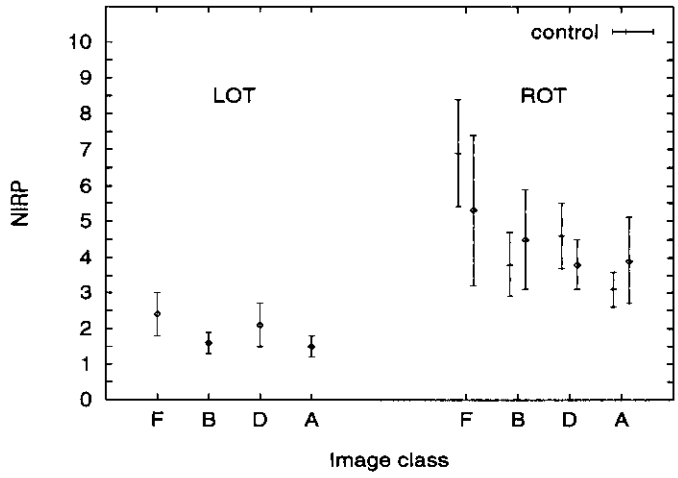

	F	B	D	A		F	B	D	A
	2.4	1.6	2.1	1.5		5.3	4.5	3.8	3.9
F		0.8	0.3	0.9			0.8	1.5	1.4
B			0.5	0.1				0.7	0.6
D				0.6					0.1

Figure 4.3: FT1: NIRP (autistic subjects)
Upper: graphical representation of the cohort means and standard deviations of NIRP values for the two channel groups LOT and ROT for the image classes of task FT1. The values for the control subjects have been added for comparison in ROT (see Figure 3.4). Lower: numerical values of the cohort means together with the matrix of moduli of the differences between the mean values corresponding to the image classes. The statistical evaluation of the differences gives $F_{3,24} = 0.89$, $p \leq 0.5$ for LOT and $F_{3,24} = 0.24$, $p \leq 0.9$ for ROT.

The NIRP values shown in Figure 4.4 were evaluated separately for first and second images in a pair, disregarding, in the latter case, the distinction between matching and non-matching images. There are no significant differences. The qualitative patterns are unaltered when taking into account this distinction.

Face Task 3

As in normal controls, identification of emotional expression exerts no significant influence on the signal power. Neutral faces evoke slightly stronger responses than smiling faces in both regions LOT and ROT (Figure 4.5).

4.3.4 NIRP analysis comparing LOT and ROT responses

In all tasks, the responses associated with a given stimulus are stronger in group ROT than in LOT according to the NIRP values. However, the differences are only significant

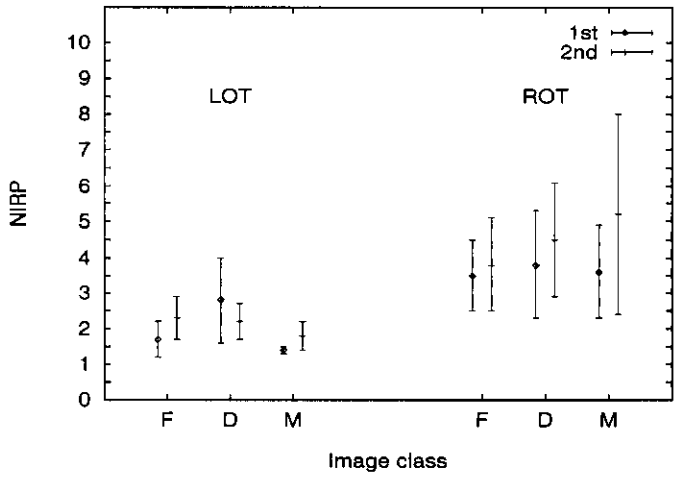

	F	D	M		F	D	M
	1.7	2.8	1.4	1st image	3.5	3.8	3.6
F		1.1	0.3			0.3	0.1
D			1.4				0.2
	2.3	2.2	1.8	2nd image	3.8	4.5	5.2
F		0.1	0.5			0.7	1.4
D			0.4				0.7

Figure 4.4: FT2: NIRP (autistic subjects)
The NIRP calculations were carried out separately for first and second images. The statistical evaluation of the differences gives: for first images $F_{2,18} = 1.1$, $p \leq 0.4$ for LOT and $F_{2,18} = 0.017$, $p \leq 1.0$ for ROT; and for second images $F_{2,18} = 0.28$, $p \leq 0.8$ for LOT and $F_{2,18} = 0.12$, $p \leq 0.9$ for ROT.

in the case of motor bike and animal images in FT1.

4.3.5 The influence of target conditions on NIRP values

As in the normals, the analysis according to target condition (e.g. dot patterns or faces in FT1) did not yield any quantitatively different results for both tasks FT1 and FT3.

4.3.6 Comparisons of NIRP values across tasks

The inter-task comparisons show a consistency similar to normal subjects (Table 4.1). There is some evidence that face responses are stronger in the first task than in the third according to the individual's ratio of unnormalised power (IRP).

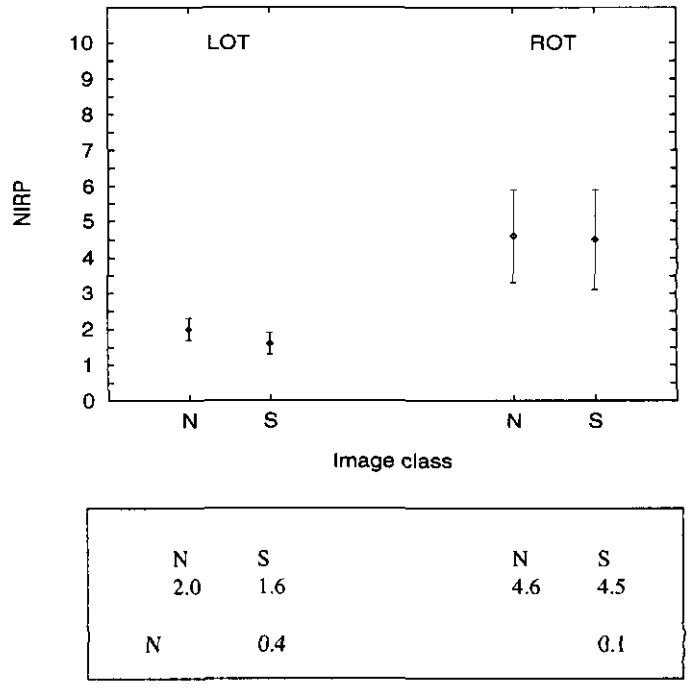

Figure 4.5: FT3: NIRP (autistic subjects)
The statistical evaluation of the differences gives $F_{1,12} = 1.0$, $p \leq 0.4$ for LOT and $F_{1,12} = 0.0$, $p \leq 1.0$ for ROT.

Comparison	Mean power ratio
FT1 F/FT1 D	1.1±0.2
FT2 F 1st/FT2 D 1st	1.0±0.1
FT1 F/FT2 1st	1.1±0.2
FT1 F/FT3 N	1.3±0.1
FT1 F/FT3 S	1.2±0.2

Table 4.1: ROT: inter-task comparisons (autistic subjects)

4.3.7 Reproducibility of NIRP values

This issue was not systematically pursued in the case of the autistic subjects.

4.3.8 Source localisation using task FT1 data

As with the normal control group, source localisation based on equivalent current dipoles complemented the power analysis. The calculations were carried out according to the scheme for the normal subjects, no MRI images were available. Again, only a relatively low number of good fit sources emerged, with face responses being most easily modelled. The proportion of rejected dipoles are similar to the normal group making proper statistical analysis impossible due to the low number of autistic subjects measured. Within these limitations, the results do not suggest differences in location

between the dipole sources corresponding to responses following face and other object images.

4.3.9 Correlation based analysis

In order to complete the analysis, NIRP rank correlations were calculated between the pairs of images of a given task for regions LOT and ROT (Table 4.2). In general, there is a lower number of significant correlations compared with the control group. The patterns are modulated by the task or sub-task. As with the normals, the inter-subject variability is conserved in FT3 and group ROT.

		LOT			ROT		
FT1		B	D	A	B	D	A
	F	---	---	---	---	---	---
	B		0.89	---		---	1.0
	D			---			---
FT2 1st			D	M		D	M
	F		0.86	---		1.0	0.89
	D			---			0.89
FT2 2nd			D	M		D	M
	F		---	---		0.94	0.85
	D			---			---
FT3				S			S
	N			---			1.0

Table 4.2: NIRP correlations, all tasks (autistic subjects)

The table shows the rank correlations coefficients (ϱ) corresponding to pairs of response in FT1 to FT3. Each value specifies a significant positive correlation of at least $p < 0.05$ significance. Each entry is based on n = 7 pairs of NIRP values corresponding to the number of autistic subjects participating in the tasks.

4.4 Discussion

It is worth reiterating that 7 high-functioning autistic subjects were flown from the United Kingdom to Finland, and were subsequently administered 3 tasks designed to study the neural mechanisms associated with the processing of images of faces and other objects. All autistic individuals managed well within an environment atypical in terms of clinical studies. The occurrence of no more than moderate problems did not jeopardise significantly the experimental flow. This is a remarkable observation given that all 7 autistic subjects had no prior experience of MEG, in contrast to the majority of control subjects.

All seven autistic subjects performed as well as the normal group in tasks FT1 and FT2 with no correlation between wrong key presses and image classes. The task performance was below normal but well above chance level in FT3. This observation is broadly consistent with previous studies which have suggested a selective impairment in the recognition of facial expressions (see section 4.1.2 for references). The profile of the cued reaction times is similar to the normal group but is shifted towards higher values.

The main observation concerning the MEG readings for this group is the absence of evidence for a differential effect in signal power between the responses following faces and other object over right occipito-temporal regions at latencies around 145 ms. The effect is subtle. In general, the responses to all stimuli are comparable in waveform, latency, and amplitude to the control group. All NIRP values are broadly comparable across the two groups of subjects, with similar mean values for the same task and stimulus for the two cohorts. The comparison with the normal data suggest that the absence of a differential effect is due to a reduced signal power of the face responses in this group of subjects.

All remarks previously made about the signals' near-independence of the task conditions hold true for this group as well. The relative differences between face response in the various tasks are less pronounced but qualitatively the same as in the control. Again, the face responses in FT3 are unaffected by the facial expression.

As with the normal group, both the normalised powers and inspection of the evoked responses provide clear indications of activity related to face and other objects at similar latencies over the left occipito-temporal region. Exactly as before, the signal power is less over the left than over the right for all image classes in all tasks. However, the differences for face responses are not significant, most probably because of the

assumed reduction in power over the right hemisphere.

The pattern of correlations varies with the task condition for both groups LOT and ROT, although there are fewer correlating pairs of NIRP values than in the control group. This may be linked to the relatively low number of subjects in this group, making the significance of pair correlations volatile. It is noted that, as in normals, all significant correlations are positive.

The small number of dipole locations obtained and the nonavailability of MRI scans precluded interpretations other than to reiterate that the results are broadly consistent with the normal group, and do not contradict the NIRP results.

It is unclear what causes, in this group of individuals, the reduction, or absence of the differential effect in signal power between face and non-face responses, which has consistently been identified in the control group. If this means a (partial) lack of face specificity for which there are supporting observations in normal subjects, then the reduced coherent neural activity might signal a reduction in but not an abolishment of the use of pathways leading to the processing of features specifically associated with faces. These might be not of preeminent importance for individuals who are self-absorbed, and for whom the face, or the individual represented by the face receives an object-centred status [115]. In this sense, the present results might be compatible with autistic individuals solving face tasks using different strategies akin to those used for objects other than faces as suggested by behavioural investigation. A lack of usage of face-specific attributes might feed through into higher order face processing deficits.

Conclusion

To date, only a weak conclusion can be drawn: the results suggest that the magnetoencephalographic approach is potentially useful in studying some neurophysiological aspects associated with the highly complex disorder of autism. It has to be explored whether the present results can be replicated in this group or extended to a larger group of individuals diagnosed autistic, or whether they might be specific to the disorder in general.

Chapter 5

Oscillatory dynamics following semantic incongruity

This chapter is a report of a study of the neural mechanisms associated with the processing of semantics conveyed in words and sentences. The study is based on a semantic violation paradigm which has often been used in neuroelectrical explorations of language processing, and which is known to elicit a robust evoked response. In this study an attempt is made to parameterise the γ-band activity associated with the neural processes, and to study its relationship to evoked responses in the time domain. This approach has been motivated by recent advances indicating a possibly specific role of higher frequency activity in language processing.

In the first section, a brief overview of the paradigm is given, followed by a description of the actual experiment. The analysis method is developed next. It centres around the technique of Gabor transforms recently introduced to the analysis of EEG and MEG signals. Then follow the presentation of the results and a discussion.

5.1 Background on neuroelectrical studies of semantic processing

Language is an essential characteristic of the human race, and has been studied by a variety of disciplines including psychology, biology, neurology, computer sciences, and philosophy (e.g. [52]). Because of its complexity, researchers have addressed certain aspects of language separately, but the part-whole relationships have also attracted a considerable inter-disciplinary interest. These relationships are found at many levels: letters or units of sound (phonemes) combine into words, words make up sentences,

and sentences form discourse. Over many decades, research has suggested that the relationships are unlikely to proceed in a strictly serial manner from the simplest to the most intricate unit, either in language comprehension or production. Since the 1960s, there has been exploration of context effects which involve meaning and which operate at the level of interactions between sentences and words; e.g. a word which forms a congruous completion to a sentence is more likely to be identified with a brief exposure period and to receive a faster response than an incongruous completion (see [160] for an overview).

At about the same time, event-related studies came into use as a means of investigating language processing. However, it was not before 1980 that encouraging results were obtained which demonstrated clearly that event-related responses following linguistic stimuli are informative. In that year, it was shown that a late negative component around 400 ms after stimulus onset, called the N400, was related specifically to semantic context [88]. The modulation of that component was demonstrated by recording the responses following semantically congruous and incongruous final words in sentences such as

It was his first day at work and He spread the warm bread with socks.

It was found that the N400 had a much larger amplitude when it followed the semantically incongruous final word compared to the congruous control word. The specificity with respect to semantics was suggested by the observation that the responses around 400 ms were not different from the (congruous) control condition when the final words fitted into the context of the sentence but were of different letter size.

The experiment sparked a huge interest in the N400 component. At least 100 subsequent studies employing mainly EEG but also MEG have provided further evidence that the N400 is elicited by semantically incongruous words in various sentence positions, or by the second word in pair of words which is semantically unrelated to the first. It is also elicited by pseudowords like *noom* used as a replacement for *moon*, but not by true non-words, i.e. phonologically illegal words like *lakb* (see [77]). The N400 has been shown to vary as a function of the expectancy of a word (the so-called 'cloze' probability when used at the end of a sentence): the more probable is the occurrence of a word in a given context, the smaller is the amplitude of the N400 [89]. This observation suggests that the N400 is more than a simple marker for semantic anomalies.

The N400 component can be elicited in both the visual and the auditory modalities, and is spatially widespread [65]. It exhibits a complex topography with, dependent on the paradigm, the strongest effects observed over frontal, anterior temporal, or centro-parietal regions. Studies based on readings from intracranial electrodes have pointed to components at the same latency sharing characteristics with the N400. The depth studies have identified a variety of anatomically different structures involved in the generation of the depth N400, including a marked bilateral contribution from the anterior medial temporal lobe [55, 56, 100].

Despite intense research efforts, the role of the N400 component within semantic processing is not yet resolved. A hypothesis supported by several independent teams maintains that the N400 component signals the process of integration of the stimulus within its context after the stages of the word recognition. Accordingly, a semantic incongruity entails greater integration effort and is seen as a higher N400 amplitude (a brief review of current N400 hypotheses can be found in [35]). In this context, a few EEG studies have considered evoked responses outside the traditional N400 time window, and have reported on a family of late positive components ($\approx$700 to 1000 ms), in N400 experiments. There is preliminary evidence that these also reflects semantic context effects [77, 99].

The problems in interpreting components identified in language processing have led researcher to explore methods different from the usual analysis of latencies and amplitudes of evoked responses. Specifically, the methods of time-frequency localisation have gained momentum. In time-frequency localisation, a signal is represented via an integral transformation in terms of suitable basis functions, most commonly chosen to be similar to the well known Fourier basis. The representation yields coefficients, or spectral estimates as a function of time and frequency. The computed coefficients are related to the task and stimulus under consideration, and a significant change of a coefficient with respect to a baseline is usually interpreted as an oscillation at that frequency and time.

Using these methods, recent studies on language processing have addressed the neural activity in the γ-band as a possibly independent marker. It has been suggested that γ-band power at 30 Hz is specifically suppressed following pseudoword presentation at latencies concomitant with the N400 [95, 125]. Other studies have pointed out that oscillatory activity at higher frequency might distinguish between the processing of language and non-language stimuli, thereby revealing specific hemispherical differences [44]. These studies indicate that it is potentially fruitful to leave the realm of the low

frequency evoked responses, and consider event-related activity at higher frequencies when studying language processing.

The present study furthers this approach by considering the time-frequency localisation of γ-band activity elicited by congruous and incongruous words completing sentences. In an extension to previous work, not only the localisation of γ-band power has been determined, but also the localisation of γ-band phase-locking, i.e. the alignment of phase with respect to the stimulus of certain frequency components at certain times.

5.2 The experiment

The chosen experimental design followed closely the original study in 1980 [88]. Specifically, the subjects read sentences displayed word by word on a screen (Figure 5.1). Each sentence's final word was either semantically congruous or incongruous with respect to the preceding context. In order to maintain the subject's attention in the sentence, the approach was reinforced by the target verification paradigm used in a more recent EEG study on the effects of semantic violation [46]. A target word followed the sentence. It was either a repetition of one of the words of the sentence or a new word. The subjects were requested to confirm or deny the target as being a repeated word by pressing with the index or middle finger respectively. The key press was cued by the appearance of a visual prompt. This kind of experiment has been a reliable tool in neurophysiological investigations of semantic processing. For the sake of notation, the experiment will be referred to as the language task LT.

Two examples are given below for each of the four possible combinations between the sentence's final and target words:

a) semantically correct (C), target repeats a word

Those glasses really suited his face.	glasses
The cut was so deep she had to go to hospital.	cut

b) semantically correct (C), target is a new word

She got into bed and turned out the light.	mass
The baby cried all through the night.	trench

c) semantically incongruous (I), target repeats a word

It rained so hard he put up his key.	hard
The interview went well and he got the steam.	went

d) semantically incongruous (I), target is a new word

He bought a pint of milk and a dozen gnomes.	whale
To keep warm Mark wore a scarf and a furry glass.	horse

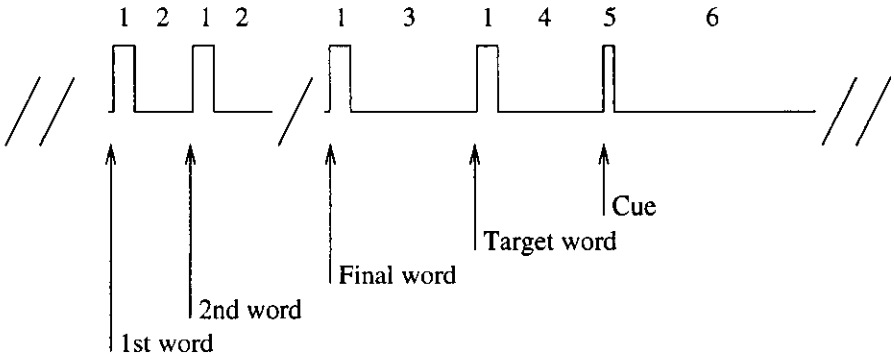

1) 200 ms
2) 550 ms
3) 1200 ms
4) 1000 +/- 200 ms
5) 100 ms
6) 1900 +/- 200 ms

Figure 5.1: Timing of a sentence cycle

The figure sketches one cycle of the language paradigm. The appearance and disappearance of an image on screen is denoted by a rectangular pulse. Horizontal (zero) lines symbolise intervals during which a grey background was displayed. A whole sentence was shown as a sequence of word images followed by a target word in red. Each cycle was completed by a visual cue prompting for the key press. A central fixation point was displayed during each cycle's final periods (4, 5, and 6). The average duration of a cycle is 9.8±1.4s based on an average number of 8.9 words per sentence (including the target word).

Each subject was presented with a total of 100 sentences with equal numbers (25) corresponding to the four possible combinations. These were split evenly into blocks of 50 sentences administered in two identical runs of the experiments. Four blocks were prepared from a data base of two hundred English sentences[1] of an average length of 8.9±1.3 words. The minimum length of a sentence was 6 and the maximum 13 words. Each sentence's final word was a noun[2] and had a length of 5.3±1.4 characters on

[1]Sentences were prepared by the English native speakers Drs Bailey and Swithenby.

[2]The sentences were designed so that the final noun or noun-phrase was syntactically correct. Within the data base some ambiguous cases might be present given the high flexibility of the English grammar in converting almost freely between nouns and verbs.

average. Care was taken to keep the range of lengths as narrow as possible (minimum = 4, maximum = 9 characters). These two provisions were made to avoid possible complications in interpreting the data arising from the use of different word types or word lengths. The target word could be of any type, and was colourised to make it clearly distinct from the sentence final word.

Subjects

A total of 9 normal volunteers were recruited for this experiment, all of whom were native speakers of the English language (see Table A.1 for an overview). The group was slightly gender imbalanced with a proportion of 6 female to 3 male participants. Subjects S17 and S18 had no prior experience of MEG studies and were introduced to the laboratory environment including a demonstration of the keypad prior to the experiment. Informed consent was obtained from all subjects who were made aware that the study concerned the response to visually presented sentences with a particular interest in the processing of semantic context. The target condition was pointed out and the subjects were reminded to press a key only after the visual prompt with no particular need for a rapid reaction.

5.3 Time-frequency localisation

In order to investigate the possibility of localised spectral characteristics associated with the brain signals, the technique of Gabor transforms was chosen. These transforms were recently added to the repertoire of neuroscience methods, and are similar to the windowed Fourier transforms which have been used extensively to estimate spectral power densities in the basic frequency bands (θ, α, β). In contrast to the latter, Gabor transforms are optimal with respect to time-width$\times$band-width uncertainty.

5.3.1 Gabor transforms

In terms common to the signal processing community, the framework of time-frequency localisation is conveniently introduced by stating a family of integral transformations of 'inner-product' type [31, 102]:

$$T : s \rightarrow < s, \Phi^{a,b} > = \int_{-\infty}^{\infty} s(x)\overline{\Phi^{a,b}}(x)dx \tag{5.1}$$

mapping a signal, s, to a (complex) coefficient dependent on two real numbers (a, b) and a (complex-valued) function of choice Φ. Both s and Φ are assumed to be square-

integrable (L^2). In this general form, Equation 5.1 comprises a spectrum of methods by which the frequency analysis of a time-dependent signal can be effected locally in time, including the windowed Fourier, the Gabor and modern wavelet transforms. The case of Gabor transforms follows by associating the integration domain and a with the time variable t, b with the frequency variable f, and defining Φ as a Gaussian shaped wave packet

$$\Phi^{t,f}(t') = e^{i2\pi ft'} g(t'-t), \text{ with } g(t) = \kappa_1 e^{-\kappa^2 t^2}, \ \kappa > 0, \kappa_1 > 0 \tag{5.2}$$

where κ and κ_1 are related by the requirement

$$\|g\|_{L^2} = \sqrt{< g, g >} = \kappa_1 \sqrt{\frac{\sqrt{\pi}}{\sqrt{2}\kappa}} = 1. \tag{5.3}$$

This completes the definition of the transformation named after its inventor Dennis Gabor [48].

The normalisation condition sets the total power of the envelope function, g, equal to 1, and implies that the wave packet is characterised by a single parameter (κ). Combining the last two equations leads to the usual expression for the transform and yields the complex coefficient

$$c(t,f) = \sqrt{\sqrt{2}\kappa/\sqrt{\pi}} \int_{-\infty}^{\infty} s(t') e^{-i2\pi ft'} e^{-\kappa^2 (t'-t)^2} dt'. \tag{5.4}$$

The signal, s, is completely determined by the Gabor coefficients via [30]

$$s(t) \sim \int_{-\infty}^{\infty} \int_{-\infty}^{\infty} \overline{c(t,f)} e^{i2\pi ft'} e^{-\kappa^2 (t'-t)^2} df dt' \tag{5.5}$$

where normalisation has been omitted.

The Gabor transform is related to the windowed Fourier transform where the window function, g, is usually compactly supported that is, for practical purposes, vanishing outside an interval. It is the specific choice of g made in Equation 5.2 which endows the coefficients of Equation 5.4 with a strong localisation property making them optimal with respect to the resolution achievable simultaneously in time and frequency. The property derives from the observation that the Gaussian shape is reproduced under Fourier transformation

$$\hat{g}(f) = \int_{-\infty}^{\infty} g(t) e^{-i2\pi ft} dt \sim e^{-\pi^2 f^2/\kappa^2} \tag{5.6}$$

where g is the envelope function and normalisation constants have been omitted. From the standard expressions for the time-width and band-width [21]

$$\Delta t = \sqrt{\frac{< t^2 g, g >}{< g, g >}} \text{ and } \Delta f = \sqrt{\frac{< f^2 \hat{g}, \hat{g} >}{< \hat{g}, \hat{g} >}}$$

respectively, it is readily derived that, for g,

$$\Delta t \Delta f = \frac{1}{4\pi} \tag{5.7}$$

whereas in general only

$$\Delta t \Delta f \geq \frac{1}{4\pi}$$

can be stated. Both g and $\hat{g}$ are concentrated around zero and $c(t, f)$ can be interpreted as the 'content' of s near time t and frequency f, thus providing a description of s in the time-frequency plane.

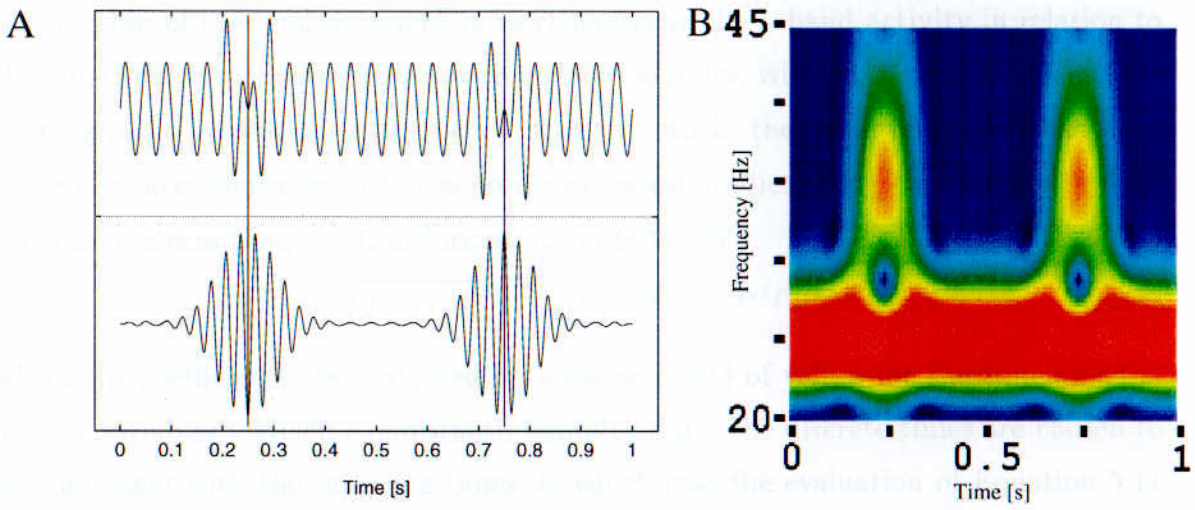

Figure 5.2: Example: Gabor transform

A: a test signal of 25Hz (f_1) with two 35Hz (f_2) bursts overlaid (upper, $y(t) = sin(2\pi f_1 t) + B(t)sin(2\pi f_2 t)$, with $B(t) = 1$ if $t \in [0.2, 0.3]$ or $t \in [0.7, 0.8]$, and $B(t) = 0$ otherwise) and the real part of $c(t, f_2)$ (K=8) as a function of time (lower). The waveform of the coefficient is here a wave packet modulated by the Gaussian envelope with maximum amplitudes at the centres of the higher frequency bursts. B: $|c(t, f)|$ colour-coded from 0 (blue) to a maximum (red, arbitrary units). The image gives an intuitive demonstration of how the signal is represented in the time-frequency plane. The phase information conveyed by the complex coefficients is lost when plotting the coefficient's modulus, so that the bursts appear to be identical with respect to the underlying signal.

Many strategies could be applied to determine the free parameter κ. Here a frequency-dependent approach is chosen by defining

$$\kappa = \frac{\sqrt{2}\pi f}{K}$$

where $K > 0$ is a constant [53]. This provision endows the transform with the usual Gaussian shape in the frequency domain with a (half-width) standard deviation

$$\sigma_f = \frac{f}{K}. \tag{5.8}$$

From this equation K may be interpreted as the (constant) ratio between the frequency and the resolution in frequency. By defining

$$\sigma_t = \frac{1}{2\pi\sigma_f} \tag{5.9}$$

the usual Gaussian shape is also obtained in the time domain, where the equations

$$\sigma_t\sigma_f = \frac{1}{2\pi},\ \Delta t = \frac{\sigma_t}{\sqrt{2}} \text{ and } \Delta f = \frac{\sigma_f}{\sqrt{2}}. \tag{5.10}$$

hold. Thus, the calculation of the coefficients $c(t,f)$ involves a family of transformations, indexed by K, where the resolution in time increases and the resolution in frequency decreases with increasing frequency. This choice of parameterisation reflects the purpose of the analysis which is to characterise the γ-band activity in relation to the time course of the evoked (low-frequency) activity, without a particular need for a fine-grained resolution in frequency. For this work, the value of $K = 8$ has been chosen, in accordance with the neurophysiological studies using this method. With this parameterisation, the transformation reads finally

$$c(t,f) = \sqrt{2\sqrt{\pi}f/K}\int_{-\infty}^{\infty} s(t')e^{-i2\pi ft'}e^{-2\pi^2 f^2(t'-t)^2/K^2}dt' \tag{5.11}$$

where the coefficients are evaluated on a discrete grid of values for the time and frequency variables[3]. Given equidistantly sampled data, the discrete times are chosen to be coincident with the sampling times, in which case the evaluation of Equation 5.11 is conveniently achieved by standard discrete convolution techniques (see Appendix B, [N-4]). In Figure 5.2, an example is given of how a signal is represented in the time-frequency plane using the Gabor transform.

5.3.2 Measures and statistics

In order to use the Gabor coefficients to study spectral properties associated with event-related paradigms, three measures, or quantities, have been suggested. These measures are derived by simple algebra and take into account that the information sought is essentially carried by a number N_e of signal epochs belonging to a certain stimulus class. The measures are defined for a given channel as follows [144]:

$$\begin{aligned}
\mathrm{P} &= \tfrac{1}{N_e}\textstyle\sum_{i=1}^{N_e}\|c_i(t,f)\|^2 && \text{(power)} \\
\mathrm{SY} &= \tfrac{1}{N_e}\left\|\textstyle\sum_{i=1}^{N_e} c_i(t,f)\right\| && \text{(synchronous activity)} \\
\mathrm{A} &= \tfrac{1}{N_e}\left\|\textstyle\sum_{i=1}^{N_e} \hat{c}_i(t,f)\right\|,\ \hat{c}_i(t,f) = \tfrac{c_i(t,f)}{\|c_i(t,f)\|} && \text{(angular alignment)}
\end{aligned} \tag{5.12}$$

[3]In case of the MEG data here, the coefficient's units are [fT/cm $\mathrm{Hz}^{-1/2}$].

where the time variable t is defined with respect to stimulus onset for each epoch. The meaning of each measure is obvious from its definition, in that phase information is disregarded in the case of P, and amplitude information is not considered in the case of A. Both types of information are taken into account for the measure SY, which, as defined, is evaluated from the averaged response instead of using single epoch data. This simplification is possible because of the linearity of the coefficients in the signal s (Equation 5.11). All three measures refer to a given point in the time-frequency plane (t, f), without making explicit this dependence.

The measures P and A have been used previously in characterising γ-band activity in terms of Gabor transforms, specifically in the context of EEG measurements employing visual stimuli (e.g. [150], see also [15, 16]). These studies have indicated the need for statistical techniques to pinpoint relevant dissimilarities in the Gabor maps corresponding to different stimuli. The techniques used involved the analysis of baseline activity estimated from prestimulus intervals, and group statistics. In the present study, the use of prestimulus activity for statistical evaluation is precluded by the existence of signal correlations preceding the congruous C and incongruous I events, most likely due to entrainment in a sequence of stimuli. This coherence of baseline activity renders it useless as an independent reference signal to which responses following different types of stimuli could be related. Group statistics, at least in the early stages of the analysis, are equally inappropriate because of considerable inter-subject variability of the resultant maps.

A further complication arises in using the measure A for analysing synchronised activity. Preliminary calculations showed spurious cancellations where coefficients derived from reasonably strong signal amplitudes were eliminated by coefficients derived from signals close to system noise level through the normalisation to unit absolute value. Possibly, the variability of signals inherent to all measurements of brain functions is more marked in very complex paradigms like the one investigated. This might lead to suppression of activity at times which in turn causes the cancellations.

Thus the measures P and SY have been chosen as the main tools to investigate differences between C and I stimuli with respect to either asynchronous or synchronous γ-band activity. SY seems to be the canonical choice when viewing synchronicity as an emergent (macroscopic) feature detected over many epochs. The approach attempts to emphasise individual over group statistics.

Statistics of the measure P

The measure P is the mean of the $\|c_i\|^2$ across epoch, and standard statistical reasoning can be applied. For each time-frequency point, let P(C) and P(I) denote the values of the measure corresponding to C and I stimuli respectively[4]. The statistical test reads in words

$$\text{T-P} = \text{T-value of the difference P(I) - P(C), DF=2}(N_e - 1) \tag{5.13}$$

where the number of degrees of freedom DF apply to an unpaired test for equal variance.

Statistics of the measure SY

This case is more difficult to deal with in that the measure is a nonlinear function of the averaged signals. Additionally, the Gabor transform constitutes a complex manipulation. Thus, finding appropriate statistics might be very cumbersome or even impossible given a lack of fundamental insight into the details of the brain dynamics. A solution to the problem was sought via a re-sampling strategy, which was introduced in 1979 and has become an accepted, powerful method to assign estimates of accuracy to measures in general.

[4]A similar notation is used for measures SY and A.

▷ **Excursion: A bootstrap method** For present purposes, the most basic technique within the framework of so called bootstrapping methods has been chosen. Despite the huge amount of theoretical and practical research centring around the general framework, the basic application is intuitively appealing. It concerns the calculation of the standard error of a statistic (or function) operating on a sample of data and reads (based on [42]):

A bootstrap algorithm for calculating standard errors (5.14)

1. Given a sample $\underline{x} = (x_1, x_2, \ldots, x_N)$ of N observations of a variable X and a function (statistic) $S = S(\underline{x})$, select randomly B independent bootstrap samples $\underline{x}^b$, $b = 1, \ldots, B$ each of size N. Each bootstrap sample is drawn with replacement from $\underline{x}$ (e.g. $\underline{x}^1 = (x_1, x_1, x_2, x_1, x_3, \ldots, x_N)$).

2. Calculate the bootstrap replication for each bootstrap sample

$$\Theta_b = S(\underline{x}^b), \; b = 1, \ldots, B.$$

3. Calculate an estimation of the standard error (se) of the statistic S from the sample standard deviation of the B replications

$$seS = \left[\sum_{b=1}^{B} \left(\Theta_b - \frac{1}{B} \sum_{b=1}^{B} \Theta_b \right)^2 / (B-1) \right]^{\frac{1}{2}}.$$

The algorithm is heuristically justified by the observation that, if the function S is chosen to be the sample mean, seS converges[5] by virtue of the weak law of large numbers, to the usual standard deviation[6] of the mean as $B \to \infty$ [41]. Many numerical studies have shown that, for most applications, a value of B between 50 and 200 guarantees a reliable calculation of the standard error, assuming a sample size comparable to this study. However, no fixed prescriptions are available, and every application must involve consistency checks [42, 162]. ◁

The bootstrap algorithm is applied to SY by identifying the sample with the set of all epochs (sample size = N_e) belonging to a given channel and stimulus, and by identifying the statistic S with the composite operation of forming the averaged

[5] A quality uniform number generator is an essential ingredient for the algorithm. Here a standard library routine was used (Appendix B, [N-1]).

[6] Precisely, convergence is given up to a normalisation factor equal to $\sqrt{N/(N-1)}$ where N is the sample size. However, this correction is usually omitted.

evoked response followed by the evaluation of the Gabor transform (symbolically: S = Gabor transform $\circ$ average). In other words, SY is evaluated as defined in Equation 5.12 based on a normal, average evoked response where each of the N_e epochs occurs exactly once. This procedure is then repeated B times using an evoked response bootstrapped from a random selection of N_e epochs drawn with replacement from the original set. These B evaluations are then used accordingly to give a bootstrap standard error of the measure $se\,(\mathrm{SY})$.

Given two stimulus classes, it is possible to perform a statistical comparison between the two by simulating a T-test[7] for a given time-frequency point according to:

$$\text{T-SY} = \frac{\mathrm{SY(I)} - \mathrm{SY(C)}}{\sqrt{[se\mathrm{SY(I)}]^2 + [se\mathrm{SY(C)}]^2}}. \tag{5.15}$$

Essentially, this formula is the Pythagorean rule of the conventional T-statistic for unequal variances where empirical standard deviations are used. It is assumed that T-SY constitutes a valid statistic for the difference between SY(I) and SY(C) based on N_e epochs each, and that the statistic is characterised by a number of degrees of freedom between $(N_e - 1)$ and $2(N_e - 1)$ (see Appendix B, [N-11]). A visualisation of the procedure is given in Appendix E together with the results of various calculations to verify its consistency.

For the sake of notation, the symbol I+ (I-) is used for positive (negative) differences in conjunction with T-P and T-SY, i.e. the case where either measure assumes higher (lower) values for I-responses compared to C-responses.

Statistics of the measure A

Once time-frequency points exhibiting significant differences in SY have been located within individuals, the measure A is used to estimate the degree of angular alignment across epochs. The measure is evaluated separately for C and I responses without direct statistical comparison between the stimulus classes. In either case, a value of A is assumed to indicate significant phase alignment across epochs if the $\arcsin(\Im\hat{c}_i)$, $i = 1, \ldots, N_e$ distribute non-uniformly ($p < 0.05$) in $[-\pi, \pi]$ according to a Kolmogorov-Smirnov test (Appendix B, [N-13]).

[7]The bootstrap theory provides algorithms of hypothesis testing based on conventional statistics. However, these require the knowledge of the observed value of that statistic, which is not the case in the context here.

5.4 Results: task performance and evoked responses

Each of the 9 volunteers completed successfully two consecutive runs of the experiment showing appropriate attention. No problems were reported concerning the word display duration or understanding of the instructions given. The contamination of brain signals following the sentences' final words due to movement or eye artefacts was negligible across all subjects[8], and the two data sets were combined as if obtained from a single run.

The task performance as measured by scores was high for the subject group as a whole (0.95±0.01) and, individually, no exceptional deviations were found. It is noted that incorrect key strokes and no-press events occurred in about equal proportion. Evaluation of the reaction times (after the visual prompt) did not reveal any specific variation of vigilance during the run-time of the experiment[9]. Neither scores nor reaction times indicate a correlation with the sentence's final word being a semantic violation.

Signals following both types of final word class stimuli show complex morphologies, and wide spread differences between the responses can be identified in all subjects by visual inspection. The differences are observed in a wide range of latencies from 180 to 1000 ms after stimulus onset and are located over the medial to anterior regions of the brain and more over the left than over the right. In an interval of approximate length of 300 ms centred around 400 ms, channels can be found in each subject where I-responses have higher amplitudes than C-responses. In order to further quantify the differences between the two waveforms, grand mean responses[10] were calculated from the data of all subjects together with with a T-test for each time slice to assess the significance of deviations between the C and I conditions.

In general, as with the individual responses, the grand mean signals exhibit a complex spatial pattern around a latency of 400 ms as well as longer latencies. A total of 6 channels over mainly left anterior to left temporal regions can be identified where the differences between the C and I signals reach a significance level equal to or better than 5% within the time span of the N400m complex (Figure 5.3 A). For this group

[8]Not more than 4 out of 100 epochs had to be rejected per subject due to eye-blinks except for one subject, who had a higher rejection rate (10). Head locations immediately before and after each run differed by no more than the limits of accuracy of the positioning system.

[9]A very small number of reaction times outside the interval 200 to 1200 ms were not taken into consideration.

[10]See remarks in Chapter 1. Prior to the grand mean calculations, the individual evoked responses were averaged, filtered (0.8 (0.4 roll-off) to 48 (0.5 roll-off) Hz, Appendix B, [N-2]), and drift corrected (-200 to 0 ms, Appendix B, [N-3]).

of channels, deviant N400m responses are very homogeneous in adjacent channels over left temporal areas with phase reversals occurring over left anterior and right temporal regions. The N400m complex is the most obvious difference between the signals, and two grand mean activation curves were calculated (see Equation 3.1) using the six detector sites containing the six channels (Figure 5.3 B).

A first peak at ≈160 ms after stimulus onset is identical for both response types. It is followed by a component at ≈250 ms in which C-responses evoke higher signal power than I-responses. This component is well represented by the channels exhibiting the N400m, but the significance of the differences is only evident in two channels. Next in the sequence is the strong N400m deviant response. A final complex of differential responses locates around 700 ms. Significant differences for this component are evident in as many channels as for the N400m. In this case the differential effects over the right hemisphere are more posterior than for the N400m and, therefore, are not optimally reflected in the particular grand-mean shown here.

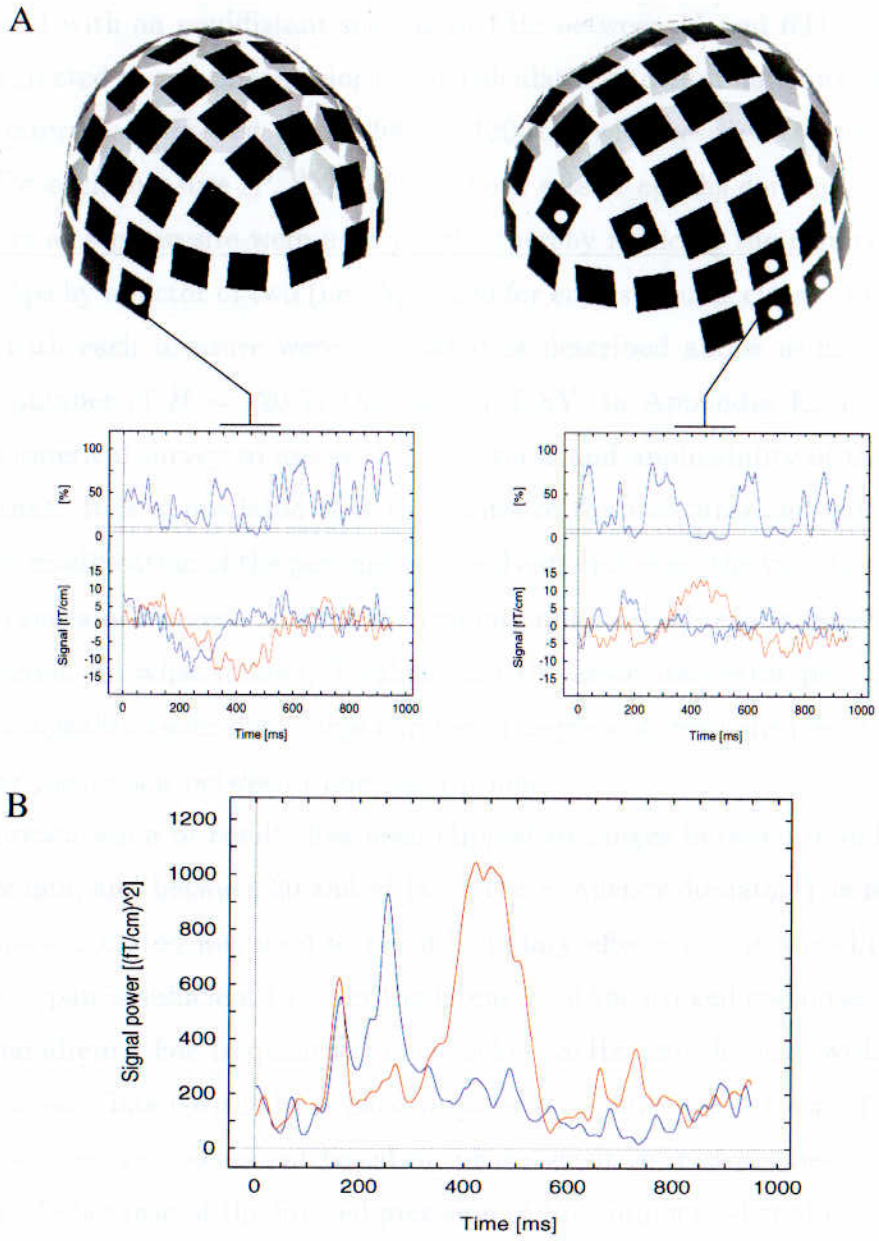

Figure 5.3: N400(m): grand mean signals

A: location of the six channels (7, 34, 39, 56, 58, and 68) where significant differences between the two grand mean waveforms (lower traces; blue C-response, red I-response) were found within the latency span of the N400m complex. The upper traces denote the significance level of the difference in amplitude at each time (DF=16; 10% and 5% levels denoted by horizontal lines). B: grand mean activation (summed signal power) based on the six sites (12 channels) containing the 'significant' channels. Most prominent is the substantial difference in power around 400 ms.

5.5 Results: Gabor transform

The Gabor coefficients were calculated from the data of all 9 subjects, separately for each channel and final word class using a wave-packet parameter of $K = 8$ and a frequency grid with an equidistant spacing of 1 Hz between 15 and 60 Hz. All signals had been corrected to zero mean prior to the calculations to eliminate unwanted offsets within an interval of interest from -200 to 1200 ms with respect to the final word stimulus. For each measure (P, SY, and A), both sets of epochs corresponding to the two detectors at a given site were used jointly, thereby reducing the resultant number of Gabor maps by a factor of two (i.e. $N_e = 100$ for each stimulus class). The statistics associated with each measure were calculated as described above using a bootstrap replication number of $B = 120$ in the case of T-SY. In Appendix E, a summary is given of a numerical survey to assess the robustness and applicability of the approach in this context. It is appreciated that the values of the measures and their statistics change upon modification of the parameters involved. However, the variations are small within the ranges of interest, so that the (mainly qualitative) results presented below are not affected. In what follows, T-values and the associated error probabilities are used interchangeably assuming a large number of degrees of freedoms (see Appendix B, [N-9] for the conversion between these descriptions).

The presentation of results has been clipped to ranges between 0 and 950 ms in the time domain, and between 20 and 45 Hz in the frequency domain. The larger array of coefficients calculated was used to avoid boundary effects due to the clipping. The reduced time span is sufficient to cover the latencies of the evoked responses associated with this paradigm. For frequencies much below 20 Hz, interference with the spectral densities associated with the evoked responses becomes too strong. Towards the higher frequencies, an assessment based on phase-sensitive measure becomes increasingly unreliable because of the limited precision of the timing of stimulus presentation (see Appendix E). The range of frequencies presented here will be called the γ-band. With a wave-packet parameter of $K = 8$, the Gabor description is characterised by ($2\Delta t \approx 90$ ms, $2\Delta f \approx 3.5$ Hz) and ($2\Delta t \approx 40$ ms, $2\Delta f \approx 8$ Hz) at the lower and upper edge frequencies respectively.

5.5.1 Statistical Gabor maps and threshold clustering

Initially, a total of 1098 statistical Gabor maps, i.e. maps associated with T-P and T-SY, were calculated. The number corresponds to 9 subjects×two measures×61 de-

tector sites. Across all maps, no T-values were found outside the interval from -4.1 to 4.9. Despite these relatively large extrema, the maps are dominated by non-significant differences as shown in Figure 5.4. The figure shows islets within the time-frequency planes where the T-values are of reasonably high significance, say $p < 0.05$, with a typical width of about 110 ms in time and 4 Hz in frequency in the case of T-SY. For T-P maps, the widths are broadly similar, but, the rate of occurrence of islets is about 4 times greater than for T-SY.

Apart from these general observations, it is difficult to extract information about temporal or spatial structures from visual inspection alone. Inter-subject variability is considerable with respect to times, frequencies and detectors. In order to identify systematic behaviour, a scheme of threshold clustering has been developed. It proceeds in three steps: 1) all sets of contiguous time-frequency points reaching a given level significance are identified in each map separately according to the sign of the statistical value, 2) each such set is identified with its (t, f)-point of maximum significance, yielding clusters cl for a given subject and detector site

$$cl = (t, \sigma_t, f, \sigma_f, \mathrm{A(I)}, \mathrm{A(C)})$$

that are endowed with resolutions and angular alignments defined at the local maximum, and 3) all clusters for all subjects and detectors are collapsed into one Gabor plane.

Thus, for each threshold, four groups of clusters[11] are obtained corresponding to the two measures used and the two possible signs for the differences between the measures (I+, I-). It is useful to define a measure of overlap OVLP of two clusters cl_i and cl_j in the Gabor plane, by

$$\mathrm{OVLP} = \begin{cases} 1 & \text{if } \frac{|t_i - t_j|}{\sqrt{\sigma_{t_i}^2 + \sigma_{t_j}^2}} \leq \sqrt{2} \text{ and } \frac{|f_i - f_j|}{\sqrt{\sigma_{f_i}^2 + \sigma_{f_j}^2}} \leq \sqrt{2} \\ 0 & \text{otherwise} \end{cases} \tag{5.16}$$

This takes into account the resolutions in time and frequency at the local maximum. OVLP is only defined if the clusters cl_i and cl_j correspond to the same subject.

Having defined the clusters, it is useful to consider profiles of the resultant populations for each group by disregarding either the time or frequency domain. Essentially, those profiles are histograms where either only the f_i or the t_i enter the calculations. However, simple histograms obtained by collecting the clusters of a given group into

[11] For reasons of numerical stability, a cluster, cl_i, is only accepted if the two T-values at $(t_{i-\delta}, f_i)$ and $(t_{i+\delta}, f_i)$ reach the same threshold as the maximal value at (t_i, f_i) representing the cluster, where δ denotes the sampling interval.

bins of constant width can be misleading and prone to instabilities across different thresholds. Therefore, a function is suggested here which assigns to a point in time or frequency a number between 0 and 1 based on all N clusters in a given group. The function produces a stable histogram-like indicator of the cluster distribution. It will be called the Gabor density GDS and defined as:

$$\text{GDS-X}(x) = \frac{\sum_{i=1}^{N} w_i e^{-\left(\frac{x-x_i}{\sigma_{x_i}}\right)^2}}{max\left[\sum_{i=1}^{N} w_i e^{-\left(\frac{x-x_i}{\sigma_{x_i}}\right)^2}\right]}, \; i = 1, \ldots, N. \tag{5.17}$$

The upper case X denotes one out of three types of functions specified in Table 5.1. The types are: 1) distribution of clusters in time (X=T), 2) distribution of clusters in frequency (X=F) adjusted for the frequency-adaptive imbalance, and 3) distribution of clusters in time weighted by the angular measure A, where I+ and I- curves have weights A(I) and A(C) respectively. The lower case x denotes either the time or frequency variable, and w_i is a weight function that varies with the choice of X. It is understood that both variables assume values only on a closed interval, which means here either $[0, 950]$ ms or $[20, 45]$ Hz.

X	x	w_i	x_i	σ_{x_i}
T	t	1	t_i	σ_{t_i}
F	f	K/f	f_i	σ_{f_i}
A	t	A_i	t_i	σ_{t_i}

Table 5.1: GDS-X: types, variables and weights

In what follows, all results were obtained using the threshold clustering as outlined. Both measures P and SY and conditions (I+ and I-) were treated equally, but, the presentation emphasises the case of I+ differences where the most interesting and interpretable patterns have been obtained so far. The case of I- differences is unresolved yet, and only a synopsis of observation is given for the sake of completeness. Currently, an interpretation in this case is too speculative and has been omitted.

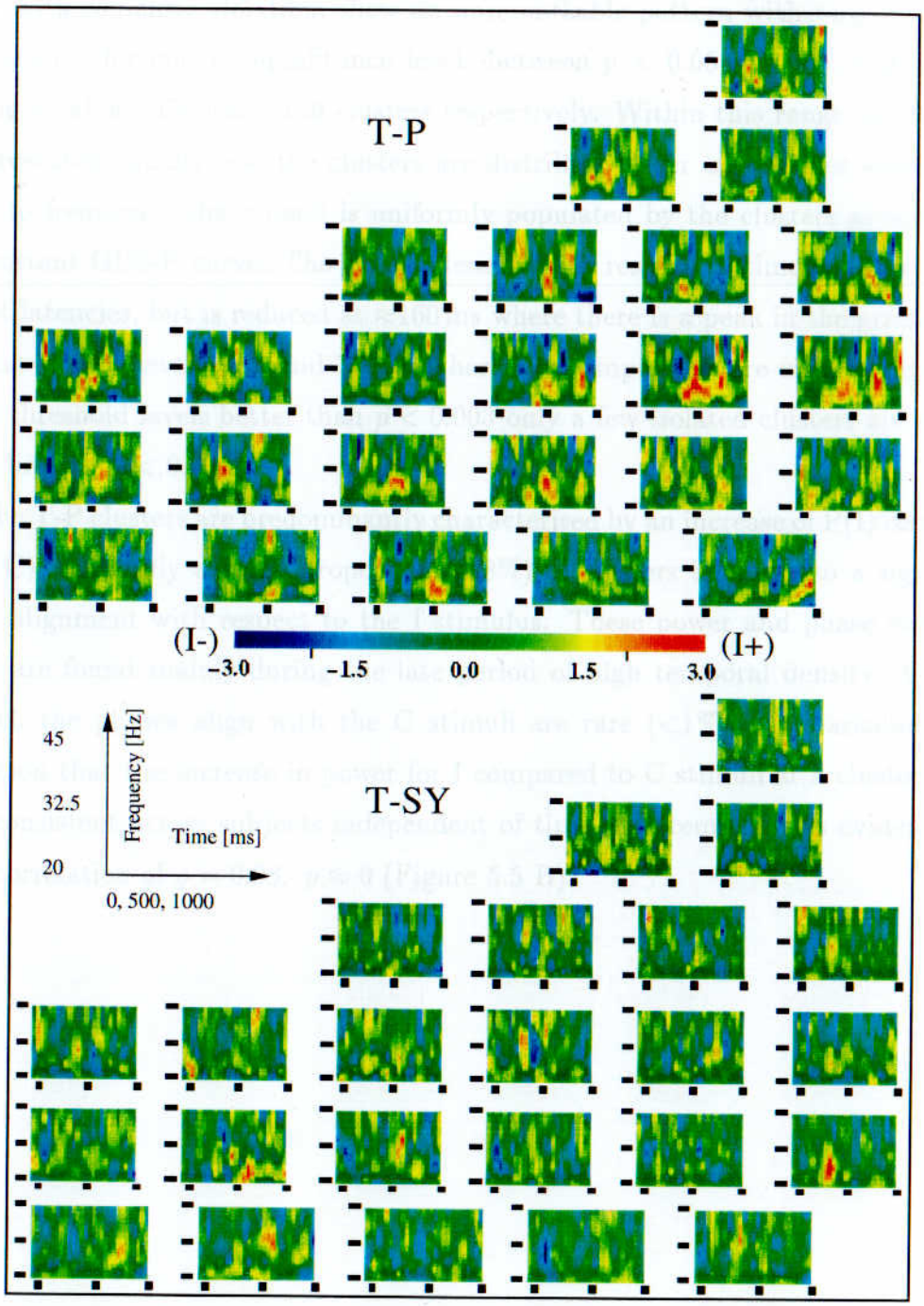

Figure 5.4: Examples: T-P and T-SY maps

The maps are shown for subject S15 and the detectors over the left anterior part of the brain (see Figure 2.4). The T-values are colour-coded (the 5%-level is indicated by the two vertical lines on the colour bar) with red corresponding to I+ significance. In general, the maps are sparsely populated by areas of elevated significance.

5.5.2 Asynchronous γ-band activity, I+ clusters

The I+ clusters of the power measure, which reflect increased asynchronous γ-band activity with semantic violation, show an unremarkable pattern with respect to time and frequency for cluster significance levels between $p < 0.05$ and $p < 0.003$ corresponding to about 1500 and 140 clusters respectively. Within this range, all subjects are represented equally and the clusters are distributed over all detector sites. With respect to frequency, the γ-band is uniformly populated by the clusters as suggested by a constant GDS-F curve. The cluster density with respect to time is also constant for most latencies, but is reduced at $\approx$160 ms where there is a peak in the grand mean power curve and elevated around 700 ms where late components are visible (Figure 5.5 A). For threshold levels better than $p < 0.003$ only a few isolated clusters are present up to a limit of $p < 0.001$.

The T-P clusters are predominantly characterised by an increase of P(I) compared with P(C), with only a small proportion ($\approx$8%) of clusters having also a significant angular alignment with respect to the I stimulus. These power and phase enhanced clusters are found mainly during the late period of high temporal density. Clusters for which the phases align with the C stimuli are rare (<1%). Remarkable is the observation that the increase in power for I compared to C stimuli at a cluster site is highly consistent across subjects independent of time and frequency, as evidenced by a rank correlation of $\varrho = 0.98$, $p \approx 0$ (Figure 5.5 B).

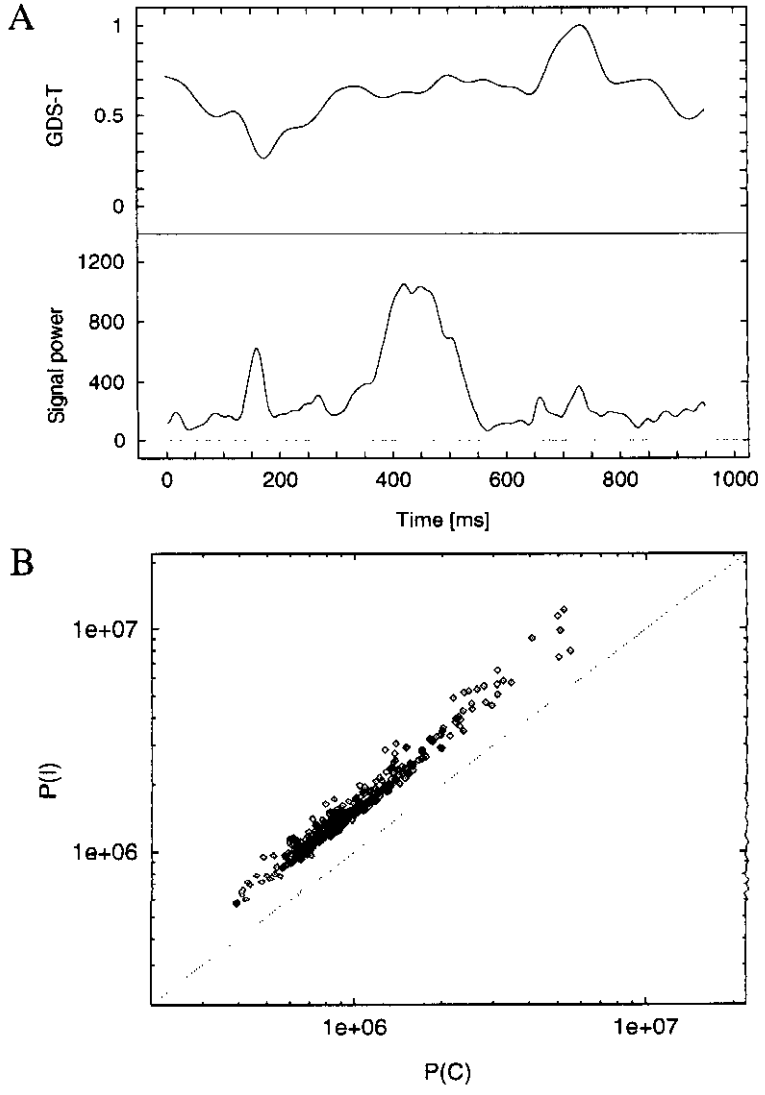

Figure 5.5: Summary statistics: asynchronous activity

A: I+ cluster density as a function of time compared with the grand mean evoked response power following incongruous final words (summed power over the six channels in Figure 5.3). The curve GDS-T is based on ≈350 clusters found with a threshold level of $p < 0.01$. B: scatter plot of P(I) versus P(C) corresponding to the clusters (units $(\mathrm{fT/cm})^2/\sqrt{\mathrm{Hz}}$). The correlation between the values is very high ($\varrho = 0.98$), and the offset indicates that the power is greater for I than for C stimuli.

5.5.3 Synchronous γ-band differences, I+ clusters

For all subjects, there are clusters identified between 0 and 950 ms. In contrast to the case of power differences, there is a distinct temporal segregation of areas in the Gabor planes populated by clusters. This emerges with increasing thresholds (Figure 5.6). Starting at $p < 0.05$, the density curves (GDS-T) smoothly transform until a stable pattern is reached at $p < 0.01$. This is characterised by three populated areas at early, intermediate, and long latency. The gap between the latter two is broad with a minimum density reached around 440 ms. This pattern continues up to $p < 0.005$, but noise does not allow higher levels of significance to be supported by the data.

Also shown in the graphs are the GDS-T curves for those clusters at each threshold for which there is no coincident T-P cluster of at least $p < 0.05$ significance. A coincidence is defined if the measure of overlap OVLP (Equation 5.16) evaluates to one for a T-SY and a T-P cluster both belonging to the same subject and detector site. The overlap is mainly present at less significant thresholds, specifically during the N400m window. At higher levels, the coincidences of changes in power are rare and isolated in time.

These observations can be extended by considering the measure of angular alignment A separately for C and I responses at the time-frequency points defined by the clusters for which there is no coincident change in γ-band power (Figure 5.7). Consistently across all thresholds, A assumes low values for C stimuli, and is characterised by a random distribution of phases (i.e. uniform in $[-\pi, \pi]$). In contrast, A assumes high values for I stimuli of about 0.25 increasing with heightened thresholds, where the distribution of phases is significantly non-random. Therefore, the pattern obtained for the measure SY, which emerges at higher levels of significance, is strongly linked to an increasing degree of alignment of phases with respect to the I but not the C stimuli.

A summary of the findings is shown in Figure 5.8 for the $p < 0.01$ level. Only clusters without coincident change in power have been considered. There are two extended plateaus of elevated cluster density, correlated with increased angular alignment, and separated by a broad gap in nearly precise anti-correlation with the N400m response (Figure 5.8). A plateau at very early latencies, just after stimulus onset, might also be present. The profile of the density with respect to frequency suggests that the effects are centred around 35 Hz, and slightly lower in case of the early synchronicity (Figure 5.8 C; the plateau at 28 Hz is dominated by the clusters up to 120 ms).

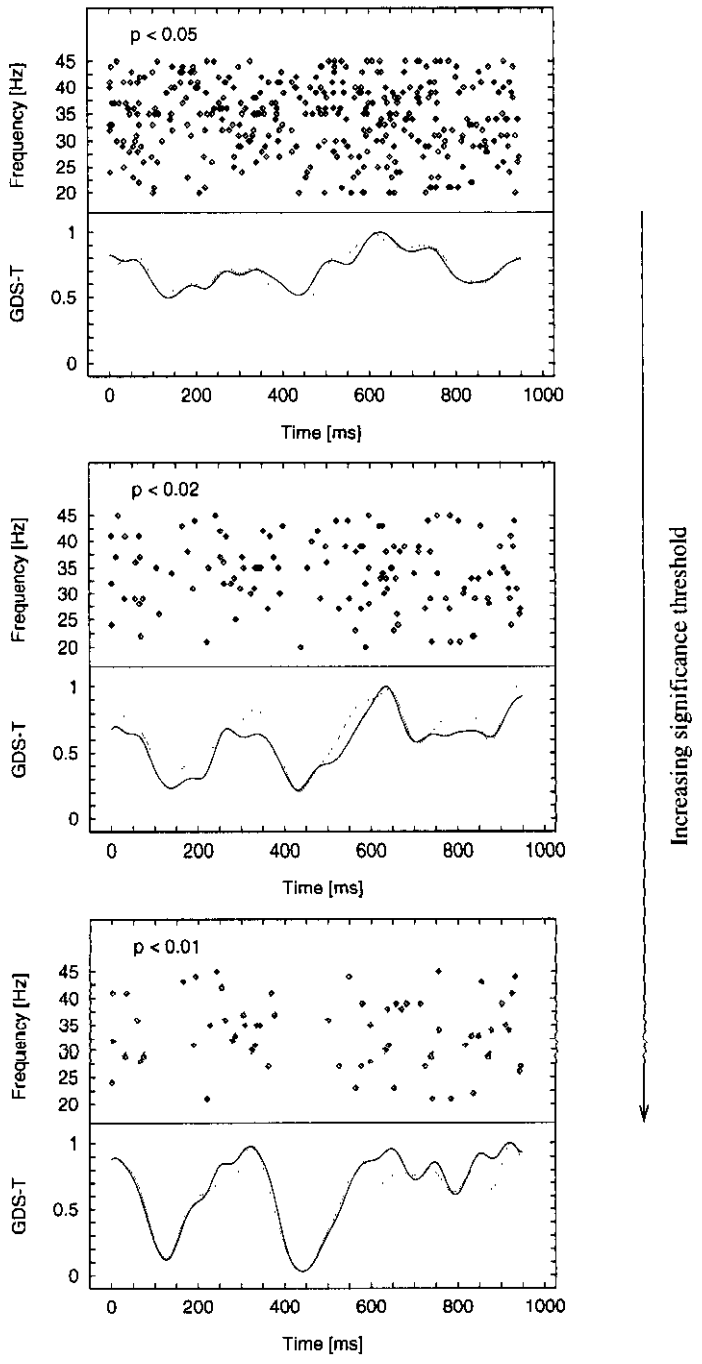

Figure 5.6: Population of Gabor planes

Distribution of I+ clusters as a function of the significance threshold. Each point represents one cluster at that time and frequency. There are 346, 128, and 63 clusters in the maps. The curves show the cluster density with respect to time for all clusters at a given threshold (solid), and the density for only those clusters which do not coincide with a T-P cluster within the range defined by the overlap measure (dashed). At higher thresholds, the difference between the two curves appear to be pronounced occasionally despite the rare coincidence in power changes. This is due to the small number of clusters and the normalisation.

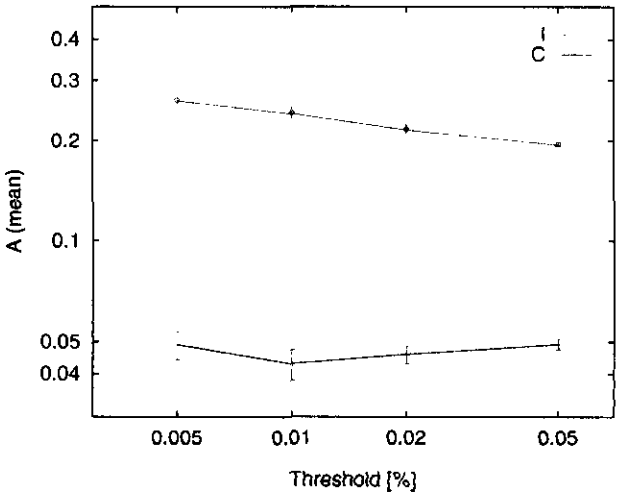

Figure 5.7: Measure A versus the threshold

The mean values and standard deviations refer to the clusters shown in Figure 5.6 evaluated separately for the C and I responses (the level $p < 0.005$ is not shown in that figure).

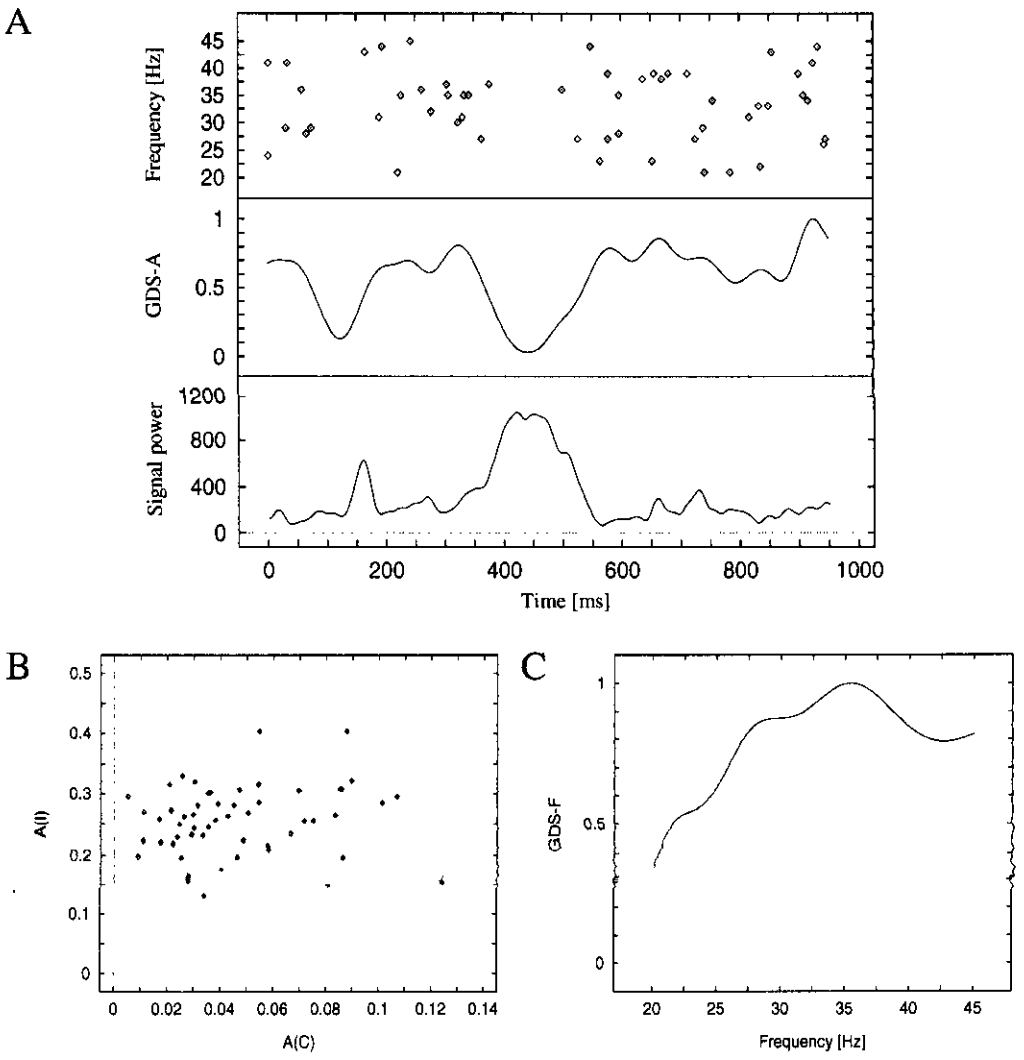

Figure 5.8: Summary statistics: synchronous activity

A: distribution of clusters not coincident with a change in γ-band power in relationship to the grand mean evoked response following I-responses (summed power over the six channels in Figure 5.3). B: scatter plot of A(I) versus A(C) corresponding to the clusters. There is no correlation because of the randomness of phases with respect to C-stimuli (Figure 5.7). C: density of clusters with respect to frequency. All graphs correspond to the $p < 0.01$ threshold.

Subject representation and spatial distribution

The analysis was taken a step further by slicing the time-frequency plane into three time segments according to the pronounced minima of the GDS-A curve (Figure 5.8 A), and investigating the resultant groups of clusters separately. Only clusters that are not coincident with a power change were considered. The following are general observations:

- Early latency plateau (0 to 120 ms) The representation of subjects is unclear. Even at $p < 0.05$, clusters are only found for 7 out of the 9 participants. A spatial pattern is not detectable.

- Middle latency pattern (120 to 450 ms) All subjects are represented, but the representation is not balanced over the two hemispheres. A spatial pattern is not detectable in the group distribution.

- Late latency pattern (450 to 950 ms) All subjects are represented with clusters in both hemispheres. At higher levels of significance, the spatial distribution suggests a reduced incidence of clusters over right anterior regions, and, possibly over occipital and medial areas (Figure 5.9 A and B). In general, the clusters over the left hemisphere are distributed evenly over this latency span, whereas the clusters over the right are predominantly within the interval 500 to 750 ms. There is some evidence for clusters coinciding in time and frequency across the two hemispheres. The (local) relationship between a cluster and the characteristics of the individual's evoked responses at that time is unpredictable (Figure 5.9 C).

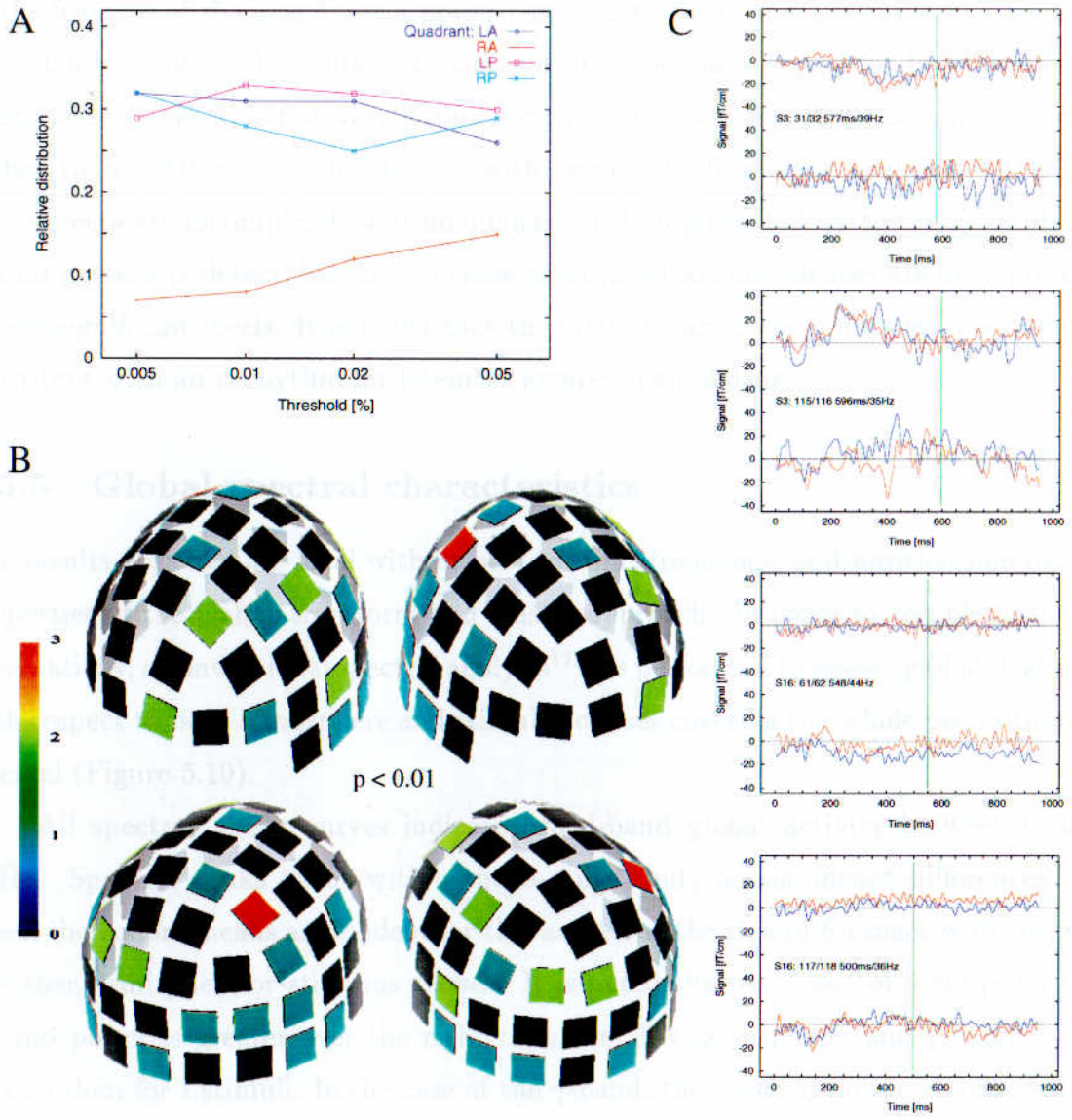

Figure 5.9: Spatial distribution of clusters

All graphs are based on the late (> 450 ms) clusters that are identified at a given threshold and are not accompanied by a change in γ-band power. A: distribution across quadrants of the helmet normalised to 1 for each threshold (LA: left anterior to RP: right posterior). B: distribution over sites at $p < 0.01$, colour-coded in terms of the numbers of clusters found at that site. C: the position of four clusters within the individual's evoked responses (blue C response, red I response).

5.5.4 Synopsis: γ-band activity of both measures, I- clusters

In general, I- clusters have about the same rate of occurrence as their I+ counterparts for both measures. All remarks made for asynchronous clusters (T-P) hold basically here as well. The corresponding GDS-T curve exhibits even less fluctuations unrelated to the features of the grand mean power curves both for C and I responses.

The case of T-SY is different from the situation encountered for I+ clusters: a) clusters are either found at very early latencies between 0 and $\approx$90 ms or at latencies higher than $\approx$310 ms, b) the density with respect to frequency peaks at 40 Hz, c) the subjects are incompletely and inhomogeneously represented by the clusters, d) no spatial pattern is detectable, and e) cross hemispherical coincidences are only present at less significant levels. It is noted that the GDS-A curves show fluctuations broadly consistent with an α-rhythm for latencies greater than 500 ms.

5.5.5 Global spectral characteristics

The results obtained are local with respect to time, frequency, and position due to the properties of the Gabor transform and cluster approach. In order to complement the observations, a conventional spectral analysis[12] was performed to assess 'global' features with respect to both hemisphere and stimulus classes covering the whole post-stimulus interval (Figure 5.10).

All spectral power curves indicate broad-band global activity between 0 and 45 Hz. Spectral peaks occur within the α-range, but, no significant differences between the cohort means are evident for this as well as the β, and θ-ranges with respect to either hemisphere or stimulus classes. It is noted that, in 7 out of 9 subjects, the α-band power is greater over the right than over left hemisphere, and greater for C stimuli than for I stimuli. In the case of the γ-band, the spectral power is consistently higher over right than over the left hemisphere in all subjects, however, the differences between the cohort means are not significant with respect to hemisphere or to stimulus classes.

[12] All epochs were individually transformed into frequency space using a maximum entropy method (30 poles, Appendix B, [N-7]) applied to the epoch's full length (0 to 950 ms). For each individual, the spectral densities were averaged over all epochs corresponding to the same stimulus and all channels over the left and right hemisphere respectively.

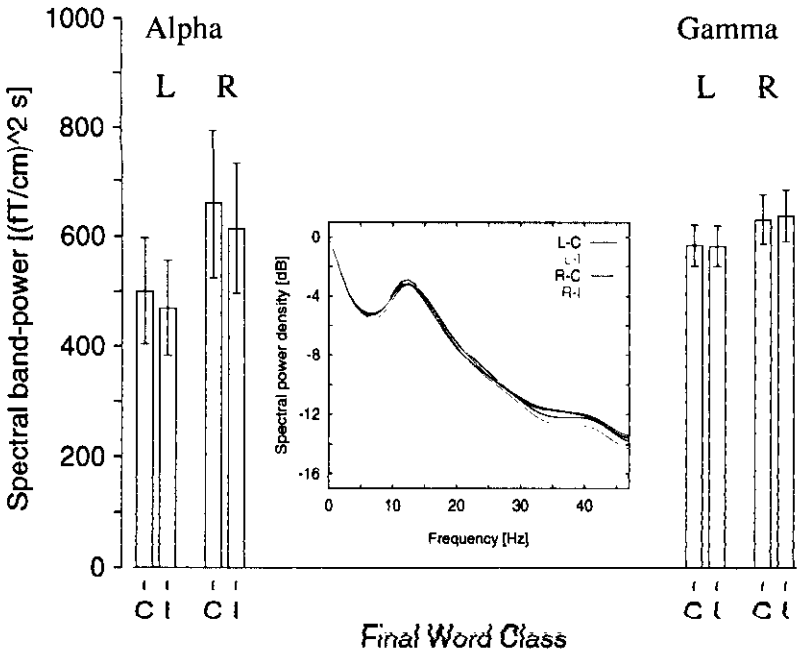

Figure 5.10: Global spectral features

Cohort means and standard deviations ($n = 9$) for the α and γ-band obtained by integration between 8 to 13 Hz and 20 to 45 Hz respectively. Inset: spectral curves for subject S2

5.6 Discussion

The main observation in the present study is γ-band activity significantly phase-locked to the incongruous stimulus. This activity can be detected in the statistics of the individual signals in a paradigm compatible with previous studies on semantic incongruity which have shown evoked responses around 400 ms. The degree of phase-locking is the only property which distinguishes the I from the C stimulus. That is, given a phase-locking event associated with the I stimulus, there is no significant difference in power between this and the C stimulus at that time and frequency. This power independence is local with respect to a given detector site, and holds for all (t,f)-points within the vicinity of the event defined by the resolution of the method.

The asynchronous γ-band power is essentially insensitive to the type of stimulus for these data. On the global scale this is evidenced by the absence of differences between the cohort means of the total post-stimulus γ-power over both hemispheres. On the local scale, a very high correlation is seen between P(C) and P(I) for all clusters, showing that the individual variability of γ-band power is not influenced by the stimulus type in this experiment. This suggest that the power measure is unspecific with respect to the stimulus. It is noted that a depression of γ-power concomitant to the N400 as reported previously is not evident [95, 125].

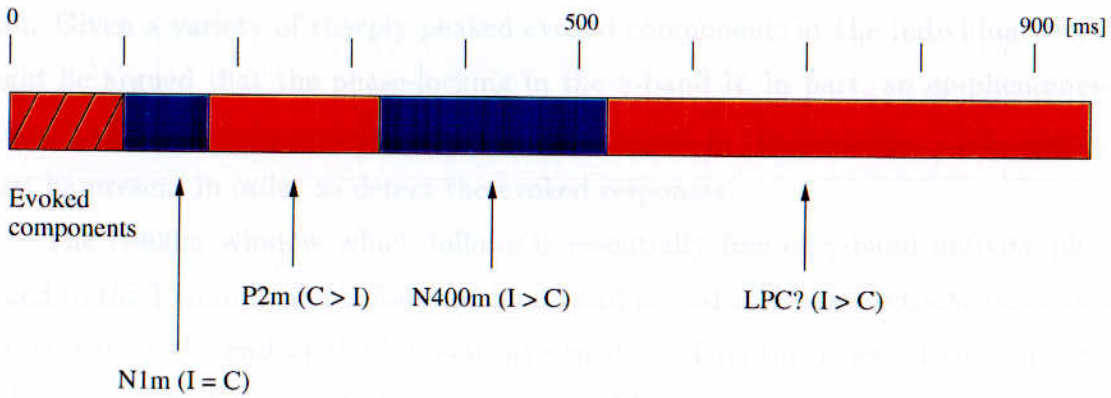

Figure 5.11: Overview of main findings

The colour bar shows a simplified distribution in time of those clusters characterised by γ-band activity significantly phase-locked to I but not to C stimuli (red: presence and blue: absence; see Figure 5.8). The mid-point of a blue interval coincides approximately with the local minimum of the corresponding GDS-A curve. The red interval marked with forward slashes denotes an incomplete representation of subjects. The evoked components listed below the bar refer to grand mean summed power curves. The components specified are those observed in previous studies on semantic processing. The relationship between the amplitudes corresponding to C and I responses is given in parenthesis. LPC = late positive component.

The phase-locking exists at all reasonable levels of significance, and its occur-

rence exhibits a clear-cut pattern with respect to latency at higher significance levels (Figure 5.11). A first period of phase-locked activity starts as early as the onset of the stimulus and lasts up to about 100 ms, in general preceding all visible evoked responses. A possible explanation could be along the lines of recent studies. These have reported unspecific phase-locked γ-band activity at $\approx$100 ms after a visual stimulus in a variety of paradigms unrelated to the present one, e.g. [151, 152]. However, in contrast to those results, the activity here is on average too early and too low in frequency to fit into previous observations. Most likely, what is seen here is predominantly related to the stimulus preceding the final word and not directly a consequence of the stimulus of interest.

A second period of phase-locked activity follows between about 180 and 320 ms, and is presumably the first directly related to the final word stimulus. The onset of this period is after the N1m and covers the P2m. Components around these latencies are widely elicited and have been consistently reported in studies on semantics. In the present study, both components are seen. They agree in latency and region of predominant occurrence with previous EEG studies. The first (N1m) component does not distinguish between the two stimulus types in accordance with other studies. The possibility of a differential effect in the case of the second component (P2m) in this data is unresolved[13]. Unresolved as well is the meaning of the γ-band activity in this latency span. Given a variety of sharply peaked evoked components at the individual level, it might be argued that the phase-locking in the γ-band is, *in part, an epiphenomenon related to activity substantially coherent with respect to the stimulus. This coherence* must be present in order to detect the evoked responses.

The N400m window which follows is essentially free of γ-band activity phase-locked to the I stimuli, and is followed by a third period of γ-band activity from about 520 to 950 ms the end of the interval investigated. This third period coincides with evoked response components between about 650 and 850 ms which are significantly different for C and I stimuli. Here, these components have been termed late positive component operationally because of the similarity in time with components observed in EEG studies [77]. The result supports the notion of late, post-N400, differential evoked responses in semantic paradigms as reported previously.

Currently, no explanation can be offered for the remarkable anti-correlation between the N400m and the phase-locking. At its peak latency, the N400m component is

[13]It is possibly that the MEG readings here are more affected than EEG readings by a partial cancellation of the P2m through the strong N400m in the case of I stimuli.

observable over virtually all cortical regions, whereas γ-band activity phase-locked to the I stimuli is almost completely absent. At later times, the phase-locked activity co-exists with strong evoked responses. It seems, therefore, unlikely that the observation can be accounted for by a simple dynamical, or physical effect independent of specific neural action.

The mere existence of significant phase-locked activity at higher frequencies is equally intriguing. It requires a timing mechanism which can cope with the nontrivial variability of the stimulus set. Although the stimuli belong conceptually to the same class, they vary to some extent with respect to the word length, cloze probability, semantic category (e.g. part of the body, a place to go, etc), and the number of preceding words. It might be argued that mechanisms at least partially independent of the semantic networks are involved to retain information about the stimulus onset. Studies in animals have pointed recently to synchronisation of oscillations of $\approx$35Hz in thalamocortical networks (e.g. [147]). Such mechanisms might be relevant here.

In summary, the present study has repeated a well known observation, has given support to recent findings about late differential, semantic related evoked responses, and, most importantly, has provided at least some further evidence that γ-band activity might play a specific, independent role within neural processing. In order to attempt a concluding suggestion for the late, highly significant phase-locked γ-activity, a brief excursion is necessary:

▷ **Excursion: the temporal coding hypothesis** *It has been hypothesised that* γ-band activity may mediate a process called the temporal coding of distributed neural networks. The principle assumes that an individual assembly or neuron can participate at different times in the representation of different objects, where the momentary context determines the significance or specificity of an individual (neuronal) response. Essentially, the principle is a model for a reintegration process of distributed activity in order to generate unambiguous representations of objects in the brain, without the need for highly selective centres (brain areas) of reconvergence. The hypothesis may be extended from object to other perception functionally specific higher order processes [143].

This idea has been conceptualised in a variety of models describing the interaction of neural assemblies (e.g. [40, 124]). However, such work suffers in practice from the ubiquity of γ-band activity in brains [37]. Indeed, oscillations are commonplace in complex dynamical systems, and it is not a question of whether oscillatory activity is

present in general, but what specific role it plays if it is to be useful as a marker and/or mediator of cognitive processes.

The temporal coding hypothesis is contentious, but has recently received some indirect support, mainly through studies in animals. These investigations have suggested that γ-band oscillations might show task and stimulus specific alterations, and zero-lag synchronicity across segregated cortical and sub-cortical areas, e.g. [128]. One study of the neural dynamics in the frontal cortex of monkeys performing a behavioural task has supported the notion that neurons can associate rapidly into a functional group. Moreover, there was an indication that the transitions in the dynamics can occur without an accompanying change in the firing rate of the neurons [158]. The latter observation might point to mechanisms that are locally independent of changes in metabolic energy. These might underlie the phenomenon of power independent phase-locking observed macroscopically here.

Observations in humans using EEG or MEG related to the hypothesis have been reported for γ-band activity accompanying the (cognitive) P300 component (referenced in [143]), early γ-band activity phase-locked to the stimulus [114, 151, 152], and phase-locked between readings from different channels [37]. The studies on language processing referenced earlier have been guided in part too by the quest for signs that (macroscopic) γ-band activity might be specifically modulated. ◁

Within the framework of these ideas, it is hypothesised that the late phase-locked γ-band activity might signal the temporal coding of large scale semantic networks as they achieve functional specificity. The anti-correlation of phase-locked activity with the N400m might indicate the unfolding of a sequence, where this evoked response signals a pre-integration stage needed to initiate the reconvergence process. The persistent existence of γ coherence over the left hemisphere[14] is broadly consistent with the activation of large scale semantic networks seen in functional imaging studies [161]. The γ-band activity over the right hemisphere is confined to a smaller area, parts of which cover regions that have been associated with the processing of words (fusiform and inferior temporal gyri [7]). On average, the activity over the right occurs earlier than over the left, and one might attribute the right hemispherical involvement to a (final) word recovery or reread strategy preceding further integration attempts. If the picture is correct, the late differential responses, might reflect some sort of control or inhibition processes, needed to dampen the γ-band oscillations which mediated the

[14]It is assumed that the left hemisphere is language dominant in all subjects.

integration.

Conclusion

The results obtained from the present study suggest that analysis of coherent phase-locked γ-band activity as proposed here might prove rewarding. Rewarding because the experimental evidence of its existence, specifically at long latency and related to the parameters of a paradigm, might constitute another window into the apparently infinite repertoire of dynamics available to neural systems. Information, so it seems, is available not only from the low-frequency evoked responses or the signal power at higher frequencies, but also from dynamical events where the brain does not need changes in (metabolic) energy which are detectable by other functional imaging techniques. Thus, the γ-coherence might support the formation of theories aimed at describing the interaction of large scale networks, be they of cortical-cortical and/or cortical-subcortical nature.

Rewarding also in that the analysis of phase-locked γ-activity might contribute to the understanding of cognitive processes. Its relationship in time with respect to 'marker' signals may indicate that these are embedded within a complex sequence of events. Thus, a question like 'what is the meaning of the marker signal X?' might have an useful extension such as 'what is the meaning of the marker signal X in relationship to subsequent changes in the neural activity of a different kind?'

Chapter 6

Pre-stimulus states

This chapter describes a further study on the neuroelectrical mechanisms underlying the processing of faces in humans. The motivation has been to learn more about the relationship between the activity evoked by face stimuli and the ongoing spontaneous activity in which it is embedded. The present study departs from conventional methods used in investigations of face processing in that the class of a particular stimulus is determined by the dynamical characteristics of the brain signals immediately preceding the presentation of that stimulus. To the knowledge of the author, this is a novel approach within the setting of face processing, although it is based on known design principles of experimentation and analysis.

In the first section, the strategy of the analysis is explained. The chapter continues with a description of the experiment, followed by presentation of the results and a discussion. As far as possible, technical details have been taken out of the mainstream presentation, and been collected into an addendum following the conclusion. The ordering of the addendum follows the order of steps of the analysis.

6.1 The approach: face responses and spontaneous activity

The interest in the relationship between evoked activity and the ongoing spontaneous activity in which it is embedded dates back to the very early days of EEG. Usually, the interest derives from the assumption that the ongoing brain activity reflects a 'functional state' of the brain which influences the fate of the incoming information (stimulus), thereby modulating the evoked responses thought to reflect the processing of the information [91]. In this sense, the internal functional state is assumed to

be defined by the neural dynamics and, therefore, reflected in certain features of the spontaneous activity.

The spontaneous versus evoked relationship is a very broad issue amenable to many different methods of investigation. However, only the so-called pre-stimulus approach is relevant here[1]:

▷ **Excursion: pre-stimulus studies** In the pre-stimulus method, the relationship between the pre and post-stimulus activity is quantified by categorising the spontaneous activity within the pre-stimulus interval into two or more categories. This yields a number of sets of epochs which may be used to calculate selective evoked responses. Subsequently, the features of the selective responses are related to the categorisation. The approach is dynamical in nature in that the momentary neural activity sets the context for a stimulus.

To date, a number of so called pre-stimulus studies have shown significant correlations between the ongoing and the evoked activity. These studies have tended to use power measures applied to EEG readings to classify the spontaneous activity within oddball paradigms where a rare stimulus elicits an endogenous component known as P300 around 300 ms after stimulus onset. Specifically, it has been shown that there is a positive correlation between the pre-stimulus α-band power and the amplitude of the P300 component. The effect has been shown to exist in experiments using visual and auditory stimuli, and is independent of the physical properties of the stimulus. Also, a P300-like component associated with the frequent stimuli of an oddball paradigm has been shown to be dependent on the spatial distribution of the total signal power about 30 to 60 ms before the arrival of the stimulus.

These studies, as well as others, have given support to the notion that significant interrelationships between the evoked activity and the ongoing activity can be detected, specifically at long latency. The results are correlational in nature and the underlying mechanisms have yet to be explored (the excursion is based on [10, 67, 71, 85, 91, 120, 129]). ◁

In this chapter, the pre-stimulus activity will be described both as the pre-stimulus state PSS, and as part of the epoch. The latter term is unbiased but the

[1]The concept of a functional state encompasses a variety of notions like level of alertness or vigilance, and physiological states like sleep. It has been studied using a variety of approaches to correlate behavioural and neurophysiological measures with the spontaneous activity. The pre-stimulus approach is the most accessible for the present study.

former makes implicitly an assumption about the notion of a 'state' having meaning.

Following the traditional approaches of pre-stimulus analysis (see next section for the experiment), it became clear in preliminary calculations that power measures were not sufficient to yield information specific to the face experiment[2]. Therefore, a change in strategy was made and a different discriminator to classify the epochs was sought.

The choice of a different measure has been motivated by the advances made in the analysis of neural signals using nonlinear approaches. Recently, interest in phenomenological, mainly linear-stochastical models of the irregular signals emanating from the brain have been giving way to examinations of nonlinear, deterministic systems. Determinism implies a system that may be described without stochastical terms, and which usually links to continuity and differentiability requirements. A deterministic system's behaviour is predictable for all times if the initial conditions are known precisely.

Mathematical theories have shown that nonlinear, deterministic systems defined in a low number of dimensions can exhibit a surprising variety of dynamical behaviour, from stable points, to a bifurcating hierarchy of stable cycles, to apparently random fluctuations. Despite the deterministic nature of the equations, predictability can be lost in a practical sense because of sensitive (i.e. exponential) dependence on initial conditions even for one dimensional systems [131].

Since the early 1980s, a powerful framework has been made available to the experimentalist providing rules and algorithms to partially reconstruct and investigate a system underlying a given time series. Essentially, a signal is converted into a set of vectors in Euclidean space, the dimension of which is determined by the dynamical features of the signal. The process is called embedding and the dimension of the reconstructed space is denoted as the embedding dimension [149]. Measures exist to quantify the set of vectors with respect to certain, often very subtle, geometrical and dynamical features. The framework has gained importance in neuroscience over the last 15 years, where studies in diverse areas of interest have suggested that this methodology may provide additional information [39, 43, 101].

The embedding framework is based on general mathematical assumptions, and is applicable to any time series. For the present purposes, a scheme has been developed to divide the epochs into two classes according to whether an epoch passes both of the following tests.

[2]As demonstrated and discussed below, the P300 versus pre-stimulus α-power relation is confirmed by the data from this experiment. The P300 is most clearly seen in oddball paradigms but is ubiquitous in all experiments requiring rapid decisions [75].

Test 1 Is the epoch stationary?

Test 2 Is the epoch deterministic?

The scheme emphasises fundamental properties of the signals. The first test is independent of the embedding. The test has been neglected in many studies, although the stationarity of a signal plays an important role within the framework [43]. The second test operates on the vectors of the reconstructed space, and implies a test of nonlinearity. For this test an auxiliary measure is needed to determine the optimal embedding dimension. The test follows recent recommendations of strategies with which to analyse brain signals in general [156].

It should be noted that the use of nonlinear techniques to analyse neural signals still has many loose ends where approaches are impossible to justify rigorously [68]. The present scheme is an attempt to shed some light on the mechanisms involved in face processing by making a crude distinction as to whether the pre-stimulus signal reflects a stationary process which is not described appropriately by random fluctuations.

Remark While developing this scheme, the author learned about an EEG investigation carried out in 1994 [70], which has one feature in common with the strategy here, i.e. the use of an embedding technique for the analysis of pre-stimulus intervals. The study seems to be the only one of its kind, and is preliminary in nature. For one subject, responses following visual stimuli were analysed using a clustering method which grouped vectors embedded in 3 dimensions. No interpretation of the tentative result has been offered by the authors other than pointing to a strong correlation with the spectral power content of the epochs. Nevertheless, the author of this thesis considers the study to be a precursor to the present investigation.

At this point, it may be helpful to read the Addendum in its entirety (Section 6.5) so as to gain an overview of the the analysis method used. At later points in the chapter, individual parts of the the Addendum will be identified, as appropriate.

6.2 The Experiment

A face identification experiment was designed to probe the effects of pre-stimulus states on face processing. It will be referred to as FPT (face 'pre-stimulus' task). The task is similar to the second run of FT1 discussed in Chapter 3. It consists of a randomised sequence of 60 images each displayed for a constant, short period and separated by

extended inter-stimulus intervals ISIs (see Figure 6.1 for details of the timing). Each image either shows an adult face (30 images) or a distractor, non-face object (motor bikes and animals, 15 each, see Figure 2.7). The images are all different and previously unseen by the subjects. The target is always a face image. As before, the appearance of a target face requires the subject to press with the index finger (of the right hand) and to press with the middle finger for a non-face object. FPT differs from FT1 in three major aspects:

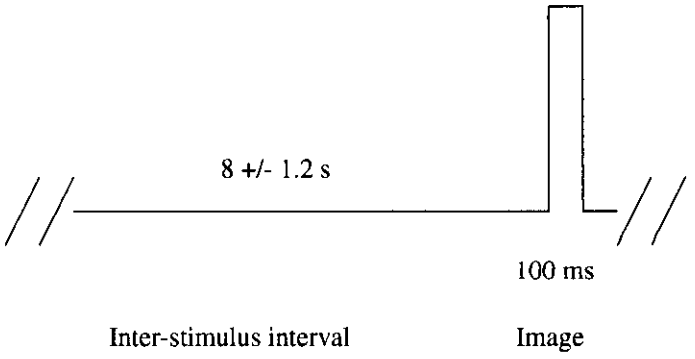

Figure 6.1: Timings
One presentation cycle is shown. A randomised, relatively long pre-stimulus interval (grey background) is followed by a short presentation of an image. The subjects press the appropriate button immediately after the image.

Equal numbers of face and non-face images This provision is to ensure equal probabilities for target and non-target images, therefore avoiding the well documented effect of stimulus probability on late components[3]. This effect may well interfere with the effects assumed to arise from the pre-stimulus classification.

Absence of a visual cue The subjects are instructed to press the appropriate key immediately after the appearance of the image. This requirement links directly the pre-stimulus state and the behavioural response without an intervening, forced wait period and an additional visual stimulus, and makes it possible to measure a reaction time (RT). This facilitates the analysis of possible correlations between the behavioural and nonlinear measures.

Prolonged inter-stimulus-interval Each ISI contains the post-stimulus interval of the previous image followed by the pre-stimulus period of the next image during

[3]Typically, P300 and, in the case of face stimuli, P300b responses are enhanced for low target probabilities. P300b is around 600 ms after stimulus onset (e.g. [36]).

which the pre-stimulus state is measured. On the one hand, a long ISI is desirable to ensure: separation of the transient brain activity following a stimulus from the pre-stimulus state preceding the next image, avoidance of unintended external priming[4], and a sufficiently long data sequence to ensure robust analysis.

On the other hand, a short ISI is desirable to ensure the subject's comfort and attendance and the stationarity of the signals. The value for the ISI of 8 ± 1.2 s (Figure 6.1) is a compromise. Preliminary tests showed that the subjects found it increasingly difficult to maintain a relaxed gaze and to avoid unnecessary movements for an ISI longer than 10 to 15 s in this paradigm and environment.

6.2.1 Subjects

A total of 6 normal volunteers were recruited for this investigation. All subjects had previously participated in face processing experiments (see Table A.1). Preference was given to individuals who had shown a low incidence of eye blinks in the previous experiments. There was no selection on the basis of the subject's evoked responses following face presentation. Informed consent was obtained from all subjects who were made aware that the study concerned the response to complex visual stimuli with a particular interest in face processing. The subjects were also aware that, this time, extended inter-stimulus intervals would occur. The subjects were instructed to press the button immediately after the presentation of the image. No specific instructions were given for subject behaviour for the period between images other than the need to direct gaze on the fixation point.

6.3 Results

Each of the six volunteers completed successfully one run of the FPT experiment. The same script for the task was used in all cases. Therefore, each subject was presented with exactly the same sequence of images and of intervals between images. Across the subjects, only 3 inappropriate key presses occurred.

Eye blinks were unavoidable (in $\approx$7% of all trials), however, all the corrupted data stretches were located well within the unused period between the transient evoked responses and the following pre-stimulus interval. All epochs associated with face

[4]Studies have shown that, for ISIs longer than $\approx$4 s, stimulus probability effects vanish [117]. Although these results are not directly applicable to the present paradigm, the threshold of 4 s seem to be appropriate here as a means of compensating for possible inadequacies of the random sequence.

stimuli were useable for the analysis of transient components for latencies from 0 to 650 ms. Also, each epoch contained at least 5020 ms of 'clean' pre-stimulus data[5]. Therefore, the analysis of each PSS was based on the 5 seconds preceding the stimulus to achieve a homogeneous numerical treatment of all data. The post-stimulus data for non-face stimuli were of similar quality, but were only used to replicate the main finding obtained with face tasks FT1 and FT2 and otherwise discarded. Artefacts due to movement were not observed. Each subject maintained a constant head position during the run of the task.

6.3.1 Replication of the early component's face specificity

Analysis of evoked signal power yielded results qualitatively similar to the ones obtained for FT1. As shown in Figure 6.2, face responses were significantly different from non-face responses according to the NIRP measure using the same integration interval at early latencies (145 ms response) and the same channels over the right occipital-temporal region (ROT). However, for this task, late components around 400 ms following face presentation are more clearly identified in many channels within and in the vicinity of this region. Usually, these deflections are recognisable in the regional power curves as being clearly distinct from pre-stimulus levels (Figure 6.2).

[5]Here, 'clean' means uncorrupted by eye blink and other artefacts as well as separated from preceding transient responses. The length of 5020 ms corresponds to 1872 time slices at a sampling rate of 373 Hz.

Subject	F	NF
S3	2.2	0.9
S9	2.5	1.0
S10	4.9	1.5
S12	2.8	1.0
S13	4.5	2.0
S15	4.1	2.1

Means ($p < 0.01$):
F 3.5 +/- 0.5
NF 1.4 +/- 0.2

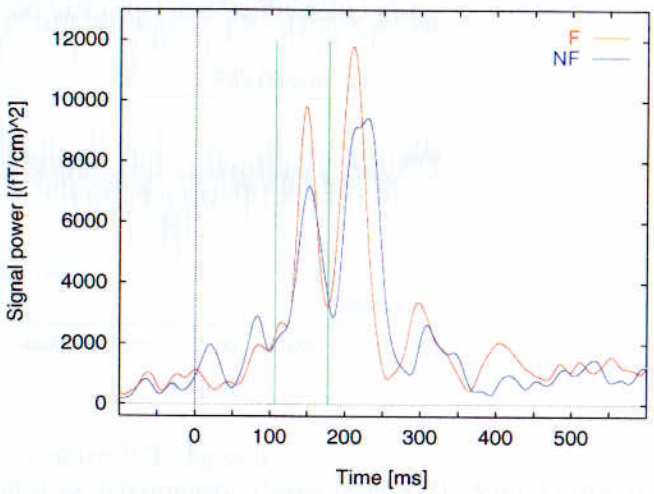

Figure 6.2: Evidence for face specificity in Task FPT

Left: individual NIRP values (channel group ROT, same as for FT1 to FT3) for the six subjects together with cohort means. Responses following face (F) presentation are compared with responses following images of non-face (NF) objects. For the latter, the responses belonging to the two distractor image classes were averaged together. The cohort mean values are clearly different, reflecting face specificity for this task.

Right: summed signal power (Equation 3.1) as a function of time for subject S12 and group ROT. The average evoked responses for each channel were filtered (0.8 (0.4 roll-off) to 48 (0.5 roll-off) Hz, Appendix B, [N-2]) and drift corrected (-200 to 0 ms, Appendix B, [N-3]) prior to the power calculations.

6.3.2 Classification of pre-stimulus states

The pre-stimulus state classification was attempted for a set of detector sites consisting of the group ROT extended by surrounding channels (coloured sites in Figure 6.4). In these channels robust and specific face responses are found at early latencies as well as strong late and possibly cognitive components. The classification scheme is explained fully in the addendum. In Figure 6.3, an example of an epoch is shown. All epochs were corrected to zero mean, but not filtered prior to the classification analysis.

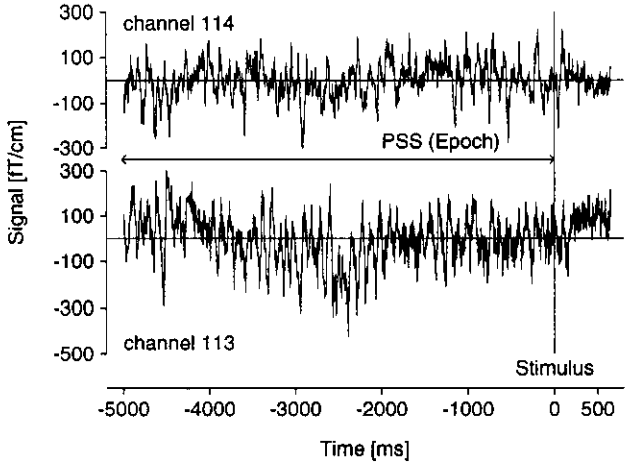

Figure 6.3: Epoch

An example of a 2-vector epoch classified as deterministic (taken from S13). Visual inspection is of no value in predicting whether an epoch will pass or fail a particular test.

A total of 1980 epochs (6 subjects×11 detector sites×30 face cycles) were tested using the ST measure, yielding 307 epochs that were stationary and rapidly decorrelating according to this measure. (The test is described in the first part of Section 6.5.2). The ST measures for these epochs exhibit a highly erratic behaviour as a function of the lag, a pattern that is broadly similar to that found for model systems used (Figure 6.4 A). Usually, the onset of convergence ($ST_k < 1,\ k > k_c$) locates well before the threshold. The majority of epochs (1673, or $\approx 85\%$), however, failed the criterion set. For these epochs, the ST-graphs show an erratic variation with lag, as before, but are overlaid with broad peaks of increased amplitude of the autocorrelation function. These peaks are usually about 200 lags wide, and are separated by 300 to 500 lags from each other.

The distribution of stationary epochs is spatially inhomogeneous, as shown in Figure 6.4 B. Clearly, these epochs gravitate over the more temporal regions of the target group of sites analysed. This non-uniformity extends to the individual level in that the subjects' contributions to the number of accepted epochs differ vastly for a

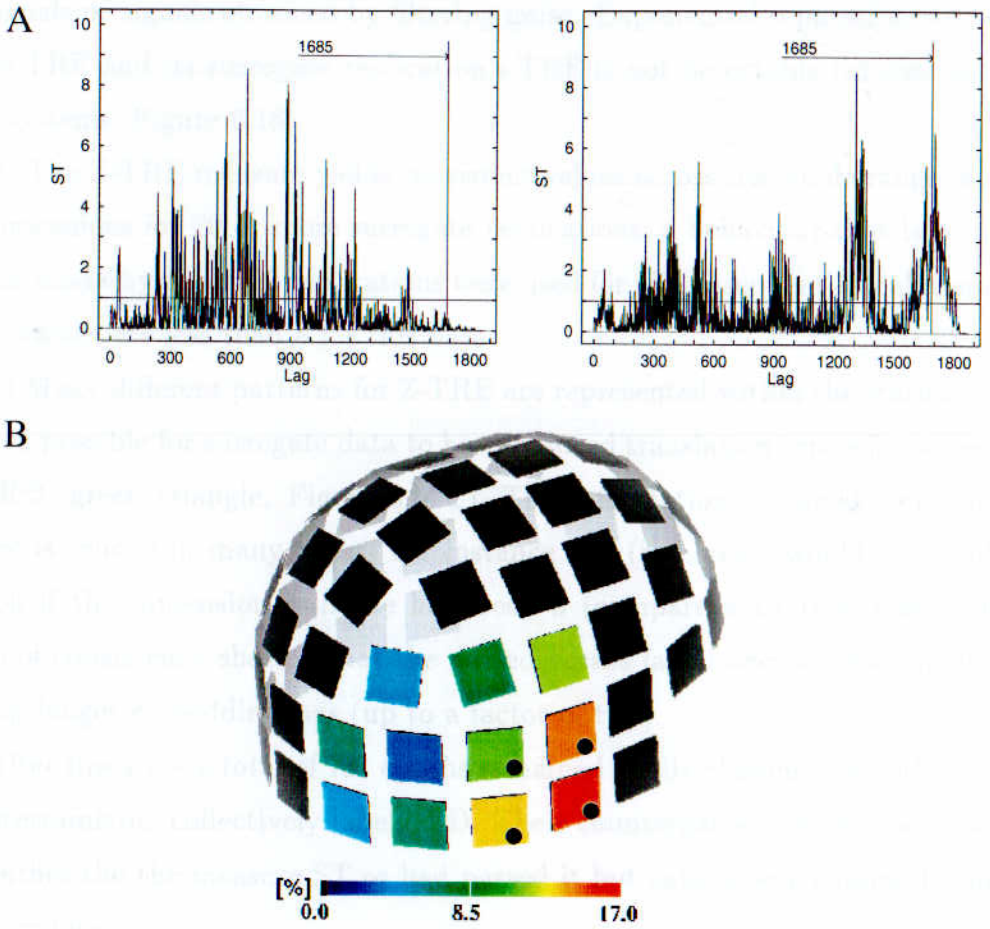

Figure 6.4: ST Measure: examples and spatial distribution

A: an example of a stationary and rapidly decorrelating epoch (left), and an example of an epoch (right) not fulfilling the condition set for this measure. The vertical line denotes the lag by which the onset of convergence is required (i.e. at a lag of 1685≡90% of 1872). B: the spatial distribution of stationary epochs. The colour-coded detector sites constitute the target group of channels. The colour-code itself is normalised to all stationary epochs found. The four dots denote the sites used in the final analysis.

particular site.

Having identified stationary epochs, effective embedding dimensions were sought for this group using the FNN method. In general, unremarkable profiles of percentages of false nearest neighbours emerged. The estimates for the embedding dimensions are all between 2 and 5 corresponding to reconstruction spaces of dimensions 4 and 10 respectively. Most often a dimension of 3 is assumed.

The next step, using the proper values for embedding lag and dimension, was to evaluate the measure Z-TRE for the 307 stationary epochs. (The measure and the associated test of determinism are discussed in the latter part of Section 6.5.2). This yielded the following observations (see Figure 6.5).

1) The data is associated with translation errors comparable to those of ran-

dom signals or signals obtained by filtering noise. Exponential separation between the epoch's TRE and its surrogate replication's TRE is not detectable (in contrast to the model systems, Figure 6.18).

2) The Z-TRE measure yields consistent values across the whole range of embedding dimensions for 20 or more surrogate replications, a behaviour that is compatible with the model systems (30 replications were used for all subsequent calculations). The Z-TRE values are less than 8 for this data.

3) Many different patterns for Z-TRE are represented within the stationary data. It is even possible for surrogate data to have reduced translation errors for some epochs (e.g. R:3, green triangle, Figure 6.5 C). The information obtained from the FNN measure is crucial in many cases. For instance D:4 (red cross) would have failed the criterion if the dimension estimate had been 3 (compare with D:3, blue rhombus). Checks of consistency showed that the passed versus failed decision was unaltered by choosing longer embedding lags (up to a factor of two).

After this step, a total of 131 epochs remained finally classified as both stationary and deterministic, collectively labelled D. Their counterparts, the rejected epochs R, failed either the the measure ST or had passed it but subsequently failed to meet the Z-TRE criterion.

For each subject, D epochs are found in the signals of at least 3 detector sites. In five subjects there is only one site with six or more D epochs, and there are two such sites for the remaining subject[6]. Given this outcome and the requirement that more than 5 epochs are needed for the reliable identification of the evoked response components, analysis was subsequently restricted to the small set of 6 site-subject combinations shown in Table 6.1. The sites comprise a group that is comparable in location to the group ROT considered previously, but shifted anteriorly. The mean values of k_0 (corresponding to the first zero of the autocorrelation function) are listed in the table for each subject and class. In four subjects, this shortest (linear) time scale seems to be dominated by α-waves[7] for both D and R epochs. In two subjects, decorrelation is slower, particularly for R epochs.

In summary, the analysis of the pre-stimulus interval has separated the epochs

[6]For this subject the two sites have 16 and 10 pre-stimulus states classified as D with an overlap of 7 in the epochs to which they refer.

[7]A pure sine-wave has a cosine auto-correlation function. For α-frequencies between 8 and 13 Hz, the first zero of the cosine function at $\pi/4$ translates to an interval lying between

$$\frac{1}{4 \times 8\,\mathrm{Hz}} = 31.3\,\mathrm{ms} \text{ and } \frac{1}{4 \times 13\,\mathrm{Hz}} = 19.2\,\mathrm{ms}$$

Subject	Site	#D	$\overline{\text{zero}}$ [ms]	#R	$\overline{\text{zero}}$ [ms]
S3	4	10	66 ± 15	20	92 ± 21
S9	114	9	32 ± 2	21	31 ± 2
S10	114	17	30 ± 1	13	32 ± 2
S12	4	16	22 ± 2	14	24 ± 2
S13	112	11	60 ± 12	19	127 ± 22
S15	2	13	26 ± 1	17	26 ± 1

Table 6.1: ST and Z-TRE measures: summary statistics

For each subject, the site (see also Figure 6.4) is given where at least 6 D epochs were found for that subject. In the case of S12, a second such site (site 112, 10 D epochs) exists. The number of epochs in each class is given in the #D and #R columns respectively, followed by the mean first zero lag (translated to a time scale).

into those that are deterministic (denoted as D epochs) and those that are not (denoted as R epochs). The main thrust of the rest of the chapter will be the comparison of these two groups in the post-stimulus period. In making this comparison the precise technical details underlying the classification are not essential.

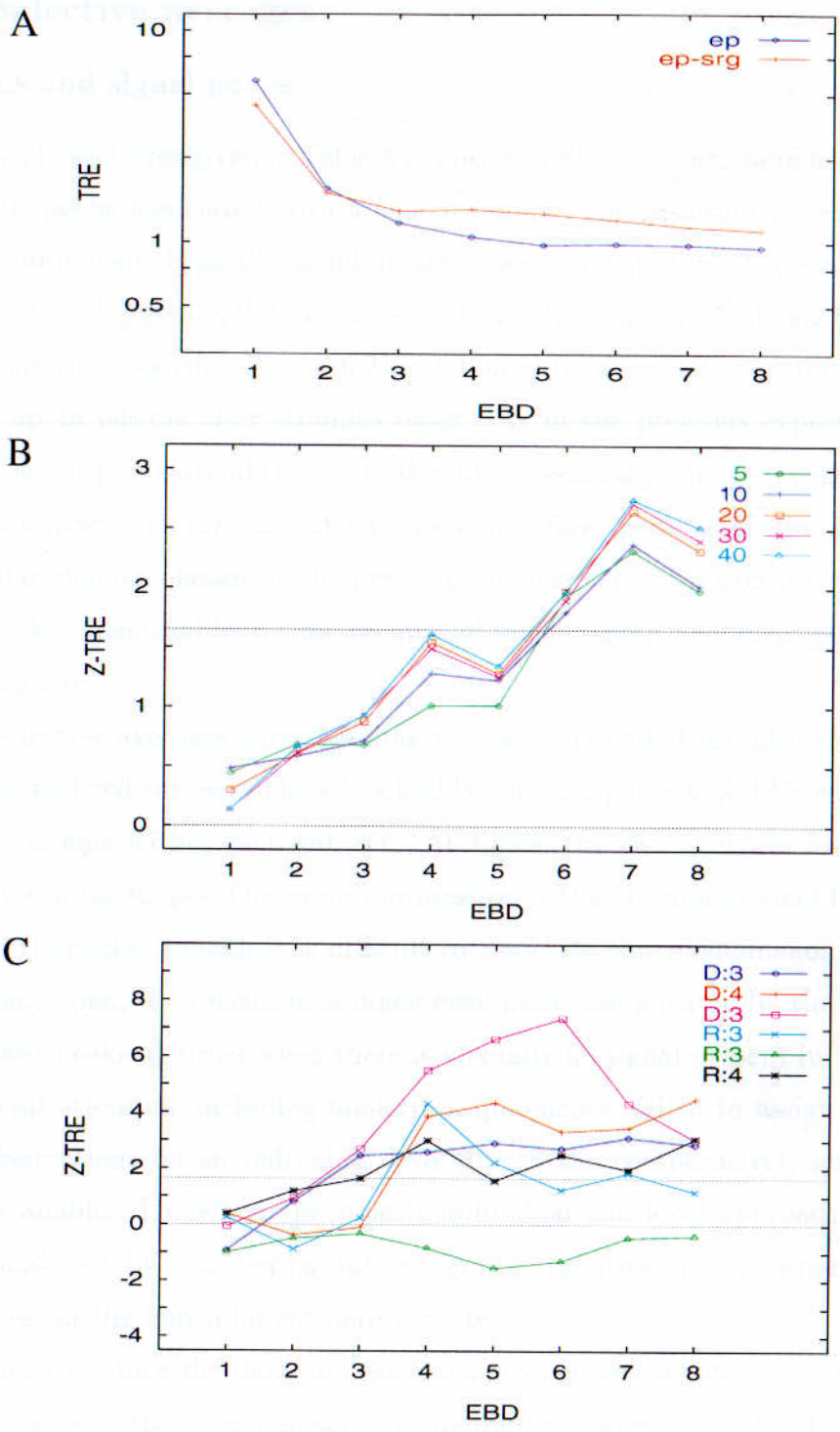

Figure 6.5: TRE measure: overview

A: Translation error (TRE) as a function of the embedding dimension for one stationary epoch (blue) and one of its surrogate replications (red). In general, brain signals yield TRE values comparable to the surrogate replications of standard deterministic model systems. The exponential separation between original and replication found in those systems is not seen here. B: The measure Z-TRE as a function of embedding dimension for several surrogate replications. This epoch passed the stationarity criterion and had an EBD=4 according to FNN. It did not pass the Z-TRE criterion. Reasonable stability of the measure is observed for 20 and more replications. C: Z-TRE (30 replications) versus EBD for some deterministic and rejected epochs. The number in the curves' legends refers to the EBD value estimated by the FNN measure. R denotes rejected by the Z-TRE criterion. The 1.65 statistical threshold is denoted by the dotted line.

6.3.3 Selective averages

Waveforms and signal power

For all subjects and sites given in Table 6.1, post-stimulus averages were first calculated using all 30 epochs associated with a face stimulus. The resultant power waveforms exhibit all components typically found in face processing experiments over the occipito-temporal cortex (Figure 6.6 dotted curves). A clearly identifiable, strong peak around 140 to 150 ms (face-specific, Figure 6.2) is followed by a cascade of later components continuing up to 600 ms after stimulus onset. As in the previous experiments, FT1 to FT3, inter-subject variability is considerable, specifically for the evoked responses at higher latencies. In the case of S3, the early 'face' peak is of low amplitude in the particular channel chosen by the pre-stimulus state classification procedure. However, the peak is identifiable in time because of much higher coincident peak-power in neighbouring sites.

The selective averages corresponding to classes D and R are also shown in Figure 6.6 (blue and red curves). There is a highly complex pattern of differences between the average signals within each subject. At times, the two averages for the classes exhibit very similar shapes The overall impression is that R epochs yield higher signal power than D epochs, though it is difficult to associate this phenomenon with a particular latency span. The scenario is made even more complicated by the existence of isolated power peaks at times when there is virtually no signal present in the total average. Several attempts, including bootstrap approaches, failed to assign significance to these observations on an individual level due to the comparatively small number of epochs available. Therefore, the strictly individual and local approach pursued so far was abandoned by considering subject group statistics and ignoring the spatial distinctiveness of the four different detector sites.

In order to reduce the data and establish any consistent differences between the D and R responses, the cohort mean of a dissimilarity measure of local signal power was calculated as a function of time, disregarding that the data applies to different sites. The measure is defined as:

$$\mathrm{DISSIM} = \frac{\mathrm{LP}_D(t) - \mathrm{LP}_R(t)}{\mathrm{LP}_D(t) + \mathrm{LP}_R(t)} \tag{6.1}$$

where the local power LP is given by

$$\mathrm{LP}_{D/R}(t) = \left\| S_{D/R}(t) \right\|^2 .$$

The subscripts D/R denote the (selective) averages of signals over all epochs belonging

to either the D or R set. The DISSIM measures achieves within-subject normalisation of signal power, but it does not incorporate pre-stimulus data which are used here as a selection criteria. The measure's modulus takes values between 0 and 1, corresponding respectively to the same activation in classes D and R and to an activation present in one class only.

As shown in Figure 6.7, the use of the DISSIM measure revealed a remarkable feature. Evoked responses corresponding to R pre-stimulus states carry significantly more signal power than evoked responses following D states at latencies around 480 ms. From about 360 ms to about 560 ms, the dissimilarity generally exceeds the 5% significance level with the peak achieving better than 0.5% significance.

It is worth pointing to two observations without giving details: a) in the case of S12, a second site containing an useable number of D epochs yields differential effects fully compatible with the results presented, and b) in all subjects, the variance of the pre-stimulus signals decreases with an increasing number of averages independently of the D versus R classification.

Spatial continuity of the effect on signal power

Visual inspection without any further quantification revealed a degree of continuity of effects across sites. That is, the deviations between the D and R (power) waveforms are very similar across a number of sites within each subject, and not only found in the subject's maximal site. A very clear example is shown in Figure 6.8. In other subjects, the continuity is less pronounced, but there are always at least two sites that show a pattern comparable with the maximal one. It is noted that, for random selections of epochs, continuity is less marked but does not vanish completely.

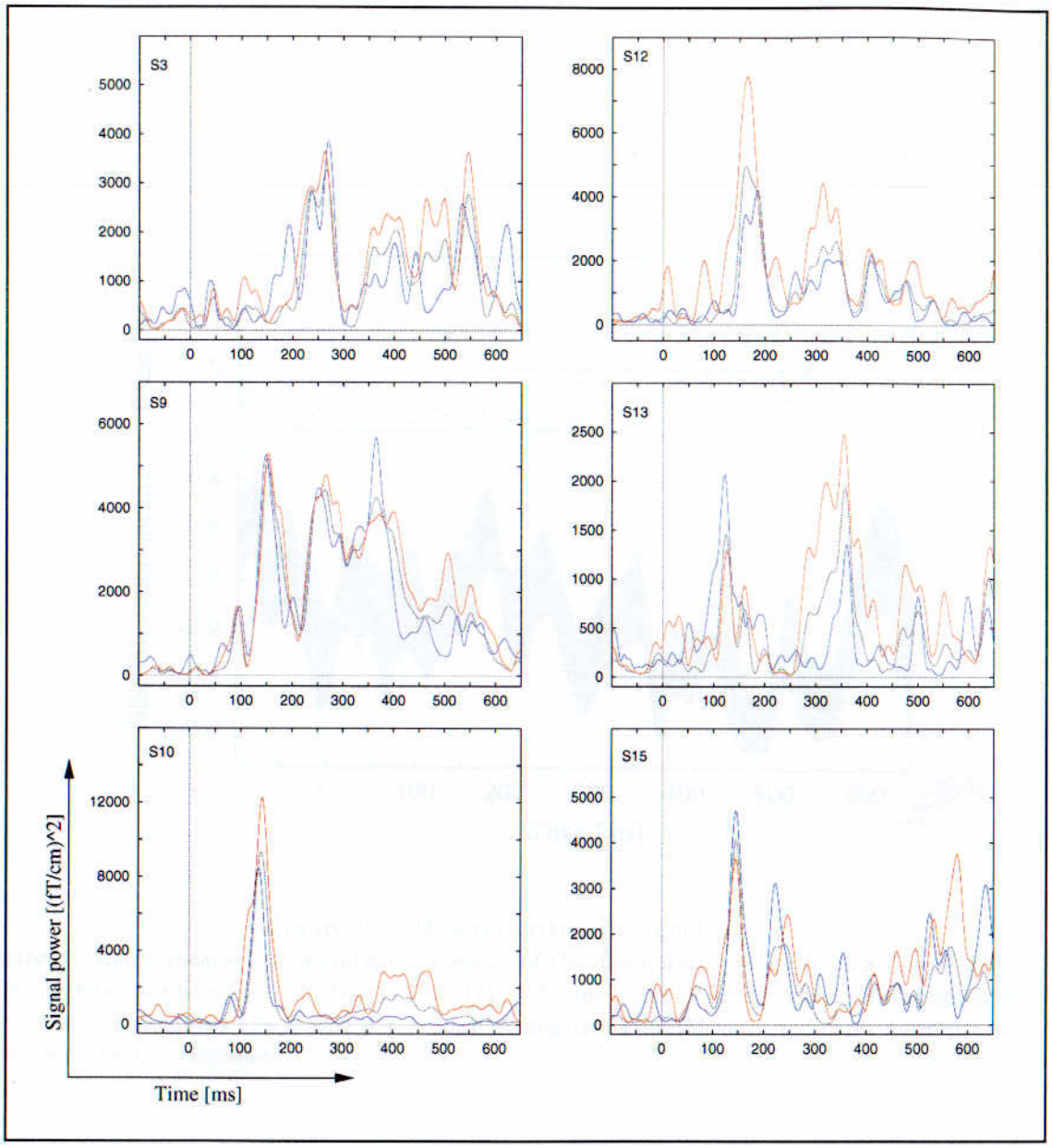

Figure 6.6: Waveforms: D versus R epochs

The local power curves for the six sites that meet both criteria corresponding to the selective averages of D (blue) and R (red) epochs, as well as the total averages (black dotted).

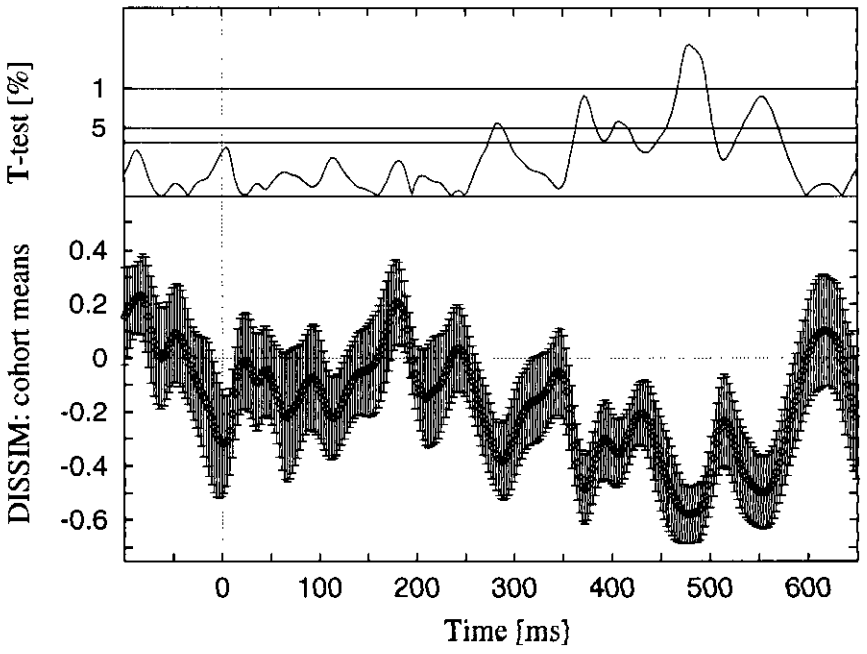

Figure 6.7: Dissimilarities in signal power

Bottom: cohort means with standard deviations of the dissimilarity measure as a function of time. Top: significance level as a function of time (T_5; 10%-line without label). The highest significance is found at about 480 ms ($T_5 = 5.7$, $p \leq 0.003$). A negative DISSIM value indicates more power in R than in D evoked responses.

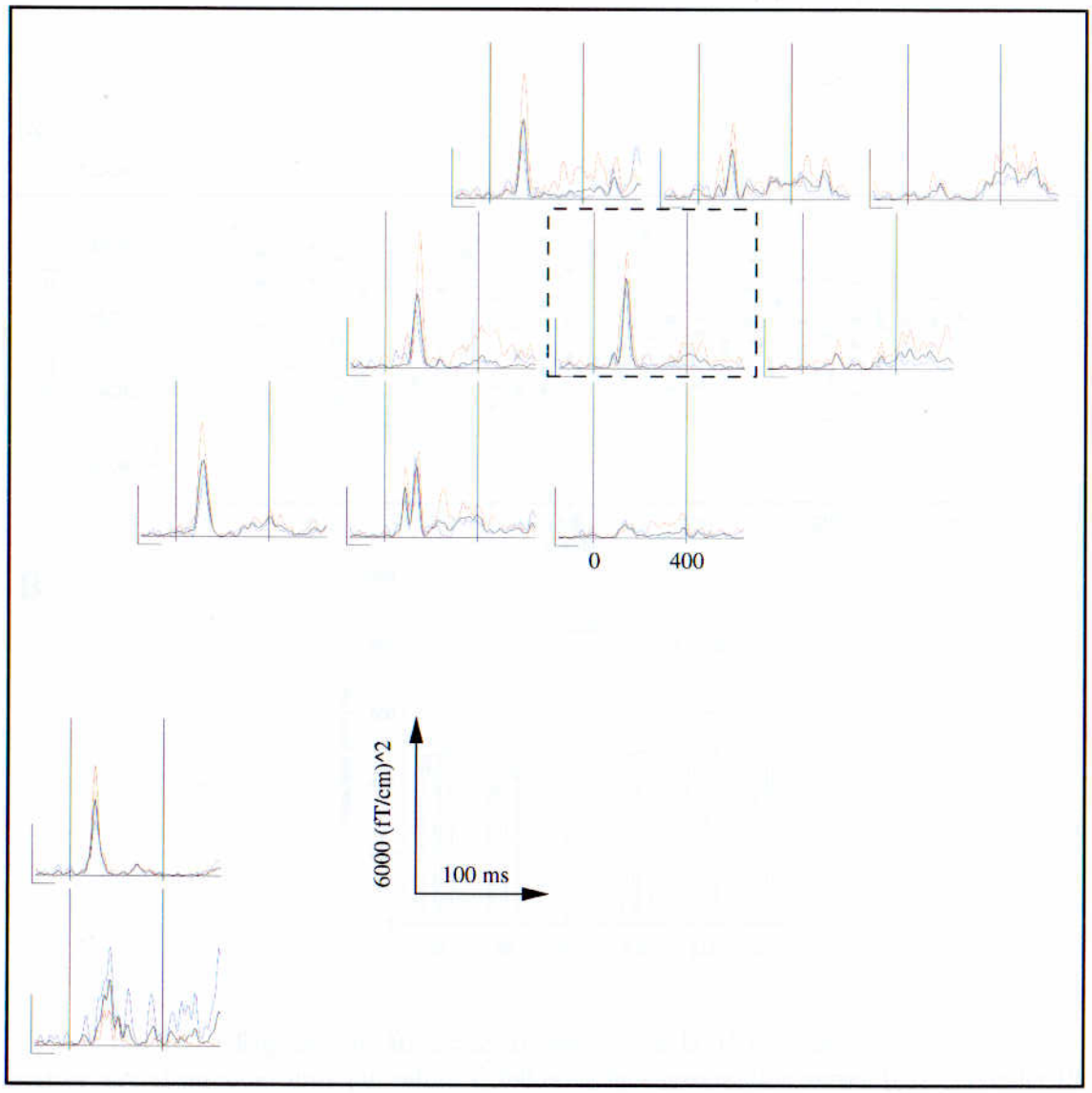

Figure 6.8: Local power: D versus R epochs (all sites)

Shown are the signals of subject S10 in all of the detector sites considered for the analysis. The coding of the curves is as before (black: all epochs, blue: deterministic, red: rejected). Detector 114, the maximal site for this subject is enclosed in the dashed box. This subject's signals are a very clear example of the general observation that the effects are 'continuously' represented in neighbouring sites. Specifically, this holds true for higher latencies, but can also apply to the earlier times.

Behavioural responses

The only behavioural measures in this task were score and reaction times. As stated above, the subjects achieved scores indistinguishable from 100% making this measure useless for further analysis. This section will concentrate on reaction times.

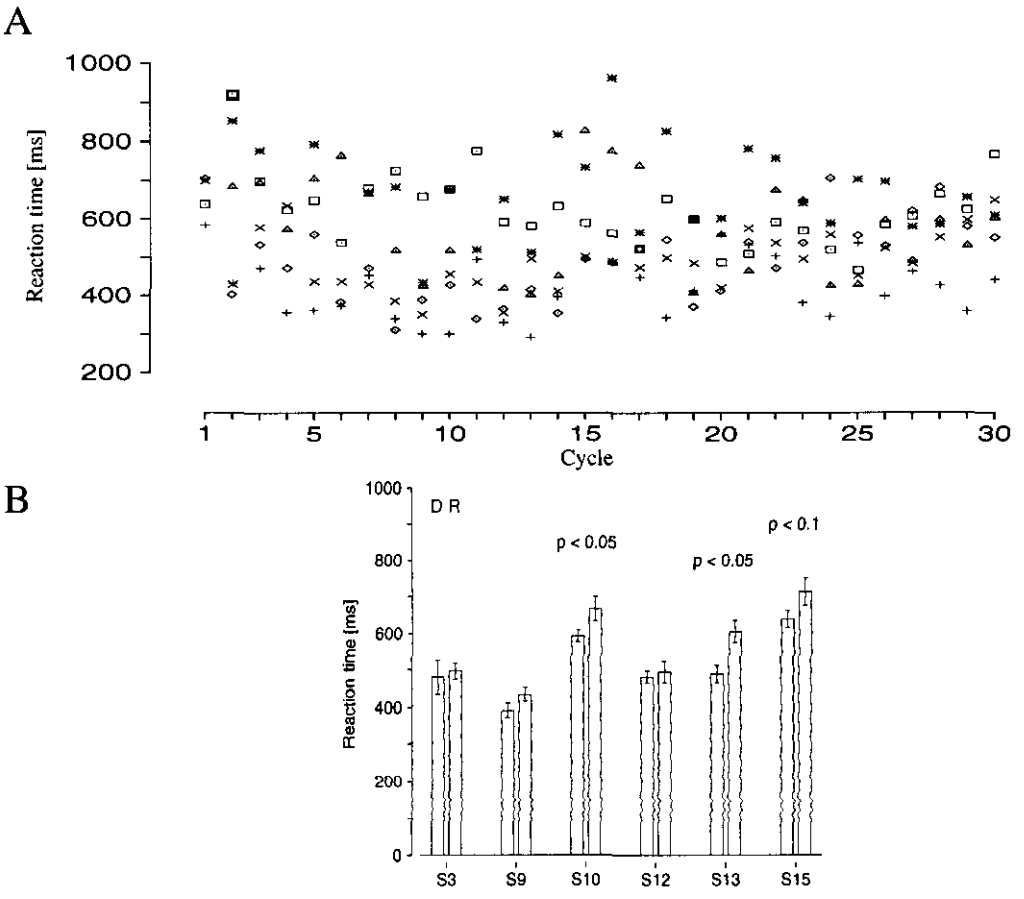

Figure 6.9: Reaction times versus D/R epochs

A: scatter plot of reaction times (all subjects) following face presentation versus (face) cycle for the 30 epochs. B: selective means of reaction times according to the classification of the epochs (D left, R right). Significant difference are marked by probability levels (S10: $T_{28} = 2.2$, $p \leq 0.05$, S13: $T_{27} = 2.4$, $p \leq 0.05$, and S15: $T_{26} = 1.7$, $p \leq 0.1$).

After each appearance of a face image, each subject responded within 300 to 1000 ms by pressing the appropriate button. The four reaction times that fell outside this range have been excluded from the analysis. The overall profile of reaction times as a function of (face) cycle is unremarkable (Figure 6.9 A). However, averaging reaction times according to the dynamical classification of the preceding pre-stimulus state revealed a pattern (Figure 6.9 B). Each subject responded faster on average in D epochs. This difference is significant in two subjects and weakly significant in one

subject.

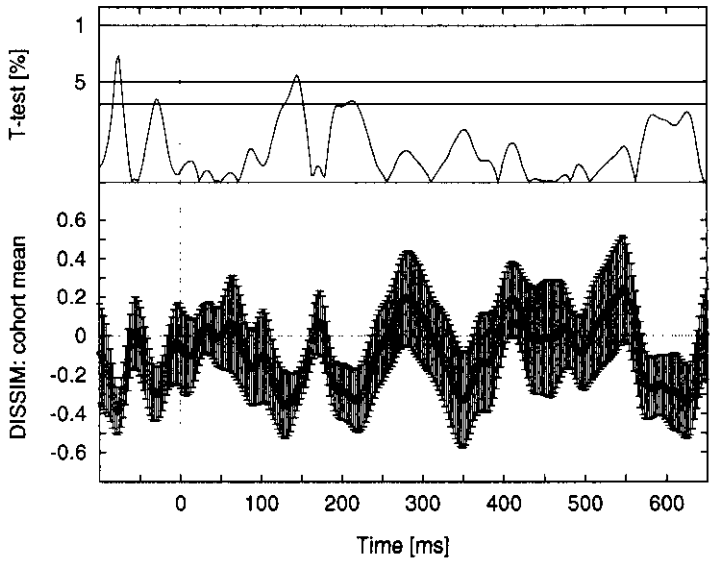

Figure 6.10: Signal power: classification according to RT
Impact on signal power with classification according to high and low reaction times (10%-line without label).

In order to assess further how strongly this correlation binds to the brain signals observed, a two-way classification of the 30 epochs according to fast and slow reaction times was performed. Each subject's epochs corresponding to the 15 lowest reaction times were grouped into one class and the ones corresponding to the 15 highest into a second class. For consistency with the evaluation above, the group of epochs associated with the 15 lowest (15 highest) reaction times entered the calculations as the 'D' ('R') epochs. In essence, this is a post-stimulus classification used to test whether variations in motor responses[8] are sufficient to explain the differential effect of signal power at long latency.

Selective averaging of epochs with the reaction time classification gives the results shown in Figure 6.10. According to the DISSIM calculations, the pattern presented in Figure 6.7 is lost, i.e. there is no significant differences in the power curves at long latency.

6.3.4 Investigation of correlations

Having established a classification of the pre-stimulus state based on dynamical features, it is reasonable to ask whether this classification has any particular status in relation to the experiment, the brain signals and behaviour. Clearly, it is not possible

[8]The variations are considerable in that the difference between the means of the low and high reaction time groups is highly significant for each subject.

to unambiguously prove the classification to be of unique relevance, given the large number of combinatorial[9] possibilities. The following investigations focus on a set of questions the answers to which should reveal more about the meaning and status of the classification.

Correlation with the image sequence

Possible correlations of the classification with the details of the image sequence were analysed. The main findings are summarised in Figure 6.11. There is no indication that the D-R classification correlates with either the length of the time intervals between image presentations, or with the position of a face within the image sequence. The image class of the preceding stimulus is also uncorrelated to the classification.

Despite the absence of any significant correlations, the idea of dissociations of effects was pursued a little further with respect to the proportion of images of each class in the preceding stimulus. Each subject's (face) epochs following the presentation of a (previous) face image[10] were grouped into one class and the ones following a (previous) non-face image into a second class. Selective averaging leads to the result shown in Figure 6.12. As is evident from the graphs, the DISSIM measure does not suggest any difference in signal power between the two classes of epochs, and the reaction times are not different for these groups.

[9]For example, the number of ways of selecting 13 epochs randomly out of 30 without replacement is given by the (binomial) coefficient:

$$\binom{30}{13} \approx 1.2 \times 10^8.$$

[10]The ratio is 14:16 epochs instead of 15:15 due to randomisation.

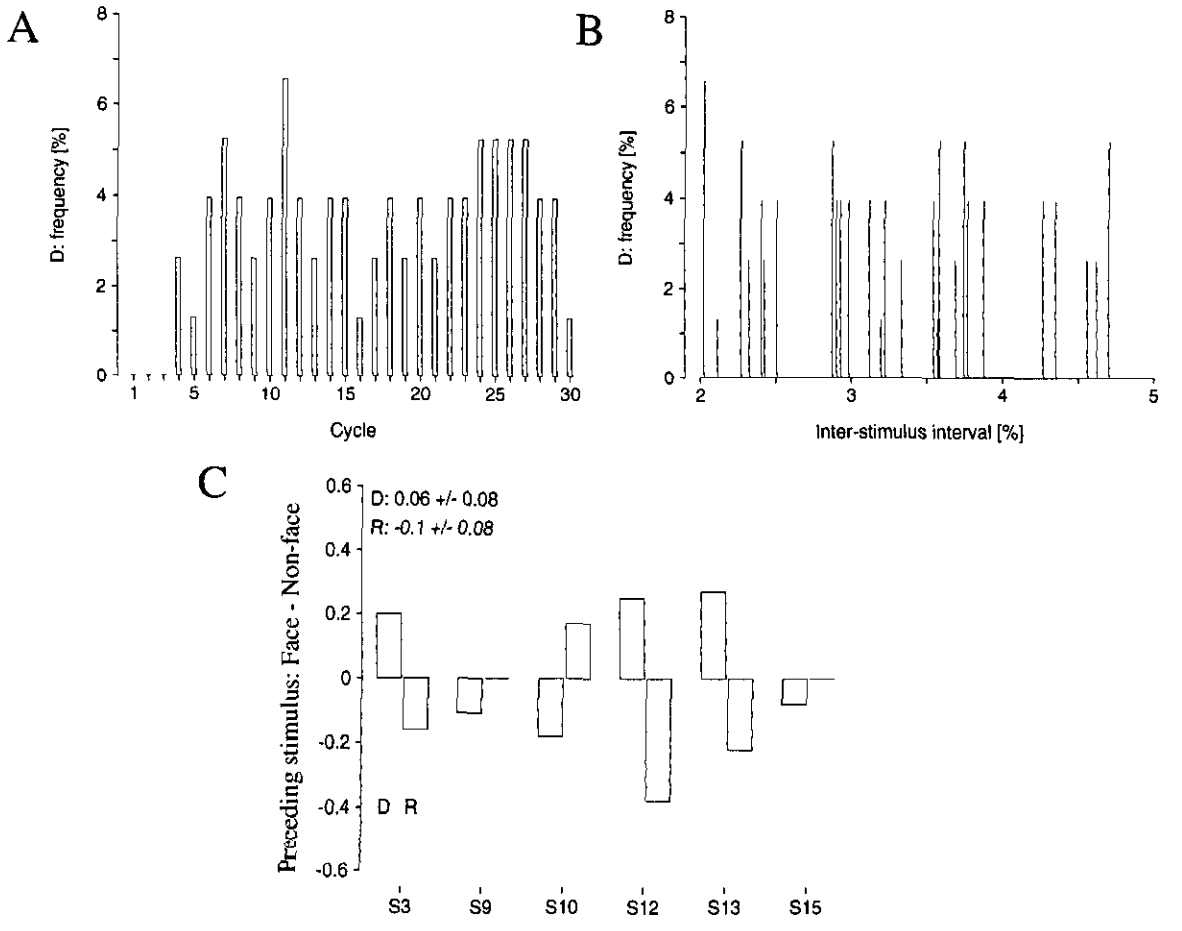

Figure 6.11: Epoch classification in relationship to the image sequence
A: Distribution of the D epochs as a function of the cycle number for the 30 epochs. The probability is normalised to the total number of 76 D epochs. B: Distribution of D epochs as a function of the inter-stimulus interval (the length of the inter-stimulus interval is normalised to the total length over all 30 cycles). There is no significant relationship between the occurrence of a D epoch and the time elapsed since the last stimulus. C: the relative proportions of face and non-face images in the stimulus preceding D and R epochs. The quantity plotted is $(N_f - N_{nf})/(N_f + N_{nf})$. Also shown are the cohort mean values, which are not significantly different from zero.

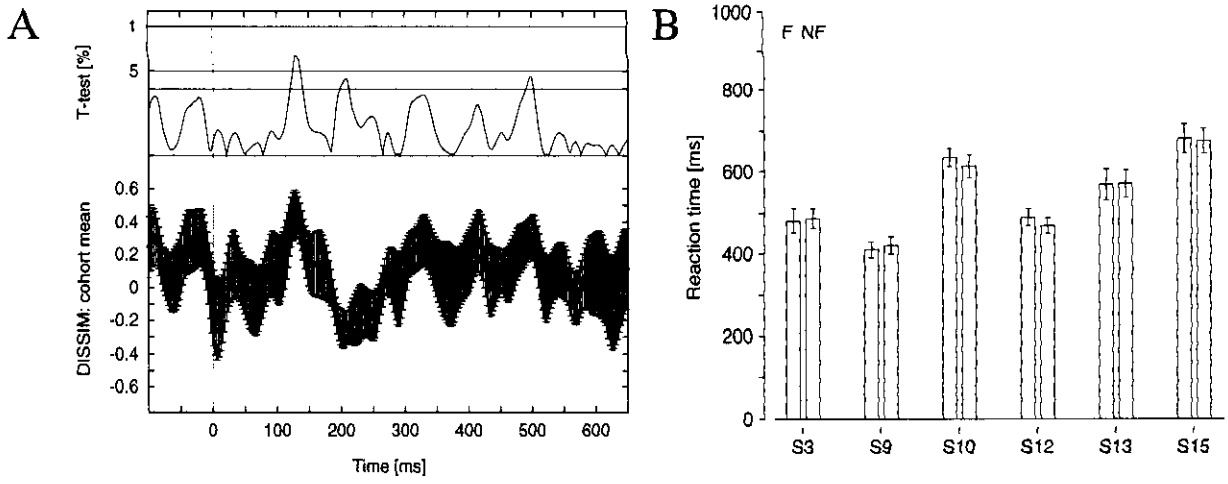

Figure 6.12: Relationship to the preceding image class

Effects on signal power (A) and reaction time (B) for a classification according to the nature of the preceding stimulus. In both cases, no differential effects are observable.

Correlations with spectral power

Correlations were sought with respect to the spectral properties of the signals. Spectral power[11] was calculated in the α, β, and θ bands, separately for D and R epochs.

The results of these calculations are given in Figure 6.13. There is no evidence that the dynamical classification correlates with the spectral power in that neither the D nor the R class of epochs is consistently associated with either higher or lower spectral power in any of the bands.

Notwithstanding the absence of clear evidence for a correlation, the graphs might suggest that D epochs are characterised by higher spectral power, specifically in the α-band. This feature was further investigated by considering a classification according to the α content of the epochs. Each subject's 15 epochs that were highest in α-band power were grouped into one class and the 15 lowest into a second class. For each subject, the difference between the means of the high and low α power groups is highly significant.

Selective averaging according to this α classification yielded the results given in Figure 6.14. The changes with respect to signal power are such that the consistent and significant pattern obtained initially is lost. In all but one subject, low α power is accompanied by faster key presses, however, the differences do not assume significance.

For reasons to be explained below, the same analysis was carried using the pre-stimulus θ instead of the α-band power. As with the α power, the difference between the mean high and low θ power is highly significant for each subject. The changes with respect to signal power are such that the pattern obtained initially is lost. The differences between the reaction times are neither significant nor consistent in sign across the subjects

[11]Spectral band powers for each epoch were calculated using the periodogram method (Appendix B, [N-6]), separately for subjects and channels within the detector site designated. Thus, each detector contributed two spectral estimates for a given band, which were averaged.

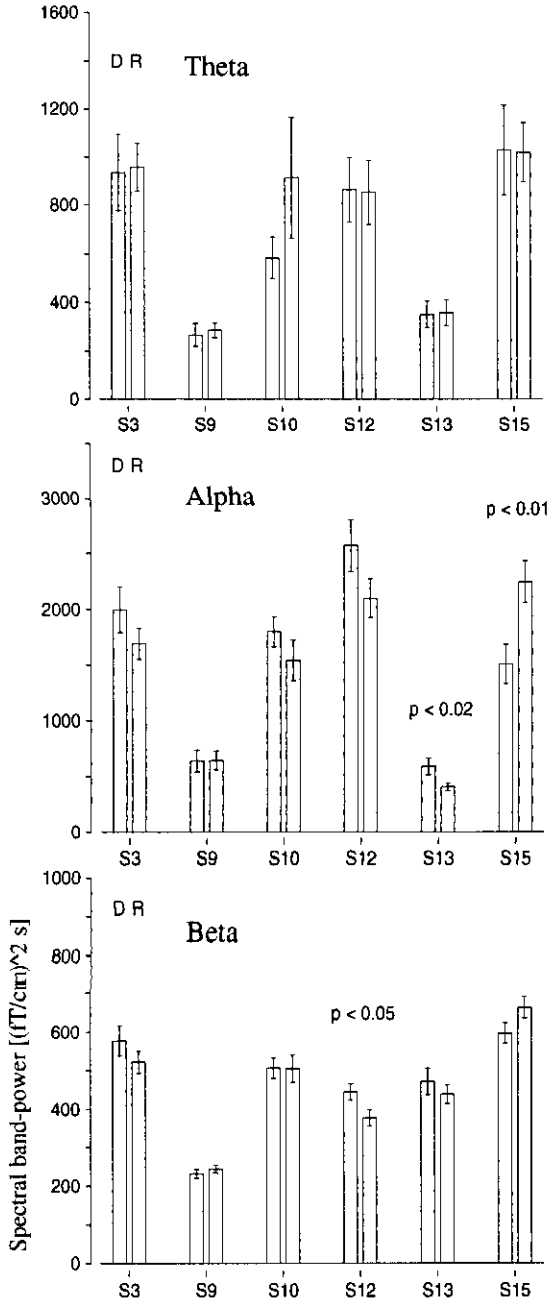

Figure 6.13: Spectral content of D and R epochs

Spectral content of D and R epochs in the α, β, and θ bands. For some individuals, differences between the two classes assume significance in the α and β bands (α S13: $T_{58} = 2.5$, $p \leq 0.02$, S15: $T_{58} = 2.8$, $p \leq 0.01$; β S12: $T_{58} = 2.3$, $p \leq 0.05$).

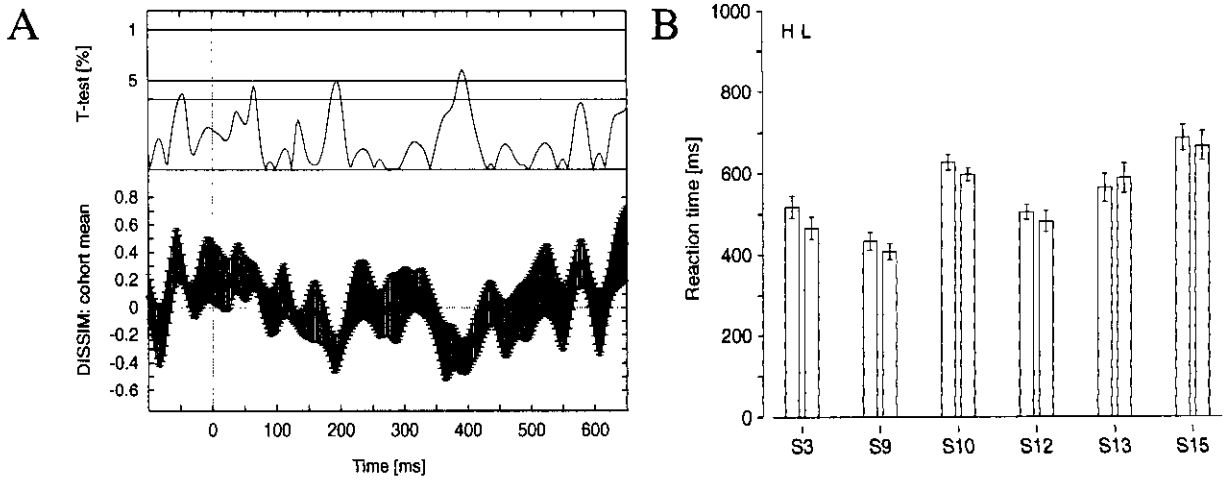

Figure 6.14: *Relationship to the α-band power*

Effects on signal power (A) and reaction time (B) for a classification according to the pre-stimulus α-band power (high and low power). In general, the effects seen initially are not reproduced using this classification.

6.4 Discussion

A classical measure of complexity in conjunction with a nonlinear framework has been used to identify a number of epochs from a large background group. These D epochs are stationary, at least within the 5s detection interval[12], rapidly decorrelating, and deterministic as well as nonlinear according to the assumption of surrogate testing. The D epochs are detectable predominantly in a small number of detectors over occipito-temporal and temporal regions across all subjects.

Pre / Post	D	R
Late power	low	high
Reaction time	fast	slow

Figure 6.15: Summary of observations

A pattern of significant differences in signal power between the selective evoked responses corresponding to D and R epochs has been obtained based on each subject's site with the maximum number of D epochs. Using the same classification scheme, a consistent although only partially significant effect has been obtained for the behavioural responses (reaction times) associated with the two classes of epochs. The findings are summarised in Table 6.15 simplified so as to highlight the main points. The power difference is present at long latency and does not affect the face-specific response at early latency.

Essentially, two questions arise from these results: a) what are the underlying neural mechanisms which have led to the distinction between D and R epochs, and b) what is the neurophysiological meaning of the effect observed for the post-stimulus signal power and reaction times? To date, only tentative answers can be offered because of the restriction of the analysis to one experiment only with a relatively small number of epochs.

With respect to the first issue, the most parsimonious view is to consider that both classes, D and R, represent a whole variety of dynamical states, and a given class is not necessarily associated with the the same underlying process. Each individual epoch could represent a multitude of simultaneous, possibly deterministic and partially

[12]This is broadly consistent with reports that stationarity can be detected up to 30 s (see [43]).

correlated processes. This could account for the recurrent broad bursts seen in the correlograms of the majority of R epochs. The multitude of processes could still be deterministic enough to make the epoch pass the second test as observed in numerical checks. Nevertheless, the processes in the two classes are distinct enough as a whole to cause a significant effect on the post-stimulus signals even though this is not reflected in pre-stimulus classifications based on conventional power methods or based on the parameters of the experiment.

At present, it is not known what causes the seemingly spontaneous transitions between the D and R states. Clearly, the transitions are not induced by the sequence of images or other parameters of the task, but could be related to inevitable fluctuations in vigilance or task attendance, measured in term of the θ-band[13] activity according to conventional electroneurophysiology. As stated above, considerable fluctuations in θ-power have been found within each subject. However, neither the differences between the mean θ power associated with the D and R epochs nor the classification according to low and high θ suggest that the D versus R classification is related to fluctuations in vigilance according to these calculations.

Regarding the second question, it is noted that the effect of P300 enhancement by high pre-stimulus α-power observed in previous studies is also detectable in the present study. The effect may be observed by comparing high and low α epochs yielding a broad interval centred around 300 ms where the high α P300 amplitudes are greater than the corresponding low α P300 amplitudes, as predicted by previous studies[14] (compare Figures 6.7 and 6.14). Simultaneously, the effect observed initially is destroyed, albeit not completely because the classification has produced an imbalance where D states have slightly more α power than R epochs in some subjects. Thus, the two effects seem to be dissociated.

Taken together, the results suggest that the phenomenon observed at long latency is not related to the task parameters, the fluctuations in vigilance, or the effects observed in previous pre-stimulus studies. In order to offer a hypothesis, a brief excursion is needed.

▷ **Excursion: the contextual modifications of face processing** It is known that certain behavioural responses associated with word, or more generally language pro-

[13]Some researchers have included the δ-range above 1.5 Hz [129]. For consistency, the same provision was used in calculations not reported here. The results are qualitatively identical to the case of using only θ activity.

[14]The channels determined by the classification are not optimal with respect to the P300 effect, which is more pronounced over other regions.

cessing extend to the processing of faces. Specifically, persistent repetition-priming[15] effects have been found in the behavioural responses to familiar faces that must either be identified or discriminated from unfamiliar faces. The effects are usually revealed in lower recognition thresholds, decreased reaction times, or increased accuracy of identification of primed faces. An analogue of the semantic priming for words has also been shown to exist for faces, in that decisions of face familiarity are facilitated when the test face is preceded by a face to which it is related (e.g. a familiarity decision for Oliver Hardy is facilitated by a previous image of Stan Laurel).

Recently, electrophysiological studies of face processing have investigated whether these non-linguistic contextual effects are associated with changes in the neural activity. Specifically, EEG studies have given evidence that the late components in the responses following face presentation can be modulated by priming. These components are found between 320 and 560 ms after stimulus onset with potentials peaking around 450 ms. In general, there is a complex, paradigm dependent topography which is widespread but mainly over bilateral temporo-parietal, and frontal regions. These components are reduced in amplitude when they follow the presentation of a primed face in paradigms requiring the subjects to make a decision.

These effects can be induced by repetition of identical faces with a time interval that may be less than a second but may be up to several minutes. Priming may also be induced by repetition of facial expression, where the second image of a pair of images presented sequentially is primed because the facial expression depicted matches the one of the first image. The same phenomenon is also observed within a semantic context, where, for instance, the amplitude of the late potential elicited by the face of a known politician is smaller when preceded by the face of another known politician than it is when preceded by the face of a known person belonging to a different semantic category (e.g. an actor).

These late components are usually referred to as 'N400-like' or 'face-N4' in a functional sense, because of the similarity of some of the features with the much studied N400(m) component elicited by words. Depth electrode studies suggest that the face-N4 generation involves widely distributed cortical networks overlapping to some extent with networks participating in word-N4 generation. The functional significance of the N400-like components has not been resolved. According to the most common, though not unchallenged hypothesis, N400-like components are enhanced when the evoking

[15]The term 'priming' is used in the sense of 'preparing' or 'providing with information beforehand'. Usually, 'repetition-priming' refers to a paradigm in which there is no explicit requirement for a decision to be made regarding context and/or meaning.

stimulus activates a memory representation other than one that has been primed (the excursion is based on [12, 13, 17, 36, 55, 56, 110, 118]). ◁

One is tempted to postulate, on the basis of a simple comparison of the power and (weak) behavioural effects, an association between D and primed states on one side, and R and unprimed states on the other. Then, one could interpret these mental states as states of varied expectation providing different contexts for incoming information, given that the correlations with respect to reaction times and signal power bear resemblance with the priming phenomena observed in psychological and neurophysiological face studies. In this sense, deterministic D states are associated with some sort of expectation or context with respect to which the incoming face image is processed, yielding a small amplitude at high latencies and a speeded reaction time. Non-deterministic R states are then associated with the absence of expectation or context. In this interpretation, states of expectation might reflect a reduction of the system's overall diversity by focusing on fewer processes, thereby inhibiting unnecessary activity. This in turn might have been detected as an increase in apparent determinism.

With this interpretation, the absence of D states in the first 3 epochs shows that the occurrence of states of (face) expectation has low probability at the beginning of the experiment, which is intuitively reasonable. The data also suggest that the occurrence of a state of expectation was not influenced by the preceding image. This makes it unlikely that there is a simple relationship between the state and the memory imprint of the previous image. The state of expectation might act as a sort of 'template' against which the stimulus is primed and processed. It might be useful to label the D state as endogenous priming.

As far as the spontaneous transitions between D and R states is concerned, the participation of large networks in occipito-temporal cortex is suggested by the spatial extent of deviations of post-stimulus waveforms as well as by the spatial extent of occurrence of deterministic epochs. Again, faces are a crucial 'entry point' into social interactions, and the ever adapting brain might find useful a rhythm of waxing and waning anticipation of faces.

Conclusion

The results suggest that the late components associated with face processing contain significantly different 'histories' not seen when using conventional techniques of averaging. Much has to be clarified, but there is some indication that the methods derived

from nonlinear theories are potentially useful in studying the neural dynamics associated with the processing of facial images. It is suggested that those methods in conjunction with the pre-stimulus approach may provide more information on the hidden mechanisms in large scale networks which mediate the perception of faces within a variable context.

6.5 Addendum

In this addendum, the dynamical approach chosen for the pre-stimulus classification is further specified. The approach emphasises two general properties of a signal representing an underlying process, namely stationarity and determinism. The latter is relatively unexplored [5, 106]. The approach relies on the technique of state space reconstruction used in different neurophysiological contexts (e.g. [121]).

In the first section of the addendum, the reconstruction method is introduced. In the second section, two tests are developed. These are used in turn to divide the epochs into two classes; rejected R and deterministic D, where the latter contains only those epochs which pass both tests. The methods involved in the tests have been validated using known dynamical systems (referred to as model systems) derived from mathematical or physical considerations. They yield time series supposed to reflect generic dynamical properties, and are very common as test cases in all approaches using techniques similar to the ones here (e.g. [1]). In the example given below, one of these systems is named explicitly which is the Ikeda system or Ikeda map. The map iterates a vector in $\mathcal{R}^2$ ($x_{n+1} = f(x_n)$) yielding a two component (2-vector) time series. The map is usually defined in terms of a complex variable z [66].

$$\text{Ikeda map: } z_{n+1} = 1 + 0.9 z_n \exp\left(i0.4 - \frac{i6.0}{1 + |z_n|^2}\right).$$

6.5.1 State space reconstruction

The concept of state space reconstruction is based on the assumption that an experimentally observed time series has been generated by a low-dimensional dynamical system, i.e. a system which is described by the time evolution of a small number of variables forming a trajectory in some suitable space. The observed time series is seen as an 'image' of the trajectory under some function Φ constituting the measurement process. The goal is to re-build the original trajectory by a set of vectors extracted from the time series. These vectors are usually defined as elements of an Euclidean space $\mathcal{R}$. Mathematical theories are needed to specify under which conditions the reconstruction is faithful, i.e. the reconstruction reflects the geometrical and dynamical characteristics of the underlying dynamical system [111].

Recently, a scheme called time-delay embedding has attracted considerable theoretical and experimental interest [113, 149]. It has been shown mathematically that the scheme yields faithful representations under fairly general assumptions regarding the

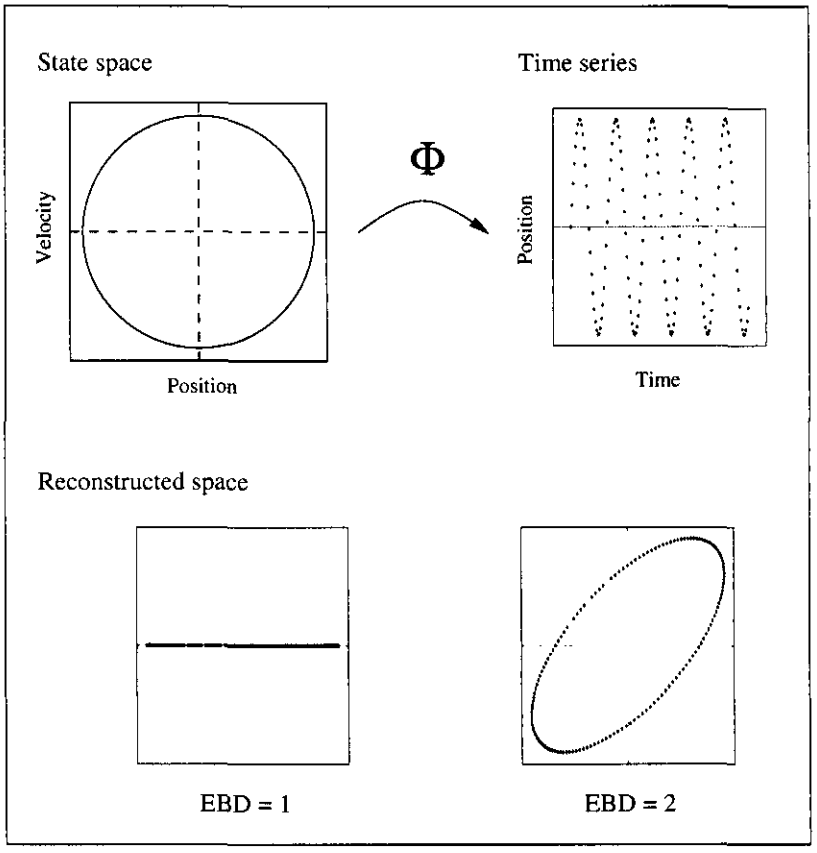

Figure 6.16: State space reconstruction

The figure visualises the embedding process using a one-dimensional simple harmonic motion as an example. The dynamics are characterised by a trajectory (circle) in a two-dimensional state space spanned by the position and velocity axes (upper left). The system is observed via a measurement process symbolised by Φ, here arbitrarily chosen to be observation of the position. The measurement yields a discrete time series (upper right). The sequence of values measured is transformed into vectors (or points) of an Euclidean space of a given dimension EBD according to the embedding rule (lower left and right). If faithful, the transformation yields a reconstructed trajectory which can be used to study the dynamics of the system.

underlying system and the map Φ representing the measurement [136]. The time-delay embedding process is stated here as a rule [68, 121] (see also Figure 6.16):

> Given an experimental time series $(s_1, s_2, \ldots, s_{N_t})$ corresponding to measurements regularly spaced in time. Each measurement comprises ν simultaneous observations, i.e. $s_i \in \mathcal{R}^\nu$. From the s_i, a sequence of vectors (or points) $x_j \in \mathcal{R}^{m\nu}$ is obtained by taking
>
> $$x_j = [s_j, s_{j+L}, s_{j+2L}, \ldots, s_{j+(m-1)L}].$$
>
> There are $N_t - (m-1)L$ vectors, the value being dependent on the parameters L and m known as the embedding lag and embedding dimension respectively.

In theory, there is a considerable freedom in choosing the embedding lag and the embedding dimension, requiring only a lower bound for the latter in order to achieve a faithful representation. In practice, given a finite data size, both parameters have to be estimated from the data as explained below. The embedding dimension m is also denoted by EBD.

For the present work two simultaneous measurements are given by the field gradients $\partial\vec{B}_z/\partial x$ and $\partial\vec{B}_z/\partial y$ at each detector site, i.e. $\nu = 2$. This allows the use of a local approach, where simultaneous measurements obtained from different sites are not considered [122].

For illustration, an embedding scheme is described here for a time series of length 10 ($N_t = 10, s_i \in \mathcal{R}^\nu$) and $L = 2$. Chosing embedding dimensions of 3 and 4 generates 6 (=10 − (3 − 1) × 2) and 4 (=10 − (4 − 1) × 2) vectors respectively in the reconstructed 3 and 4 dimensional spaces.

$$\left.\begin{array}{rcl} x_1 &=& (s_1, s_3, s_5) \\ x_2 &=& (s_2, s_4, s_6) \\ x_3 &=& (s_3, s_5, s_7) \\ x_4 &=& (s_4, s_6, s_8) \\ x_5 &=& (s_5, s_7, s_9) \\ x_6 &=& (s_6, s_8, s_{10}) \end{array}\right\} \begin{array}{l} \text{EBD} = 3 \\ N = 6 \\ x_i \in \mathcal{R}^{3\nu} \end{array} \quad \text{and} \quad \left.\begin{array}{rcl} x_1 &=& (s_1, s_3, s_5, s_7) \\ x_2 &=& (s_2, s_4, s_6, s_8) \\ x_3 &=& (s_3, s_5, s_7, s_9) \\ x_4 &=& (s_4, s_6, s_8, s_{10}) \end{array}\right\} \begin{array}{l} \text{EBD} = 4 \\ N = 4 \\ x_i \in \mathcal{R}^{4\nu}. \end{array}$$

The existence of these sets of vectors leads to three notions:

Nearest neighbour (NN) of a vector $x_i \in \mathcal{R}^{m\nu}$. The nearest neighbour of x_i is the vector x_j, $i \neq j$ which is at the smallest Euclidean distance from x_i.

Time evolution of a vector x_i. The time-ordered sequence of measurements gives rise to a trajectory in reconstructed space with time as a parameter: $(x_i \mapsto x_{i+\delta} \mapsto x_{i+2\delta} \ldots)$. Here, the increment δ between successive vectors is chosen equal to 1, where x_{i+1} is called the time image of x_i.

Dimensional image of a vector x_i upon incrementing the embedding dimension by 1. This is the higher-dimensional vector with the same index. If an index is available in dimension m but not in dimension $m + 1$, the dimensional image is not defined.

In this context, it is convenient to introduce definitions for a centre and an extent of the data by considering an embedding of ν dimensional data with $m = 1$. Obviously,

this yields N_t ν-dimensional vectors x_i for which for the centre and extent are defined as

$$< s >= \frac{1}{N_t}\sum_{i=1}^{N_t} x_i \text{ and } \ll s \gg = \sqrt{\frac{1}{N_t - 1}\sum_{i=1}^{N_t} \|x_i - < s >\|^2} \tag{6.2}$$

respectively. In the case of scalar measurements ($\nu = 1$), the usual mean and standard deviation of the time series are recovered.

Estimation of the embedding lag

The choice of embedding lag L influences strongly the extent to which the embedded trajectory reflects the underlying system. A very low value promotes correlations between the vectors available and prevents the acquisition of information about transitions between vectors. On the other hand, a very high value can either reduce dramatically the number of vectors available, or decorrelate their components to such an extent that the initial dynamics is no longer represented by the finite number of vectors. According to the most commonly used method, the appropriate embedding lag may be calculated as the smallest positive integer k_0 for which the autocorrelation coefficient

$$a_k = \frac{\sum_{i=1}^{N_t}(s_{i+k} - < s >)(s_i - < s >)}{\sum_{i=1}^{N_t}(s_i - < s >)^2}, \; k \geq 0 \tag{6.3}$$

of a given scalar ($\nu = 1$) time series is zero [1]. (Note that k_0 is synonymous with the previously defined embedding lag L.) It is well known that, on average over the observations, s_i and s_{i+k_0} are linearly independent. Thus, the suggested rule stipulates a lag corresponding to the shortest linear time scale inherent in the series.

In the case of a vector time series, it is suggested here that a_k is estimated by

$$a_k = \frac{\text{Trace}\left(\frac{1}{2}M^T M_k\right)}{N_t - 1} \tag{6.4}$$

where

$$M = \begin{pmatrix} \tilde{s}_1^1 & \tilde{s}_1^2 \\ \vdots & \vdots \\ \tilde{s}_{N_t}^1 & \tilde{s}_{N_t}^2 \end{pmatrix}, \text{ with } (M_k)_{i,j} = M_{i+k,j} \tag{6.5}$$

is the covariance matrix associated with the component time series $\tilde{s}^j$ standardised to zero mean and unit standard deviation ($i = 1, \ldots, N_t$, $j = 1, 2$). The matrix M is extended in the obvious way if $\nu > 2$. In effect, this new quantity neglects cross-correlations between the component time series. Its definition has been motivated by the properties of the detector system used, i.e. two gradiometers at each site which measure independent components of the fields. It is noted that $a_0 = 1$ holds in both cases.

Estimation of the embedding dimension EBD

On theoretical grounds, the number of embedding dimension has to exceed a certain value if the system is to be recreated, but there is no upper bound. Practically however, an embedding dimension close to the minimum needed for faithful embedding is desirable. This is because high dimensional spaces become very sparsely populated by the finite vectors making calculations prone to noise corruptions.

The method chosen here to estimate the embedding dimension has become known under the name of the false nearest neighbours algorithm FNN [1, 82]. It is designed to seek an appropriate embedding dimension that is as low as possible. It is based on a simple geometrical consideration. In an embedding space that has too low a dimension to unfold the dynamics properly, points are found which are close to each other, but which move apart in the next higher dimensional space (see the two embeddings in Figure 6.16). The value of FNN is calculated as follows (from [82]).

False nearest neighbour (FNN) algorithm in m dimensions (6.6)

1. Let x and x' be a vector and its nearest neighbour in the reconstructed space of dimension m. Denote the distance between the two vectors by $D_m = \|x - x'\|$.

2. Compute the embedding for $m+1$ dimensions and identify the dimensional images of x and x' as y and y' respectively. Denote their separation by $D_{m+1} = \|y - y'\|$.

3. Decide whether the following three inequalities are true or false:

$$\begin{aligned} \sqrt{\frac{D_{m+1}^2 - D_m^2}{D_m^2}} &> c_a && \text{(cond1)} \\ D_m &< c_b \ll s \gg && \text{(cond2)} \\ D_{m+1} &> 2c_b \ll s \gg && \text{(cond3)} \end{aligned}$$

   where c_a c_b are two thresholds and $\ll s \gg$ is as defined earlier.

4. Count x' as a false nearest neighbour if condition 1 is true and either but not both of conditions 2 and 3 are true.

5. Repeat steps 1 to 4 for all vectors in m dimensions and calculate the measure

$$\text{FNN} = 100 \times \frac{\text{number of false nearest neighbours}}{N}$$

   where N denotes the number of vectors for which the corresponding dimensional images exist.

The condition cond1 quantifies the growth of distance with increase of the embedding dimension. The conditions cond2 and cond3 are corrections needed because of the finite data size in all practical applications, where nearest neighbours are not necessarily close to each other, specifically in higher dimensions.

In order to estimate the appropriate value for the embedding dimension, the measure FNN is calculated for $m = 1$ and then for successively higher values of m. The lowest dimension for which the percentage of false nearest neighbours becomes less than 1% is considered the minimal faithful embedding dimension. Extensive numerical studies have found $c_a = 20.0$ and $c_b = 0.8$ to give robust and reliable dimension estimates in that they make the algorithm reasonably insensitive to variations of the embedding lag.

EBD	1	2	3	4	5	6	7	8
FNN [%]	95.2	19.2	2.71	0.251	0	0	0	0

Table 6.2: FNN measure

FNN method applied to a scalar embedding of the Ikeda map. A time series of a length of 2000 points has been used to replicate a previous result indicating that a 4 dimensional space (FNN<1%) is needed to unfold the dynamics of this map from the its x-component (see remarks in [82, p 3408]). In contrast, a ($\nu = 2$) vector embedding of the Ikeda map gives FNN equal to 0 for all dimensions, indicating EBD = 1 according to the 1% rule. This exactly reproduces the map.

The implementation of the algorithm has been verified using known dynamical systems. Typically, a profile of false nearest neighbours is obtained as shown for the Ikeda map in Table 6.2. An extensive survey using data from the experiment showed that embedding dimensions higher than 5 were not needed, and the maximum dimension considered was limited to 8.

6.5.2 The tests

Test of stationarity

The purpose of this test is to give an indication as to whether an epoch can be considered as stationary in the sense that its mean, variance, and autocorrelation remain constant over time. A time series with this property is usually called weakly station-

ary[16] [86]. The test uses the measure ST defined as:

$$\mathrm{ST}_k = k a_k^2, \; k \geq 0, \tag{6.7}$$

and is based on the observation that

$$\lim_{k\to\infty} \mathrm{ST}_k < 1 \;\text{ implies }\; \lim_{K\to\infty} \sum_{k=1}^{K} a_k^2 \;\text{ is finite}$$

for the autocorrelation coefficients a_k using a standard convergence argument. The expression on the right is a sufficient condition for weak stationarity in the case of a scalar time series [51]. The same argument is applied here for the a vector time series thereby neglecting cross-correlations of the component time series.

Length	1000	1500	2000	2500	3000	10000
k_c/Length (mean)	0.82	0.84	0.84	0.85	0.85	0.87

Table 6.3: ST: onset of convergence

For each of 1000 examples of the 2-vector Ikeda map of the lengths listed, the value k_c for which $\mathrm{ST}_k < 1$ holds for all lags greater than k_c was calculated. The Table lists the means normalised to the lengths. In each case the standard deviation was ≈0.002.

Following this reasoning, a test of stationarity amounts to a test as to whether the measure ST is bounded by 1 for large k. In order to establish how to interpret 'large' in the case of finite data size, an extensive survey was carried out using model time series with lengths between 1000 and 10000 points. For each system, the number k_c which serves as the minimum lag which conforms to the 'large' criterion was established empirically by studying 1000 examples, i.e. the mean value for which $\mathrm{ST}_k < 1$ holds for all $k > k_c$ was computed. For the span of lengths relevant to the present study (≈2000), the mean of the ratios between k_c and the length of the time series are approximately constant (Table 6.3). Based on this observation, the calculation were repeated for a length of 1872 points corresponding to the epoch available, yielding a maximum ratio very close to 0.9. This ratio, called the onset of convergence, was taken to establish the rule for the first test:

Test 1: *Given an epoch, classify it as non-stationary if $ST_k > 1$ holds for some value of k greater than an empirical maximum determined as 0.9 times the length of the epoch.*

[16]The condition reads in standard notation for continuous times t and t':

$$\mathrm{E}[X(t)] = \mu, \; \mathrm{E}[X(t) - \mu]^2 = \sigma^2, \; \mathrm{E}[(X(t) - \mu)(X(t - t') - \mu)] = \sigma^2 \rho(t'), \text{ for all } t \text{ and } t'$$

with the expectation E, and a function, ρ, only dependent on the lag t'.

The test is uncritical in that the onset of convergence is the lower the more a signal is corrupted by noise. Stationary epochs enter the next test.

Test of determinism

The quantitative assessment of an epoch's inherent determinism is based on its representation in reconstructed space, and comprises three steps. In the first step, each epoch is assigned a measure which quantifies the amount of determinism (or continuity, or lack of stochastic behaviour) present in the dynamics. The measure is called the translation error TRE [163].

In the second step, a number of surrogate replications is constructed from the epoch. The surrogating chosen here is a shuffle operation applied to the data such that if the original data is compatible with a Gaussian process observed via some nonlinear function, than the amount of determinism will not change significantly upon shuffling. The surrogate method has become known under the name Amplitude Adjusted Fourier Transform AAFT [155].

In the third step, the measure TRE is calculated for each of the surrogate replications to yield an empirical estimate of the amount of determinism which can be achieved with a correlated noise process compatible with the original data. The significance of the difference between the estimate and the initial TRE value is then assessed with a simple z-score like expression.

All three steps are repeated for a successive number of embedding dimensions, and the epoch is accepted as representing a process that is significantly deterministic if its TRE values are different from the surrogate replications for all embedding dimensions equal to or greater than the one needed for faithful representation.

The translation error TRE The measure reads (adapted from [163]):

Translation error (TRE) algorithm in m dimensions (6.8)

1. Let x and x' be a vector and its nearest neighbour in the reconstructed space. Denote their time images by y and y' respectively.

2. Define translation vectors $v = y - x$ and $v' = y' - x'$ and calculate the mean value

$$\bar{v} = \frac{1}{2}(v + v').$$

3. The local translation error at x is then defined as:

$$\mathrm{TRE}(x) = \frac{1}{2}\left(\frac{\|v - \bar{v}\|_m^2 + \|v' - \bar{v}\|_m^2}{\|\bar{v}\|_m^2}\right)$$

4. Repeat steps 1 to 3 for all vectors in m dimensions and calculate a global translation error as the mean over all local ones:

$$\mathrm{TRE} = \frac{1}{N}\sum_{i=1}^{N}\mathrm{TRE}(x_i)$$

where N denotes the number of vectors for which the corresponding time images exist.

Essentially, the measure quantifies the normalised mean squared displacement experienced by the vectors in m dimensions under the action of the (hypothetical) function $x \mapsto y(= f(x))$. Assuming that this function is continuous, the translation errors become arbitrarily small if x and x' are sufficiently close together, which immediately follows from the ϵ, δ-definition of continuity in normed spaces:

$$\|v - v'\| = \|y - y' - (x - x')\| \leq \|y - y'\| + \|x - x'\| \leq \epsilon + \|x - x'\|$$

for $\|x - x'\| \to 0$, which entails

$$\|v - v'\| \to 0.$$

In contrast, a translation error cannot become arbitrarily small on average for a system with a stochastic content. The random walk problem is an example. For a random walk (in one dimension) the mean squared displacement is proportional to the number of steps of the walk ($\mathrm{E}[x^2] = 1$ upon normalisation for one step).

The measure TRE is zero for the case of a constant map $x \mapsto x + c$ for some vector c. It is 1 if the mean squared displacement equals the squared mean displacement, and can assume any higher value up to a maximum set by the finite set of vectors.

The amplitude adjusted Fourier transform AAFT This technique allows for testing against the null hypothesis that the data measured is linearly autocorrelated Gaussian noise observed through a static, nonlinear transform. The amplitude spectrum of the data is left unaltered by the AAFT method. The frequency spectrum is left unaltered only for large sample sizes [138, 155]. The AAFT algorithm used to generate a surrogate replication of a time series is visualised in Figure 6.17. It consists of three simple steps employing rank matching between the data and Gaussian noise.

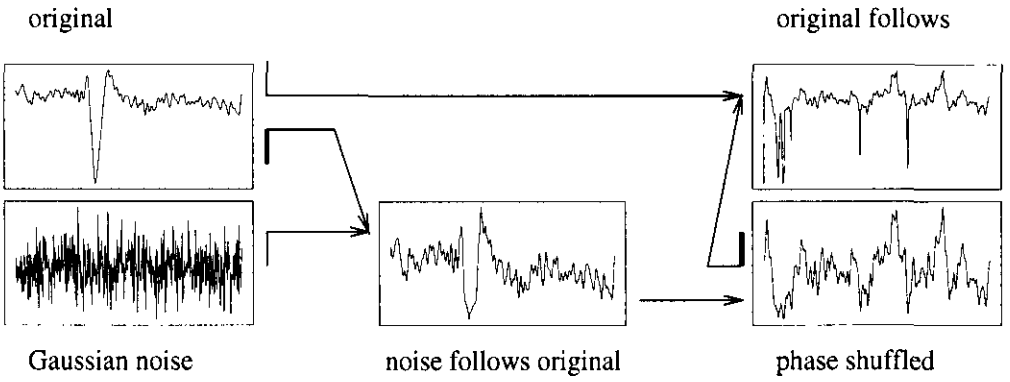

Figure 6.17: AAFT scheme

Left: a scalar time series $(s_i,\ i = 1, \ldots, N)$ and a Gaussian signal $(g_i,\ i = 1, \ldots, N)$ generated to be of the same length.

Middle: the noise is matched according to the rank of s to give a noise signal $\tilde{g}$ obtained from g. For example, if s_n is the 3rd largest value of the series s, than $\tilde{g}_n$ is chosen as the 3rd largest value of the series $\tilde{g}$.

Right: $\tilde{g}$ is phase shuffled by randomising the phases of the Fourier coefficients (lower), and s is matched according to the rank of the phase shuffled noise signal (upper), yielding the desired surrogate replication s' of the original time series.

The illustration uses an evoked (face) response from FT1. Pre-stimulus epochs which 'look' too much like noise, are useless for a visual demonstration.

The z-score statistic for the translation error Z-TRE Following general recommendations (e.g. [126]), a z-score like quantity Z-TRE is used here for the comparison between the translation errors associated with the data and its surrogate replications:

$$\text{Z-TRE} = \frac{\overline{\text{TRE}}_{srg} - \text{TRE}}{\Delta\text{TRE}_{srg}} \tag{6.9}$$

where $\overline{\text{TRE}}_{srg}$ and ΔTRE_{srg} denote the mean surrogate's translation error and the corresponding standard deviation of the samples respectively. It is generally agreed that expressions like this are best suited for surrogate comparisons, where one instantiation of a measure is compared against a mean obtained from replications. However, currently no precise prescriptions exist.

The test is now framed in terms of Z-TRE. It is chosen to be directional (>), reflecting smaller translation errors for a truly deterministic process compared to its (Gaussian) surrogate replications. A Z-TRE value greater than 1.65 is accepted as indicating a significant difference between the translation error associated with the original and surrogate data for a given embedding dimension. The threshold corresponds to the 5% right tail probability of the normal distribution.

The second test, which assesses the deterministic nature of the epoch, can be stated as follows.

Test 2: *Given an epoch, classify it as deterministic if Z-TRE* > 1.65 *holds for all embedding dimensions equal to or greater than the faithful embedding dimension estimated with the FNN method.*

As is usual in such analyses, it is assumed that an epoch passing this test represents an underlying deterministic and nonlinear process, though the latter might not always hold true [138].

The approach has been validated using known model systems. Examples and main results are given in Figure 6.18.

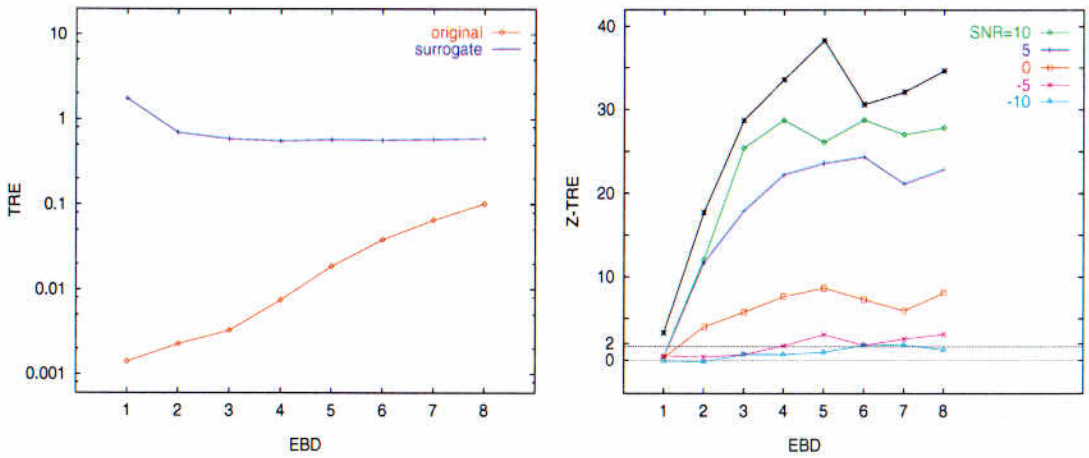

Figure 6.18: TRE and Z-TRE

Left: TRE values for the Ikeda map (red) and one of its surrogate replications (blue) as a function of the embedding dimension. Right: Z-TRE as a function of the embedding dimension for various signal-to-noise ratios (SNR in [dB]) using 30 surrogate replications. The faithful embedding dimension is 3 for all noise levels according to the FNN method. In general, the model systems are identified as deterministic for noise levels better than SNR = 0. The noise free case is depicted by the black line, in which case the faithful embedding dimension is 1. The threshold of 1.65 is denoted by a dotted line. The graphs are based on a time series of a length of 2000 points using 2-vector embedding ($\nu = 2$) with an embedding lag estimated from ST.

6.5.3 A remark on the implementation

Despite the subtlety of the underlying mathematical theories, the algorithms used here are numerically straightforward in general, with the implementations following directly the expositions given above. Only the search for nearest neighbours is computationally very demanding. Algorithms exist and have been used to alleviate the $\sim N^2$ problem of finding the nearest neighbours for all vectors in a given reconstructed space [47]. However, these algorithms are optimised for a situation with one space and a huge number of searches, whereas, for this work, many spaces have to be considered. The problem is not yet resolved, and has posed a limitation on what could be achieved for this thesis. In particular, it has restricted the number of sites that could be investigated thoroughly.

Chapter 7

Conclusion and future work

This thesis has been concerned with the neuromagnetic fields associated with the processing of faces and sentences in humans. In four, largely independent sub-projects, results were obtained using novel methods of analysis to extract neurophysiologically relevant information.

The research has led to four main suggestions:

- there are early latency face-specific neural systems in humans that are predominantly in right inferior occipito-temporal cortex.
- MEG recordings are useful in the study of autism in that autistic subjects exhibit different responses to normal subjects following face presentation.
- phase-locked γ-band activity has a specific role in semantic processing.
- the late components of responses to face images are modified by endogenous priming, which is detectable before stimulus arrival.

The new methods for treating magnetoencephalographic data comprise:

- an improved parameterisation of signal power over regions of interest.
- the use of re-sampling strategies to achieve statistical assessment of spectral coefficients within subjects.
- a pre-stimulus approach for the study of face processing using a tailored state-space representation approach.

A detailed discussion of these issues has been given in the previous chapters. It remains to point to the weakness of a particular approach, suggestions for improvement, and what should be done in the future.

Face processing

The precise processing role of the strong face-specific response is unclear. Nor is it clear how unspecific responses at earlier latencies evolve into the face-specific ones that are observed. Studies that are not reported in this thesis have been started with the aim of establishing the extent to which the face-specific component reflects a structural encoding mechanism in the cortex. A variant of task FT1 has been used in which several types of (partial) face images as well as images of control objects are presented. The partial faces are based on the boys' faces in association with ellipsoidal masks such that either the inner features of the face (eyes, nose, mouth), or the outer features of the face (lower part of the chin, upper part of the forehead, ears) are visible. The preliminary analysis of the data suggests a differential effect between the full and inner faces.

For the future, experiments are planned involving more face-like control stimuli, e.g. *moderately scrambled, but identifiable faces, cartoon faces and images showing* only a person's eyes or mouth. The use of Mooney faces is also planned [104]. A Mooney face is a peculiar 'silhouette' face which has the remarkable property that the perception of the face is strongly reduced when the image is turned upside down and therefore must to some extent decouple the face percept from standard structural encoding. It is hoped that this kind of stimulus might be a sensitive probe for face-specific responses (see also [72]).

Turning to the technique, the method of integrated regional power analysis has proven to be reliable for the present work, yielding robust results across subjects and tasks. However, the method is tightly linked at present to the specific arrangement of detectors used and it's extension to other MEG systems has not been considered. Extension to EEG measurements is a further attractive possibility. For this to happen, the integrated power measure can be converted readily into an integrated variance measure which would be independent of the particular choice of reference electrode (for reference free measures see [92]).

Face processing: autistic subjects

The main conclusions of the study of face processing in autistic subjects have been spelt out at the end of Chapter 4. Significant limitations are the restricted numbers of autistic subjects and the lack of appropriate controls. In short, the results require further validation before they could be considered to be particular to autism and therefore informative about the specific condition. The controls should include most importantly, IQ matching. Additional insights would be provided by extending the study to related disorders, e.g. Asperger's syndrome, and by investigating the development of face specificity in normal childhood. As an aside, there is already considerable language task data on (some) of the autistic subjects but the coverage is not yet sufficiently complete to be reported.

Oscillatory dynamics

The language experiment reported has only dealt with a fairly dramatic form of semantic incongruity (a violation), although it is known that semantic effects are a graded function of expectation [89]. An obvious extension is to study phase-locking at higher frequencies in the context of graded incongruity, i.e. as a function of cloze probability. In addition, analysis has already started of data from a task similar to LT, but using homographs as final words. Homographs are words which, with the same spelling, have separate meanings which are defined by the context, e.g.' bank' as in 'river bank' and 'bank account'. These homographs have been used to probe semantic range, mainly through observation of N400 effects [160].

A significantly unexplored issue in the data from the present language task LT is the phase-locked activity following semantically correct final words. Although there is no a-priori reason why phase-locking should not occur as part of a process of semantic closure, the lack of systematic behaviour in the present subject group suggests the need for both more subjects and alternative approaches to the analysis.

The present analysis method needs strengthening towards a better control over the possible spurious occurrence of clusters of phase-locked γ-band activity. So far, the approach is based on standard (T-test) statistical reasoning. It is planned to augment the current approach by techniques recently developed within the bootstrap framework which allow more rigorous error bounds associated with the statistics used [42]. This should establish better rejection rules than the ones employed here.

Pre-stimulus states

The approach presented in this thesis is very restricted and leaves open many questions concerning the underlying neural dynamics. For example, how many classes of pre-stimulus state should be assumed beyond the two postulated here? There is, after all, no reason to expect all variation to lie within two discrete sets.

A technical but crucial problem is the huge volume of calculations needed to carry out a more comprehensive analysis including all channels and the classification of pre-stimulus epochs preceding non-face control objects. This is compounded by the need for more data with longer sequences and more subjects. This will automatically improve the statistical basis of the conclusions.

Although not initially anticipated, the analysis of FPT data has led to the notion of semantic processing of non-linguistic stimuli. Thus, it is conceivable that a combination, in some form, of state analysis and the analysis of oscillatory dynamics might prove fruitful.

Endpiece

Having contributed minute but, hopefully at least, slightly relevant insights into the neural processes in the human brain, the author of this thesis is left in confusion. The brain, in an attempt to understand itself, seems to create machines which are designed to compound the enigma.

Appendix A

Subjects

This appendix lists information on the subjects, normal controls as well as autistic patients, who participated in the experiments. In case of the normal volunteers, the details are slightly fuller than is usually found in the method sections of EEG and MEG publications. For the autistic subjects, attempts have been made to include some relevant behavioural observations made during the measurements.

A.1 Control subjects

A total of 18 normal volunteers were recruited either on site in Helsinki or from the United Kingdom. All subjects were free of any neurological history and under no medication at the time of measurement. In each case, no IQ scores were available and the handedness was determined by the subject's self-assessment. No information were available concerning the subject's language dominant hemisphere. The vision of each subject was either normal or corrected to normal. The overview given in Table A.1 refers to the experiments (tasks) as discussed in Chapter 3 (face tasks FT1 to FT3), Chapter 5 (language task LT), and Chapter 6 (face task 1, pre-stimulus version FPT). After each experimental session, subjects were briefly and informally interviewed about the strategies they used in solving a particular task.

Subject	Age	Gender	Nationality	Occupation	FT1	FT2	FT3	LT	FPT
S1	39	M	English	1	x	x	x	x	-
S2	35	F	English	2	x	x	x	x	-
S3	25	F	English	3	x	x	x	x	x
S4^{L}	26	M	Australian	1	x	x	-	x	-
S5^{m}	31	F	German	1	x	-	-	-	-
S6^{m}	51	F	American	1	x	x	x	-	-
S7	55	F	English	5	x	x	x	x	-
S8^{m}	35	M	Finnish	1	-	x	x	-	-
S9^{m}	29	M	Finnish	1	x	x	x	-	x
S10^{m}	29	F	Finnish	1	x	-	x	-	x
S11	24	M	English	3	x	x	x	-	-
S12	36	M	German	4	-	-	-	-	x
S13	35	M	German	1	x	x	x	-	x
S14^{m}	37	F	Finnish	1	x	x	x	-	-
S15^{m}	46	M	English	1	x	x	x	x	x
S16	52	F	English	5	x	x	x	x	-
S17^{L}	24	F	English	6	-	-	-	x	-
S18	31	F	English	7	-	-	-	x	-
Mean age: 36 ± 10 years				Σ	14	13	13	9	6

Table A.1: Overview: control subjects

^{L} left handed subject (all other: right handed). ^{m} MR-images available. The age given refers to the subject's first participation (usually in FT1). Experiments FT1 to FT3 were performed by each subject within one session. However, gaps between this group of tasks and others were as long as 1 year in some cases.

Profession codes: 1) academic working in the field of neuroscience with at least some MEG experience, 2) academic working in the field of neuroscience without any prior contact with MEG, 3) academic working in a field unrelated to neuroscience, 4) engineer with MEG experience, 5) secretary, 6) social worker, and 7) employee in academic administration. Mostly, a minus sign indicates 'not measured', but can also mean that rejection due to artefacts precluded any meaningful analysis.

A.2 Autistic subjects

Seven high-functioning autistic subjects of English nationality were recruited. All were diagnosed during childhood and have either been monitored over the years at the Maudsley Hospital, London, or were ascertained during an epidemiological twin study. The diagnosis has been confirmed in all cases using the Autistic Diagnostic Interview. Occasional medication as well some weak epileptic symptom were not entirely ruled out within this group, but severe forms of either have not been reported. Also, to the knowledge of the author, there is no evidence for the existence of neuropathologies in these patients which could alter the emergent brain signals in a way not specifically linked to autism itself. The patients were flown to Helsinki and measured between mid 1995 and spring 1997. With one exception, they were always accompanied by a person of their confidence (usually the mother or a non-autistic sibling).

The overview given in Table A.2 refers to Chapter 4 (face tasks FT1 to FT3, performed by A1 to A7). The gender disparity in the occurrence of autism was reflected in this group, whose ages lay within a normal span. As with the control subjects, vision was either normal or corrected to normal.

Patient	Age	Gender	Occupation	FS	V	P
A1	29	M	second chef in an old peoples home	83	84	88
A2	28	M	trolley collector in a supermarket	89	91	90
A3	32	M	warehouse and delivery person	76	86	66
A4	30	F	secretary, current unknown	90	91	94
A5	35	M	artist, university degree	92	96	89
A6	37	M	artist (protected environment)	102	106	97
A7	33	M	charcoal burner (protected environment)	88	88	76

Mean age: 32 $\pm$ 3 years

Table A.2: Overview: autistic subjects

Handedness: A2 to A5 right handed, A1 and A6 left handed, and A7 semi-ambidextrous. The age given refers to the subject's first participation (FT1). All IQ scores were based on the Wechsler scale (FS: full scale, V: verbal, and P: performance; norm data: 100$\pm$15 for the respective mental age). It is noted that A3's performance score was in the mental handicap range. A5 is currently unemployed and found it difficult to cope with a job despite his degree. A1 is an identical twin, but the cotwin is unaffected. A2 is an identical twin, and the cotwin is also diagnosed autistic. No MRI-scans were available for these individuals.

Some behavioural observations Each of the seven patients was accompanied by a psychiatrist while performing the experiments within the shielded chamber. For each subject, behavioural responses were noted during the preparation period and running

of the experiments. Additionally, interviews[1] were conducted after each experimental session. This data has been briefly scanned to give a profile for each autistic subject (tasks not mentioned were fully understood and performed without any problems).

A1 Showed a slight misunderstanding of FT2. Initially, he expected the two images simultaneously. He tried to use clues such as hair style and hair grey shade (as far as visible) and found the dots the hardest. He had to be reminded to press a key within the first few trials of FT3 where he used mouth clues only. He found the right-handed keypad 'strange' in the very first trials of FT1, but he reported no subsequent problems.

A2 He had no problems at all, but reported FT2 and FT3 to be harder than FT1. He looked at all the face to solve FT3 (reported that, for smiling faces, lips were stretched without the teeth showing up and cheeks/eyes were altered).

A3 Because of a profoundly hunched posture, several head-to-dewar positioning problems occurred within the first session, most probably annoying A3. These were sorted out eventually, but repetitions of some tasks became necessary in later sessions. He reported the use of facial clues ranging from all of the face to only the mouth to solve FT3. However, reports were inconclusive and conflicting upon repetition of this task.

A4 An unremarkable performance. She reported that she looked at all the face. Seeing the boy's teeth could have been important in identifying the smiling expression.

A5 He was very anxious during the beginning of the first run of FT1. He made some premature key presses and was confused about which button to press. He had to be re-instructed during the first 5 or so trials but provided an unremarkable and good performance afterwards. He reported no particular strategies.

A6 Outstanding performance. He found identification of emotional expression 'easy'. He looked at the whole face but concentrated on the eyes, and commented on subtle frowns on some of the faces. He did not encounter problems with the right-handed keypad.

A7 He was initially very anxious and needed a practice run in which he had trouble timing the key press to the visual prompt. However, he provided an unremarkable

[1]The interviews were informal, but more elaborated than for the control subjects.

performance afterwards. He found dot patterns difficult to distinguish in FT2 and reported some expressions as borderline in FT3. He reported no particular strategies.

Appendix B

Auxiliary numerical algorithms

A variety of supplementary algorithms drawn from diverse fields of numerical mathematics have been used for the analysis of the data in this thesis. In most cases, only a reference has been given in the main text and details have been omitted. This appendix provides further details of these methods. Whenever possible, existing code has been used, and routines have been taken from three commercially available sources:

- FORTRAN object-code library routines provided by the Numerical Algorithm Group NAG [154]. These routines are specified as: NAG-*routine*
- C source-code routines provided in Numerical Recipes [119]. These routines are specified as: NR-*routine*
- HP-41C programming language routines provided by a Hewlett-Packard statistical package [62]. These routines are specified as: HP-*routine*.

The first two sources are considered accessible within a physics research environment and references given in the documentation for a particular routine are not repeated. However, in the case of the third source appropriate references are repeated. As far as these algorithms are concerned, only minor, if any modifications were made upon implementation.

Random numbers

[N-1] *Random number generators* Uniform distribution: standard C-library function 'random', and Gaussian distribution: NAG-*GO5DDF*.

Filtering and drift correction

[N-2] *Fourier filter* (based on NAG-*C06EAF*, NAG-*C06EBF*, and NAG-*C06GBF*: Discrete Fourier transform DFT and its inverse transform). The algorithm implements the recommendations given in [119, p 558] by applying the DFT to the data, multiplying the Fourier coefficients by a real and even bandpass filter function ($\mathcal{H}(f)$), and inverse transforming the coefficients via an inverse DFT. The bandpass function (or bandstop by considering $1 - \mathcal{H}(f)$) is defined in terms of two transition frequencies as:

$$\mathcal{H}(f) = \begin{cases} 0 & f \in [0, f_1 - \Delta f_1) \\ \sin^2(\tilde{f}_1) & f \in [f_1 - \Delta f_1, f_1 + \Delta f_1) \\ 1 & f \in [f_1 + \Delta f_1, f_2 - \Delta f_2) \\ \cos^2(\tilde{f}_2) & f \in [f_2 - \Delta f_2, f_2 + \Delta f_2) \\ 0 & f \in [f_2 + \Delta f_2, f_N] \end{cases}, \quad \tilde{f}_i = \frac{\pi}{2}\left[\frac{f - f_i}{2\Delta f_i} + \frac{1}{2}\right], \; i = 1, 2$$

$$f_i, \Delta f_i \in [0, fN], 0 \leq f_1 - \Delta f_1, f_2 + \Delta f_2 \leq f_N, f_1 + \Delta f_1 < f_2 - \Delta f_2$$

where f_N denotes the Nyquist frequency. The roll-off of the spectral power through the transition is -8dB at $f - \Delta f/2$, -3dB at f, and -1dB at $f + \Delta f/2$.

[N-3] *Drift correction* Let $(x_1, x_2, \ldots, x_N)$ be a sequence of equidistantly sampled, possibly pre-processed data and $I = [i_1, i_2], 1 \leq i_1, i_2 \leq N$ an index subset. The drift corrected time series is then defined as

$$\tilde{x}_j = x_j - \frac{\sum_{i \in I} x_i}{i_2 - i_1 + 1}, \; 1 \leq j \leq N.$$

This correction is widely used in MEG and EEG data analysis to ensure a zero-mean reference signal. When the interval I is located within the pre-stimulus interval, the operation is commonly called baseline correction, but the use of this term has been avoided throughout the thesis. Chosing I to be equal to the full index range, yields the usual mean of signal correction.

The methods [N-2] and [N-3] are compatible with the Neuromag software [109].

Summation

[N-4] *Discrete convolution* (based on NAG-*C06EKF*). Calculation of circular convolutions of type

$$z_k = \sum_{i=1}^{N} x_i y_{k-i}, \; i,k = 1,\ldots,N$$

where the time series x and y are assumed to be of period N. This has to be taken into account when evaluating discrete convolution integrals.

[N-5] *Time series integration* (based on NAG-*D01GAF*: four point finite-difference formula due to Gill and Miller). The routine approximates the definite integral

$$I = \int_{x_1}^{x_N} y(x)dx$$

for a time series given as N pairs (y_i, x_i) where the sequence x_i is either in ascending or descending order.

Spectral density estimation

[N-6] *Spectral power densities — periodogram* (based on NR-*spctrm*). Consecutive, overlapping segments of a given time series are subjected to a DFT (NAG-*C06ECF*) and the resulting norm-squared Fourier coefficients are summed according to the periodogram rule. The individual data segments are multiplied by a (triangular) Bartlett-Window function prior to the calculations. The spectral estimates $P(f)$ are normalised according to:

$$2\int_0^{f_N} P(f)df \;=\; \text{mean square value of data } (f_N \text{ Nyquist frequency})$$

where the integral is evaluated using the trapez rule applied to the routines output. Parseval's identity ($\int s(t)^2 dt = \int P(f)df$) is used to establish units. Integrated densities (band power) are obtained by using the integration method in [N-5].

[N-7] *Spectral power densities — maximum entropy* (based on NR-*memcof* and NR-*evlmem*). A linear prediction technique for increasing the resolution in frequency of short time series. The algorithm requires the specification of a parameter (order of prediction), which is chosen according to the recommendation given in

[119, p 574]. Normalisation and band power calculation is the same as for [N-6].

Methods [N-6] and [N-7] do not comprise a time-frequency analysis, in that the resultant spectral coefficients are time independent.

Spatial power of images

[N-8] *Spatial frequency analysis* (based on NAG-*C06FUF*: Fast Fourier transform FFT in 2 dimensions). Used in conjunction with image properties only. Each (grey-scale) pixel value (p) of the image is viewed as a complex number, which in turn gives a complex coefficient:

$$z_{k_1,k_2} = \frac{1}{\sqrt{mn}} \sum_{j_1=0}^{m-1} \sum_{j_2=0}^{n-1} p_{j_1,j_2} \times exp\left(-2\pi i \left(\frac{j_1 k_1}{m} + \frac{j_2 k_2}{n}\right)\right)$$

with $m = 180$ and $n = 225$. Averaging $|z|$ both rowwise and columnwise (over the range $m/2, n/2$ because of the symmetry given by real pixel values) yields periodogram estimates of the mean power spectral density as a function of cycles/image in the x and y-direction.

Statistics

Statistical reasoning is found throughout this thesis. With one exception, a two-tailed view has been adopted to reject a corresponding null hypothesis (e.g. same means, no correlation; no effect in general) up to an error probability of Type-I (α; reject null hypothesis although true). Significance is accepted for values $\alpha \leq 0.05$. Occasionally, effects are considered with $0.05 < \alpha \leq 0.1$ denoted as 'weakly significant'. If meaningful, the lack of significant effects is denoted by 'not significant'. Attempts have been made to avoid sophistication of statistical techniques, and the methods have been chosen for their robustness against violation of underlying model assumptions (e.g. normality and equality of variances).

In the much employed T-test, violations of the assumption of equal variances (F-test) occurred occasionally. Calculations were then repeated using the T-test for non-equal variances leaving the statistical inference unaltered in most situations

(up to a difference of 0.01). If a formerly (weakly) significant result turned into a non-significant one, the null hypothesis has not been rejected [22, 61, 81].

[N-9] *Asymptotic, DF > 30 probabilities of the Student t-distribution* [22]. The values are reproduced here for the sake of convenience.

T	1.645	1.960	2.241	2.326	2.576	2.807	2.968	3.090	3.291
P	0.100	0.050	0.025	0.020	0.010	0.005	0.003	0.002	0.001

Table B.1: Asymptotic t-distribution

[N-10] *Normal scores* (based on NAG-*G01DBF*). When normal scores are plotted against the standardised and ordered data, the degree of linearity in the resultant graphs provides an indication of the normality of the distribution of the data (see also NAG-*G01AHF*). The test is not as rigorous as other methods (e.g. [N-13]), however, in the case of small sample sizes, it is very useful when deciding whether an approach based on normality assumptions can be justified.

[N-11] *T-test and analysis-of-variance (ANOVA)* (based on NAG-*G01EBF* tail probability of the t-distribution, NAG-*G01FBF* deviate associated with tail probability of the t-distribution, NAG-*G04AEF* one-way analysis-of-variance classification, and NAG-*G01FMF* deviate associated with tail probability of the distribution of the Studentized range statistic).

Several variants of the T-test (paired and unpaired observations, equal and unequal variances) are used to assess the significance of the difference between two mean values. If the two groups of observations are of the same sample size N the unpaired tests for equal and unequal variances yield the same numerical value for the T statistic. However, the latter operates on a reduced, usually non-integral number of degrees of freedom DF (derived from [119, p 617]):

$$\mathrm{DF} = (N-1)F, \text{ with } F = \left(1 + \frac{2v_a v_b}{v_a^2 + v_b^2}\right),\ v_a, v_b > 0 \qquad \text{(B.1)}$$

where v_a and v_b denote the (empirical) variances of the two groups of observations. For $v_a = v_b$, the value of $\mathrm{DF} = 2(N-1)$ for the standard test is recovered. Otherwise, $1 \leq F < 2$ holds true ($F \to 1$ if either $v_a \ll v_b$ or $v_b \ll v_a$).

In the case of more than two treatment groups, ANOVA is used in conjunction with Tukey's honestly significant difference (HSD) to allow for a post-hoc comparison of group mean values. For convenience, the definition of HSD is repeated

here. Given a total of N observations in K groups of N_i observations, HSD is calculated as:

$$\mathrm{HSD} = q_\alpha \sqrt{\frac{rss}{\tilde{n}(N-K)}},\ \tilde{n} = \frac{2 \min N_i \max N_i}{\min N_i + \max N_i},\ 1 \le i \le K$$

where q_α denotes the deviate of the Studentized statistic for $N - K$ degrees of freedom and K groups at a level, α, not more significant than the result of the preceding ANOVA. The residual[1] within groups is denoted by rss. A one-way ANOVA is equivalent in statistical inference to a two-tailed, unpaired T-test in the case of two treatment groups.

[N-12] *Rank correlation coefficient, Spearman's* ϱ (based on HP-Σ*SPEAR*, nonparametrical statistics [50]). The implementation uses integer rank numbers greater than 0. The significance of ϱ is evaluated by using a corresponding T-statistic:

$$T = |\varrho| \sqrt{\mathrm{DF}/(1-\varrho^2)},\ \mathrm{DF} = \text{'number of rank pairs' - 2.}$$

The associated T-test is independent of the original distribution of the data to a good approximation [119].

[N-13] *Test of uniformity* (based on NAG-*G08CBF*, one sample Kolmogorov-Smirnov test). The implementation uses only one feature of this multi-purpose routine, i.e. a test against the null hypothesis that the data are a random sample of observations from a uniform distribution on a bounded interval $\{b_1, b_2\}$. Unless known from theoretical considerations (e.g. $-\pi$ and π in case of phase measures), the bounds are estimated by the routine based on the data supplied.

[1] If $y_{i,j}$ are the observations $(1 \le i \le K, 1 \le j \le N_i)$, then

$$rss = \sum_{i=1}^{K} \sum_{j=1}^{N_i} (y_{i,j})^2 - \sum_{i=1}^{K} \frac{\left(\sum_{j=1}^{N_i} y_{i,j}\right)^2}{N_i}$$

Appendix C

Source localisation

Estimation of neural generators underlying the magnetic fields measured outside the head was carried out for the responses in task FT1. The approach was based on the single equivalent current dipole ECD model assuming a homogeneous sphere as a volume conductor [134]. This model has been extensively used in previous MEG studies, and is provided by the Neuromag software [109]. Using this software, a two step procedure has been adopted as follows:

1) determination of the latency within an interval of interest where the ECD best describes (best fit) the measured magnetic fields using the origin of the individual's PAN system as the the origin of the sphere. The best fit is defined as the maximum of a quantity called goodness-of-fit (gof) which assumes values ≤ 1. The best fit dipole is only accepted if a) the gof is at least 0.7 (this is above what can be achieved for noise, [142]), and b) the 95% dipole-position confidence volume of fit is not more than 1 cubic centimeter.

2) if MRI-scans are available, step one is repeated this time chosing a best fit sphere that approximates the curvature of the skull in the vicinity of the source's location.

A current dipole constitutes a first order Taylor expansion of the Biot-Savart law of electrodynamics, assuming that the magnetic fields measured originate from a single source area G, the spatial extent of which is small compared with distances to the detectors [69]. In this approximation, the dipole can be viewed as the spatial average of all impressed currents within G. The impressed currents are due to the electromotive forces impressed by biological activity in conducting tissue. They are different from the

(compensatory) Ohmic currents which do not contribute to the magnetic fields outside the volume conductor in this model. Apart from this mathematical consideration, the approach can be partially justified on neurophysiological grounds [80].

Appendix D

Regional power analysis

This appendix lists the results obtained from various preliminary calculations carried out to verify the consistency of the normalised integrated regional power NIRP approach. The definition of the measure is repeated here for convenience:

$$\mathrm{NIRP} = \frac{\mathrm{IRP}(t_1, t_2)}{\mathrm{IRP}(-b, 0)}.$$

where IRP denotes the integrated regional power (sum over squares) of the interval of interest ($[t_1, t_2]$) and b denotes the length of the pre-stimulus baseline.

The choice of the baseline

In general, there are no fixed rules for chosing a resting, or baseline state in relation to which activity is measured. Any method relying on a ratio or subtraction may suffer from a non-trivial interaction between the processes under consideration and the baseline activity. The present approach follows common practice in that the activity in a predefined interval preceding the stimulus has been chosen as a baseline related in time to the processes associated with the stimulus (e.g. [87]).

In this context, it seems reasonable to require that IRP is approximately a linear function of the baseline length for suitable values of b. IRP measures a general power background against which the individual signals are quantified, where the total (background) power should be proportional to the time span of observation. An extensive survey has shown that the NIRP values scale according to

$$\mathrm{NIRP} \propto b^{-\alpha}, \quad \alpha \approx 1$$

for choices of b between about 80 and 300ms using real data. There is a similar functional dependence using noise data at lower NIRP values (Figure D.1 A). This dependency of NIRP on b is consistent with zero-mean, uncorrelated and constant variance

signals in the pre-stimulus interval. In which case IRP is (statistically) invariant upon time shift ($\int_{-b_1}^{-b_2} = \int_{-(b_1+\delta)}^{-(b_2+\delta)}$, with $\delta > 0$ and not too small), and linear in b ($\int_{-b\delta}^{0} = b \int_{-\delta}^{0}$).

For the purpose of the present analysis, a baseline length of $b = 200$ms has been chosen for all calculations. The value chosen is the same as for the drift correction that is applied to the evoked responses in order to enforce zero-mean signals in the baseline interval. Typically, the ratio between IRP$(-b, 0)$ values for real data and channel noise is between 4:1 and 3:1. The behaviour of the baseline power is consistent with the observation that, in general, the NIRP values are approximately normally distributed across subjects for a given stimulus and task, as verified by normal plots (Figure D.1 B). The resultant graphs are consistent with straight lines of the form $y = ax$ with $a \approx 1$ (correlation >0.85) and, therefore, are compatible with the assumptions underlying the statistical tests used for this measure.

Number of epochs averaged

Due to experimental limitations, the size of the stimulus sets varied slightly. The number of epochs available for a given stimulus affects the NIRP values by altering the signal-to-noise ratio[1]. For strong signals, NIRP decreases with a decreasing number of averages due to an increase in IRP$(-b, 0)$. However, the slight imbalance in the number of trials in some tasks presents no problem.

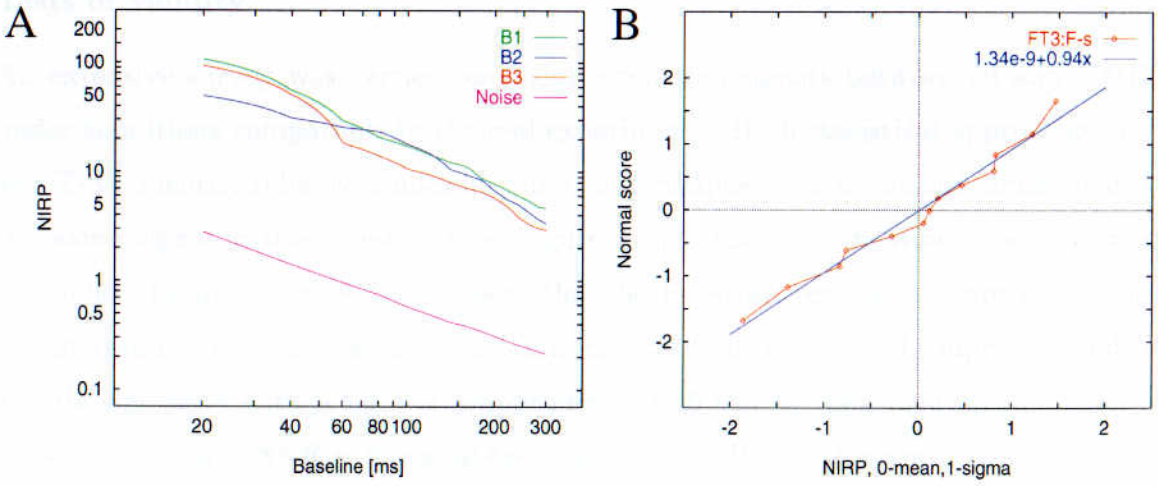

Figure D.1: NIRP: verification

A: NIRP versus the length of the baseline b for three data sets (B1 to B3) randomly chosen from all face responses. The data applies to the occipito-temporal region ROT. The curve denoted as noise corresponds to a measurement without a subject (channel noise). B: normal plot (red, blue: best line fit) of the 13 NIRP values obtained from the responses in ROT following face (smiling) presentation of all subjects who participated in FT3.

[1]Assuming the standard model of an evoked response embedded in a noisy background.

Appendix E

The Gabor transform

In this appendix, the results obtained from a series of preliminary calculations are listed. In order to evaluate differences between the two stimuli for the measures P and SY, extensions to current approaches have been introduced. As it was not known initially what ranges of values and what degree of robustness would be achieved, the procedures were validated carefully. The presentation below is complemented by Figure E.1 which explains the bootstrap procedure devised for the present study. It is convenient to think in operations applied to Gabor maps as object entities, however, all calculations are based on individual coefficients, and no matrix algebra is involved.

Tests of validity

An extensive survey was carried out using simulated signals between 20 and 100 Hz under conditions comparable to the real experiments. Both statistical approaches T-P and T-SY identify reliably sinusoidal bursts superimposed on a sinusoid signal against the same signal without bursts (see Figure 5.2). The identification is accepted at $p < 0.05$. In the cases of T-SY, more than 60 boostrap replications are needed for robust results. Typically, a burst with a duration of 100 ms at 35 Hz superimposed on a 12Hz sine wave with a ratio of amplitudes of 1:10 can be identified up to a level of noise corruption of SNR = 5 (signal-to-noise ratio in [dB]) with respect to the ongoing sine wave.

Using real data, T-SY is robust for a number of bootstrap replications $B > 100$ with respect to the threshold clustering in that upon re-evaluation of the same map: a) the same clusters of the same type (I+,I-) are identified for all significance levels equal to or better than $p < 0.1$, b) the position of the maximal (t,f)-point which identifies a given cluster does not vary by more than 3 times the sampling interval in time or

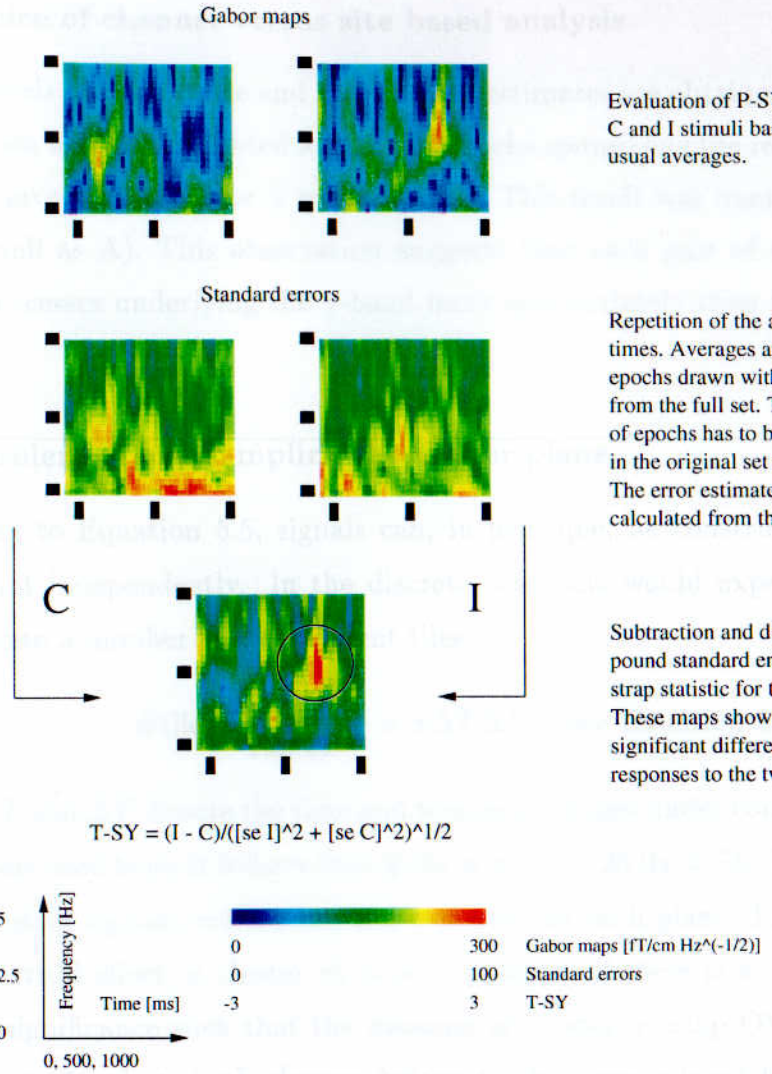

Figure E.1: A bootstrap procedure for T-SY

The example is taken from the data of S1 (channels 41 and 42, over left anterior regions). The number of bootstrap replications is denoted by B (= 120). The Gabor maps corresponding to C and I responses might indicate several γ-band events, however, only one is associated with a significant difference between the two stimulus classes. This is the cluster at 750 ms and 34 Hz.

2 Hz in frequency, and c) the variation of the maximal T-SY value does not exceed 0.3 and is generally much lower. These results were obtained by re-evaluating 50 times the signals taken from 50 detector sites randomly selected from all subjects and sites. These observations also hold true (for fixed value of B) when 1) K is varied between 6 and 10, and 2) evaluating sets of epochs randomly reduced in size by a factor of up to 5%, indicates that T-SY is within the asymptotic tail of the t-distribution.

In summary, it is reasonable to assume that the approach is sufficiently robust under real situations and not restricted to noise free conditions.

The choice of channel versus site based analysis

Higher levels of significance and more robust estimates are obtained when the measures of Equation 5.12 are evaluated for a set of epochs comprising the readings of both channels of a given detector site ($i = 1, \ldots, 2N_e$). This result was unexpected for measures SY (as well as A). *This observation suggests that each pair of channels reflects the* neural processes underlying the γ-band more appropriately than the separate channel data.

The problem of oversampling the Gabor plane

According to Equation 5.5, signals can, in principle, be constructed to sample each (t, f)-point independently. In the discrete case, one would expect each plane to be divided into a number of independent tiles

$$\#\text{tile} \approx \frac{\Delta T}{2\Delta t}\frac{\Delta F}{2\Delta f} = \pi \Delta T \Delta F \quad \text{(see Equation 5.7)}$$

where ΔT and ΔF denote the time and frequency ranges under consideration. With the parameters used here, it follows that $\#\text{tile} \approx \pi \times 1\,\text{s} \times 25\,\text{Hz} \approx 78$. Thus, at the 5%-level using random signals, $\approx$4 clusters are expected for each plane. In order to counteract this statistical effect, a cluster cl_i is only accepted if there is a cluster cl_j of at least $p < 0.1$ significance such that the measure of cluster overlap OVLP (Equation 5.16) evaluates to 1, where both clusters belong to the same subject but adjacent detector sites. With this data, the amount of cluster rejections varies between $\approx$6% and $\approx$15% dependent on a given data set, most probably due to general fluctuations in the signal-to-noise ratios.

Additionally, the calculations presented in the chapter were repeated in part using a) random signals, and b) real data but replacing the phases of the Gabor coefficients by random values. Consistently more synchronous clusters were obtained in both cases compared with the original data. These clusters were homogeneously distributed in time. This has been taken as a piece of further evidence that the inhomogeneously distributed phase-locked activity observed in the real data is related to the neural activity.

The effect of stimulus jitter

A jitter in phases is inevitably present because of experimental constraints and neurophysiological variability. A precise assessment of the effects taking into account all

sources of misalignment is not possible. However, simulations indicate that the frequency range (20 to 45 Hz) chosen for the analysis is not significantly corrupted by the experimental constraints (Figure E.2).

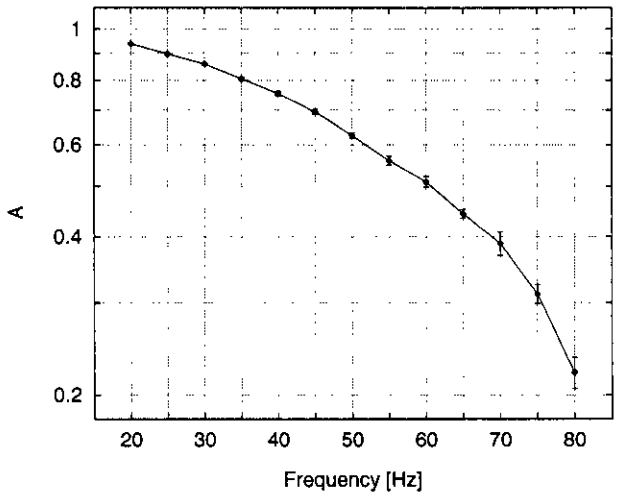

Figure E.2: Maximal phase alignment versus frequency

Mean angular alignments ($K = 8$) and standard deviations obtained for each 20 repetitions of a set ($N_e = 100$) of oscillatory responses (epochs) at that frequency. Each epoch was calculated as $y(t) = \sin(2\pi ft + \phi)$, where ϕ is distributed uniformly in $[-J2\pi f, J2\pi f]$ with a constant jitter parameter of $J = 5.1$ ms. This is the sum of 2.68 ms (sampling interval at 373 Hz) and 2.4 ms (uncertainty in time associated with the image presentation; Chapter 2, Figure 2.6). The curve represents idealised responses where the observable maximal phase alignment is restricted only by the constrains of the equipment.

Bibliography

[1] H.D.I. Abarbanel. The analysis of observed chaotic data in physical systems. *Reviews of Modern Physics*, 65:1331–1392, 1993.

[2] Advanced Visual Systems Inc. *AVS Developers's guide*, 1993.

[3] A.I. Ahonen, M.S. Hämäläinen, M.J. Kajola, J.E.T. Knuutila, P.P. Laine, O.V. Lounasmaa, L.T. Parkkonen, J.T. Simola, and C.D. Tesche. 122-channel SQUID instrumentation for investigating the magnetic signals from the human brain. *Physica Scripta*, 49:198–205, 1993.

[4] C.J. Aine. A conceptual overview and critique of functional neuroimaging techniques in humans: I. MRI/fMRI and PET. *Critical Reviews in Neurobiology*, 9:229–309, 1995.

[5] P.G. Aitken, T. Sauer, and S.J. Schiff. Looking for chaos in brain slices. *Journal of Neuroscience Methods*, 59:41–48, 1995.

[6] T. Allison, H. Ginter, G. McCarthy, A.C. Nobre, A. Puce, M. Luby, and D.D. Spencer. Face recognition in human extrastriate cortex. *Journal of Neurophysiology*, 71:821–825, 1994.

[7] T. Allison, G. McCarthy, A. Nobre, A. Puce, and A. Belger. Human extrastriate visual cortex and the perception of faces, words, numbers, and colors. *Cerebral Cortex*, 5:544–554, 1994.

[8] American Psychiatric Association, Washington (DC). *Diagnostic and statistical manual of mental disorders (DSM-IV), 4th edition.* American Psychiatric Association, Washington (DC), 1994.

[9] N.W. Ashcroft and N.D. Mermin. *Solid state physics.* Holt-Saunders International Editions, 1981.

[10] E. Başar, C. Başar-Eroglu, B. Rosen, and A. Schütt. A new approach to endogenous event-related potentials in man: relation between EEG and P300-wave. *International Journal of Neuroscience*, 24:1–21, 1984.

[11] A. Bailey, W. Phillips, and M. Rutter. Autism: towards an integration of clinical, genetic, neuropsychological, and neurobiological perspectives. *Journal of Child Psychology and Psychiatry*, 37:89–126, 1996.

[12] S.E. Barrett and M.D. Rugg. Event-related potentials and the semantic matching of faces. *Neuropsychologia*, 27:913–922, 1989.

[13] S.E. Barrett, M.D. Rugg, and D.I. Perrett. Event-related potentials and the matching of familiar und unfamiliar faces. *Neuropsychologia*, 26:105–117, 1988.

[14] S. Bentin, T. Allison, A. Puce, E. Perez, and G. McCarthy. Electrophysiological studies of face perception in humans. *Journal of Cognitive Neuroscience*, 8:551–565, 1996.

[15] S. Blanco, C.E.D. Attellis, S.I. Isaacson, O.A. Rosso, and R.O. Sirne. Time-frequency analysis of electroencephalogram series, II. Gabor and wavelet transforms. *Physical Review E*, 54:6661–6672, 1996.

[16] S. Blanco, R.Q. Quiroga, O.A. Rosso, and S. Kochen. Time-frequency analysis of electroencephalogram series. *Physical Review E*, 51:2624–2631, 1995.

[17] M.A. Bobes, M. Valdes-Sosa, and E. Olivares. An ERP study of expectancy violation in face perception. *Brain and Cognition*, 26:1–22, 1994.

[18] K. Bötzel and O.J. Grüsser. Electric brain potentials evoked by pictures of faces and non-faces: a search for 'face-specific' EEG potentials. *Experimental Brain Research*, 77:349–360, 1989.

[19] K. Bötzel, S. Schulze, and S.R.G. Stodieck. Scalp topography and analysis of intracranial sources of face-evoked potentials. *Experimental Brain Research*, 104:135–143, 1995.

[20] J. Boucher and V. Lewis. Unfamiliar face recognition in relatively able autistic children. *Journal of Child Psychology and Psychiatry*, 33:843–859, 1992.

[21] R.N. Bracewell. *The Fourier transform and its applications*. McGraw-Hill Publishers, 1978.

[22] I.N. Bronstein and K.A. Semendjajew. *Taschenbuch der Mathematik.* Verlag Harri Deutsch Thun und Frankfurt (Main), 1981.

[23] V. Bruce and A. Young. Understanding face recognition. *British Journal of Psychology*, 77:305–327, 1986.

[24] A.M. Burton, V. Bruce, and R.A. Johnston. Understanding face recognition with an interactive activation model. *British Journal of Psychology*, 81:361–380, 1990.

[25] G.A. Carlesimo and C. Caltagirone. Components in the visual processing of known and unknown faces. *Journal of Clinical and Experimental Neuropsychology*, 17:691–705, 1995.

[26] V.P. Clark, K. Keil, J.M. Maisog, S. Courtney, L.G. Ungerleider, and J.V. Haxby. Functional magnetic resonance imaging of human visual cortex during face matching: a comparison with positron emission tomography. *Neuroimage*, 4:1–15, 1996.

[27] D.J. Cohen and F.R. Volkmar, editors. *Handbook of autism and pervasive developmental disorders (2nd edition).* John Wiley & Sons, New York, 1997.

[28] S.M. Courtney, L.G. Ungerleider, and J.V. Haxby. Object and spatial visual working memory activate separate neural systems in human cortex. *Cerebral Cortex*, 6:39–49, 1996.

[29] A.R. Damasio, H. Damasio, and G.W. van Hoesen GW. Face agnosia and the neural substrates of memory. *Annual Reviews of Neuroscience*, 13:89–109, 1990.

[30] I. Daubechies. The wavelet transform, time-frequency lacalization and signal analysis. *IEEE Transactions on Information Theory*, 36:961–1005, 1990.

[31] I. Daubechies. *Ten lectures on wavelets.* Society for Industrial and Applied Mathematics (siam), 1992.

[32] J. Davies. Real-world control via LPT. *Electronic World + Wireless World*, pages 755–758, September 1994.

[33] S. Davies, D. Bishop, A.S.R. Manstead, and D. Tantam. Face perception in children with autism and Asperger's syndrome. *Journal of Child Psychology and Psychiatry*, 35:1033–1057, 1994.

[34] B. de Gelder, J. Vroomen, and L. van der Heide. Face recognition and lip-reading in autism. *European Journal of Cognitive Psychology*, 3:69–86, 1991.

[35] J.B. Debruille. Knowledge inhibition and N400: a study with words that look like common words. *Brain and Language*, 62:202–220, 1998.

[36] J.B. Debruille, J. Pineda, and B. Renault. N400-like potentials elicited by faces and knowledge inhibition. *Cognitive Brain Research*, 4:133–144, 1996.

[37] J.E. Desmedt and C. Tomberg. Transient phase-locking of 40 Hz electrical oscillations in prefrontal and parietal cortex reflects the process of conscious somatic perception. *Neuroscience Letters*, 168:126–129, 1994.

[38] R.J. Dolan, P. Fletcher, J. Morris, N. Kapur, J.F.W. Deakin, and C.D. Frith. Neural activation during covert processing of positive emotional facial expressions. *Neuroimage*, 4:194–200, 1996.

[39] D.W. Duke and W.S. Pritchard, editors. *Measuring chaos in the brain.* World Scientific Publishing, 1991.

[40] G.M. Edelman. Neural Darwinism: selection and reentrant signaling in higher brain function. *Neuron*, 10:115–125, 1993.

[41] B. Efron. Bootstrap methods: another look at the jackknife. *Annals of Statistic*, 7:1–26, 1979.

[42] B. Efron and R.J. Tibshirani. *An introduction to the bootstrap*, volume 57 of *Monographs on statistics and applied probability.* Chapman & Hall, Inc., 1993.

[43] T. Elbert, W.J. Ray, Z.J. Kowalik, J.E. Skinner, K.E. Graf, and N. Birbaumer. Chaos in physiology: deterministic chaos in excitable cell assemblies. *Physiological Reviews*, 74:1–47, 1994.

[44] C. Eulitz, B. Maess, C. Pantev, A.D. Friederici, B. Feige, and T. Elbert. Oscillatory neuromagnetic activity induced by language and non-language stimuli. *Cognitive Brain Research*, 4:121–132, 1996.

[45] M.J. Farah. Is face recognition 'special'? Evidence from neuropsychology. *Behavioural Brain Research*, 76:181–189, 1996.

[46] A.D. Friederici, E. Pfeifer, and A. Hahne. Event-related brain potentials during natural speech processing: effects of semantic, morphological and syntactic violations. *Cognitive Brain Research*, 1:183–192, 1993.

[47] J.H. Friedman, J.L. Bentley, and R.A. Finkel. An algorithm for finding best matches in logarithmic expected time. *ACM Transactions on Mathematical Software*, 3:209–226, 1977.

[48] D. Gabor. Theory of communication. *Journal of the Institute of Electrical Engineers*, 93:429–457, 1946.

[49] A.S. Gevins and A. Remond, editors. *Handbook of electroencephalography and clinical neurophysiology*, volume 1. Elsevier, Amsterdam, 1987.

[50] J.D. Gibbons. *Nonparametric statistical inference.* McGraw-Hill Publishers, 1971.

[51] J.M. Gottman. *Time-series analysis.* Cambridge University Press, 1981.

[52] R.L. Gregory, editor. *The Oxford companion to the mind.* Oxford University Press, 1987.

[53] A. Grossmann, R. Kronland-Martinet, and J. Morlet. Reading and understanding continuous wavelet transforms. In J.M. Combes, A. Grossmann, and P. Tchamitchian, editors, *Wavelets, time-frequency methods and phase space.* Springer-Verlag Berlin Heidelberg New York, 1989.

[54] V. Hakkinen, K. Hirvonen, J. Hasan, M. Kataja, A. Varri, P. Loula, and H. Eskola. The effect of small differences in electrode position on EOG signals - application to vigilance studies. *Electroencephalography and Clinical Neurophysiology*, 86:294–300, 1993.

[55] E. Halgren, P. Baudena, G. Heit, M. Clarke, and K. Marinkovic. Spatio-temporal stages in face and word processing. 1. Depth-recorded potentials in the human occipital, temporal and parietal lobes. *Journal of Physiology, Paris*, 88:1–50, 1994.

[56] E. Halgren, P. Baudena, G. Heit, M. Clarke, K. Marinkovic, and P. Chauvel. Spatio-temporal stages in face and word processing. 2. Depth-recorded potentials in the human frontal and Rolandic cortices. *Journal of Physiology, Paris*, 88:51–80, 1994.

[57] E. Halgren, T. Raij, K. Marinkovic, V. Jousmäki, and R. Hari. Magnetic fields evoked by faces in the human brain: 1. topography and equivalent dipole locations. *Society for Neuroscience*, 21:562, 1995.

[58] M. Hämäläinen, R. Hari, R.J. Ilmoniemi, J. Knuutila, and O.V. Lounasmaa. Magnetoencephalography — theory, instrumentation, and applications to noninvasive studies of the working human brain. *Reviews of Modern Physics*, 65:413–497, 1993.

[59] F. Happé and U. Frith. The neuropsychology of autism. *Brain*, 119:1377–1400, 1996.

[60] J.V. Haxby, B. Horwitz, L.G. Ungerleider, J.M. Maisog, P. Pietrini, and C.L. Grady. The functional organisation of human extrastriate cortex: a PET - rCBF study of selective attention to faces and locations. *Journal of Neuroscience*, 14:6336–6353, 1994.

[61] W.L. Hays. *Statistics.* Harcourt Brace College Publishers, 1994.

[62] Hewlett-Packard, Inc. *Statistical package for the HP-41 calculator series — manual*, 1987.

[63] R.P. Hobson. The autistic child's appraisal of expressions of emotion: a further study. *Journal of Child Psychology and Psychiatry*, 27:671–680, 1986.

[64] R.P. Hobson, J. Ouston, and A. Lee. What's in a face? The case of autism. *British Journal of Psychology*, 79:441–453, 1988.

[65] P.J. Holcomb and H.J. Neville. Auditory and visual semantic priming in lexical decision: a comparison using event-related brain potentials. *Language and Cognitive Processes*, 5:281–312, 1990.

[66] K. Ikeda. Multiple-valued stationary state and its instability of the transmitted light by a ring cavity system. *Optics Communications*, 30:257, 1979.

[67] J. Intriligator and J. Polich. On the relationship between EEG and ERP variability. *International Journal of Psychophysiology*, 20:59–74, 1995.

[68] J.-P. Eckmann and D. Ruelle. Ergodic theory of chaos and strange attractors. *Reviews of Modern Physics*, 57:617–656, 1985.

[69] J.D. Jackson. *Klassische Elektrodynamik (English edition: J.D. Jackson, Classical electrodynamics, John Wiley, 1962).* Walter de Gruyter Berlin New York, 1981.

[70] B.H. Jansen, H.N. Nyberg, and G. Zouridakis. Selective Averaging of evoked potentials using trajectory-based clustering. *Methods of Information in Medicine*, 33:49–51, 1994.

[71] P. Jasiukaitis and G. Hakerem. The effect of prestimulus alpha activity on the P300. *Psychophysiology*, 25:157–165, 1988.

[72] D.A. Jeffreys. The influence of stimulus orientation on the vertex positive scalp potential evoked by faces. *Experimental Brain Research*, 96:163–172, 1993.

[73] D.A. Jeffreys and E.S.A. Tukmachi. The vertex-positive scalp potential evoked by faces and by objects. *Experimental Brain Research*, 91:340–350, 1992.

[74] D.A. Jeffreys, E.S.A. Tukmachi, and G. Rockley. Evoked potential evidence for human brain mechanisms that respond to single, fixated faces. *Experimental Brain Research*, 91:351–362, 1992.

[75] R.J. Johnson. The amplitude of the P300 component of the event-related potential: review and synthesis. In P.K. Ackles, J.R. Jennings, and M.G.H. Coles, editors, *Advances in Psychophysiology, Vol. 3*, pages 69–138. JAI Press, Greenwich, CT, 1988.

[76] M. Jueptner and C. Weiller. Review: does measurement of regional blood flow reflect synaptic activity? — implications for PET and fMRI. *Neuroimage*, 2:148–156, 1995.

[77] K. Juottonen, A. Revonsuo, and H. Lang. Dissimilar age influences on two ERP waveforms (LPC and N400) reflecting semantic context effect. *Cognitive Brain Research*, 4:99–107, 1996.

[78] E.R. Kandel, J. H. Schwartz, and T. M. Jessell. *Principles of neural science.* Prentice Hall International Editions, 1991.

[79] L. Kanner. Autistic disturbances of affective contact. *Nervous Child*, 2:217–250, 1943.

[80] T. Katila. On the current multipole presentation of the primary current distributions. *Nuovo Cimento*, 2:660–664, 1983.

[81] M.G. Kendall and A. Stuart. *The advanced theory of statistics*, volume 3. Griffin, London, 1969.

[82] M.B. Kennel, R. Brown, and H.D.I. Abarbanel. Determining embedding dimension for phase-space reconstruction using a geometrical construction. *Physical Review A*, 45:3403–3411, 1992.

[83] B.W. Kernighan and D.M. Ritchie. *The C programming language.* Prentice Hall Software Series. Prentice Hall, 1988.

[84] C. Kittel. *Einführung in die Festkörperphysik.* R. Oldenbourg Verlag, München Wien, 1983.

[85] I. Kondákor, R.D. Pascual-Marqui, C.M. Michel, and D. Lehmann. Event-related potential map differences depend on the prestimulus microstates. *Journal of Medical Engineering & Technology*, 19:66–69, 1995.

[86] S. Kotz and N.L. Johnson, editors. *Encyclopedia of statistical sciences*, volume 9. John Wiley & Sons, New York, 1988.

[87] M. Koukkou and D. Lehmann. Brain functional states: determinants, constraints, and implications. In M. Koukkou, D. Lehmann, and J. Angst, editors, *Functional states of the brain: their determinants*, pages 13–20. Elsevier, Amsterdam, 1980.

[88] M. Kutas and S.A. Hillyard. Reading senseless sentences: brain potentials reflect semantic incongruity. *Science*, 207:203–205, 1980.

[89] M. Kutas and S.A. Hillyard. Brain potentials during reading reflect word expectancy and semantic association. *Nature*, 307:161–163, 1984.

[90] T. Langdell. Recognition of faces: an approach to the study of autism. *Journal of Child Psychology and Psychiatry*, 19:255–268, 1978.

[91] D. Lehmann, C.M. Michel, I. Pal, and R.D. Pasqual-Marqui. Event-related potential maps depend on prestimulus brain electric microstate map. *International Journal of Neuroscience*, 74:239–248, 1994.

[92] D. Lehmann and W. Skrandies. Reference-free identification of components of checkerboard-evoked multichannel potential fields. *Electroencephalography and Clinical Neurophysiology*, 48:609–621, 1980.

[93] D. Lehmann and W. Skrandies. Spatial analysis of evoked potentials in man — a review. *Progress in Neurobiology*, 23:227–250, 1984.

[94] S.T. Lu, M.S. Hämäläinen, R. Hari, R.J. Ilmoniemi, O.V. Lounasmaa, M. Sams, and V. Vilkman. Seeing faces activates three separate areas outside the occipital visual cortex in man. *Neuroscience*, 43:287–290, 1991.

[95] W. Lutzenberger, F. Pulvermüller, and N. Birbaumer. Words and pseudowords elicit distinct patterns of 30-Hz EEG responses in humans. *Neuroscience Letters*, 176:115–118, 1994.

[96] H. Macdonald, M. Rutter, P. Howlin, P. Rios, A. Le Conteur, C. Evered, and S. Folstein. Recognition and expression of emotional cues by autistic and normal adults. *Journal of Child Psychology and Psychiatry*, 30:865–877, 1989.

[97] K. Marinkovic, T. Raij, E. Halgren, and R. Hari. Magnetic fields evoked by faces in the human brain: 2. cognitive profile. *Society for Neuroscience*, 21:562, 1995.

[98] R.A. Martin, G.E. Berry, T. Dobranski, M. Horne, and P.G. Dodgson. Emotion perception threshold: individual differences in emotional sensitivity. *Journal of Research in Personality*, 30:290–305, 1996.

[99] W. McCallum, S. Farmer, and P. Pocock. The effects of physical and semantic incongruities on auditory event-related potentials. *Electroencephalography and Clinical Neurophysiology*, 59:477–488, 1984.

[100] G. McCarthy, A.C. Nobre, S. Bentin, and D.D. Spencer. Language-related field potentials in the anterior-medial temporal lobe: I. Intracranial distribution and neural generators. *Journal of Neuroscience*, 15:1080–1089, 1995.

[101] T.M. McKenna, T.A. McMullen, and M.F. Shlesinger. The brain as a dynamical system. *Neuroscience*, 60:587–605, 1994.

[102] Y. Meyer. *Wavelets - Algorithms and applications.* Society for Industrial and Applied Mathematics (siam), 1993.

[103] T. Miyashita. Discrimination of facial components in autistic children (English abstract). *The Japanese Journal of Psychology*, 59:206–212, 1988.

[104] C.M. Mooney. Closure with negative after-images under flickering light. *Canadian Journal of Psychology*, 10:191–199, 1956.

[105] J. Morton and M.H. Johnson. CONSPEC and CONLEARN: A two-process theory of infant face recognition. *Psychological Review*, 98:164–181, 1991.

[106] W. Mühlnickel, N. Rendtorff, Z.J. Kowalik, B. Rockstroh, W. Miltner, and T. Elbert. Testing the determinism of EEG and MEG. *Integrative Physiological and Behavioral Science*, 29:262–269, 1994.

[107] T.F. Münte and M. Matzke and S. Johannes. Event-related brain potentials and face processing. *Journal of Psychophysiology*, 10:83–84, 1996.

[108] Neuromag. *Technical Documentation of the Neuromag-122*, 1994.

[109] Neuromag. *XFIT - Source modelling, Reference manual, Version 4.1*, 1994.

[110] E. Olivares, M.A. Bobes, E. Aubert, and M. Valdes-Sosa. Associative ERP effects with memories of artificial faces. *Cognitive Brain Research*, 2:39–48, 1994.

[111] E. Ott. *Chaos in dynamical systems.* Cambridge University Press, 1993.

[112] S. Ozonoff, B.F. Pennington, and S.J. Rogers. Are there emotion perception deficits in young autistic children? *Journal of Child Psychology and Psychiatry*, 31:343–361, 1990.

[113] N.H. Packard, J.P. Crutchfield, J.D. Farmer, and R.S. Shaw. Geometry from a time series. *Physical Review Letters*, 45:712–716, 1980.

[114] C. Pantev, S. Makeig, M. Hoke, R. Galambos, S. Hampson, and C. Gallen. Human auditory evoked gamma-band magnetic fields. *Proceedings of the National Academy of Sciences, USA*, 88:8996–9000, 1991.

[115] W. Phillips, J.C. Gomez, S. Baron-Cohen, V. Laa, and A. Riviere. Treating people as objects, agents, or 'subjects': how young children with and without autism make requests. *Journal of Child Psychology and Psychiatry*, 36:1383–1398, 1995.

[116] Polhemus - A Kaiser Aerospace & Electronics Company. *ISOTRAK II (3Space), User's manual*, 1993.

[117] J. Polich. Probability and inter-stimulus interval effects on the P300 from auditory stimuli. *International Journal of Psychophysiology*, 10:163–170, 1990.

[118] D.D. Potter and D.M. Parker. Dissociation of event-related potential repetition effects in judgements of face identity and expression. *Journal of Psychophysiology*, 11:287–303, 1997.

[119] W.H. Press, S.A. Teukolsky, W.T. Vetterling, and B.P. Flannery. *Numerical recipes in C.* Cambridge University Press, 1992.

[120] W.S. Pritchard, M.E. Brandt, S.A. Shappell, and T.J. O'Dell. P300 amplitude/prestimulus EEG power relationships. *Psychophysiology*, 22:609–610, 1985.

[121] W.S. Pritchard and D.W. Duke. Measuring 'chaos' in the brain: a tutorial review of EEG dimension estimation. *Brain and Cognition*, 27:353–397, 1995.

[122] W.S. Pritchard, K.K. Krieble, and D.W. Duke. On the validity of estimating EEG correlation dimension from a spatial embedding. *Psychophysiology*, 33:362–368, 1996.

[123] A. Puce, T. Allison, M. Asgari, J.C. Gore, and G. McCarthy. Differential sensitivity of human visual cortex to faces, letterstrings and textures: a functional magnetic resonance imaging study. *Journal of Neuroscience*, 16:5205–5215, 1996.

[124] F. Pulvermüller. Hebb's concept of cell assemblies and the psychophysiology of word processing. *Psychophysiology*, 33:317–333, 1996.

[125] F. Pulvermüller, C. Eulitz, C. Pantev, B. Mohr, and B. Feige. High-frequency cortical responses reflect lexical processing – an MEG study. *Electroencephalography and Clinical Neurophysiology*, 98:76–85, 1996.

[126] P.E. Rapp, A.M. Albano, T.I. Schmah, and L.A. Farwell. Filtered noise can mimic low-dimensional chaotic attractors. *Physical Review E*, 47:2289–2297, 1993.

[127] E. De Renzi, D. Perani, G.A. Carlesimo, M.G. Silveri, and F. Fazio. Prosopagnosia can be associated with damage confined to the right hemisphere: an MRI and PET study and a review of the literature. *Neuropsychologia*, 32:893–902, 1994.

[128] P.R. Roelfsema, A.K. Engel, P. König, and W. Singer. Visuomotor integration is associated with zero time-lag synchronization among cortical areas. *Nature*, 385:157–161, 1997.

[129] A. Romani, R. Callieco, and V. Cosi. Prestimulus spectral EEG patterns and the evoked auditory vertex response. *Electroencephalography and Clinical Neurophysiology*, 70:270–272, 1988.

[130] I. Roth, editor. *Introduction to psychology*, volume 2. Lawrence Erlbaum Associates, 1992.

[131] D. Ruelle. *Chaotic evolution and strange attractors.* Cambridge University Press, 1989.

[132] M. Rutter. Autism research: prospects and priorities. *Journal of Autism and Developmental Disorders*, 26:257–275, 1996.

[133] M. Sams, J.K. Hietanen, R. Hari, R.J. Ilmoniemi, and O.V. Lounasmaa. Face-specific responses from the human inferior occipito-temporal cortex. *Neuroscience*, 77:49–55, 1997.

[134] J. Sarvas. Basic mathematical and electromagnetic concepts of the biomagnetic inverse problem. *Physics in Medicine and Biology*, 32:11–22, 1987.

[135] S. Sato, editor. *Magnetoencephalography*, volume 54 of *Advance in neurology.* Raven Press New York, 1990.

[136] T. Sauer, J.A. Yorke, and M. Casdagli. Embedology. *Journal of Statistical Physics*, 65:579–616, 1991.

[137] R.F. Schmidt and G. Thews, editors. *Physiologie des Menschen.* Springer-Lehrbuch. Springer-Verlag Berlin Heidelberg New York, 1990.

[138] T. Schreiber and A. Schmitz. Improved surrogate data for nonlinearity tests. *Physical Review Letters*, 77:635–638, 1996.

[139] M. Seeck and O.J. Grüsser. Category related components in visual evoked potentials: photographs of faces, persons, flowers and tools as stimuli. *Experimental Brain Research*, 92:338–349, 1992.

[140] J. Sergent, S. Ohta, B. MacDonald, and E. Zuck. Segregated processing of facial identity and emotion in the human brain: a PET study. *Visual Cognition*, 1:349–369, 1994.

[141] J. Sergent and J.L. Signoret. Functional and anatomical decomposition of face processing: evidence from prosopagnosia and PET study of normal subjects. *Philosophical Transactions of the Royal Society London, B*, 335:55–62, 1992.

[142] R. Siedenberg, D.S. Goodin, M.J. Aminoff, H.A. Rowley, and T.P.I. Roberts. The correlation coefficient and the goodness of fit in source localization of noise recorded by magnetoencephalography. *Brain Topography*, 9:95–100, 1996.

[143] W. Singer. Synchronization of cortical activity and its putative role in information processing and learning. *Annual Reviews of Physiology*, 55:349–374, 1993.

[144] J. Sinkkonen, H. Tiitinen, and Näätänen R. Gabor filters: an informative way for analysing event-related brain activity. *Journal of Neuroscience Methods*, 56:99–104, 1995.

[145] D. Smith. *Programmer's guide to PC and PS/2 video systems.* Addison-Wesley Publishing Company, 1994.

[146] R.S. Snell. *Clinical neuroanatomy for medical students.* Little, Brown and Company, 1992.

[147] M. Steriade, D. Contreras, F. Amzica, and I. Timofeev. Synchronisation of fast (30-40 Hz) spontaneous oscillations in intrathalamic and thalamocortical networks. *Journal of Neuroscience*, 16:2788–2808, 1996.

[148] S.J. Swithenby, A.J. Bailey, S. Bräutigam, O.E. Josephs, V. Jousmäki, and C.D. Tesche. Neural processing of human faces: a magnetoencephalographic study. *Experimental Brain Research*, 118:501–510, 1998.

[149] F. Takens. Detecting strange attractors in turbulence. *Lecture Notes in Mathematics*, 898:366–381, 1981.

[150] C. Tallon-Baudry, O. Bertrand, C. Delpuech, and J. Pernier. Stimulus specificity of phase-locked and non-phase-locked 40 Hz visual responses in human. *Journal of Neuroscience*, 16:4240–4249, 1996.

[151] C. Tallon-Baudry, O. Bertrand, C. Delpuech, and J. Pernier. Oscillatory gamma-band (30-70 Hz) activity induced by a visual search task in humans. *Journal of Neuroscience*, 17:722–734, 1997.

[152] C. Tallon-Baudry, O. Bertrand, C. Wienbruch, B. Ross, and C. Pantev. Combined EEG and MEG recordings of visual 40 Hz responses to illusory triangles in human. *NeuroReport*, 8:1103–1107, 1997.

[153] D. Tantam, L. Monaghan, H. Nicholson, and J. Stirling. Autistic children's ability to interpret faces: a research note. *Journal of Child Psychology and Psychiatry*, 30:623–630, 1989.

[154] The Numerical Algorithm Group Limited. *NAG FORTRAN library manual, Mark 15*, 1991.

[155] J. Theiler, S. Eubank, A. Longtin, B. Galdrikian, and J.D. Farmer. Testing for nonlinearity in time series: the method of surrogate data. *Physica D*, 58:77–94, 1992.

[156] J. Theiler and P.E. Rapp. Re-examination of the evidence for low-dimensional, nonlinear structure in the human electroencephalogram. *Electroencephalography and Clinical Neurophysiology*, 98:213–222, 1996.

[157] R.F. Thompson. *The brain — a neuroscience primer.* W.H. Freemann and Company, 1993.

[158] E. Vaadia, I. Haalman, M. Abels, H. Bergman, Y. Prut, H. Slovin, and A. Aertsen. Dynamics of neuronal interactions in monkey cortex in relation to behavioural events. *Nature*, 373:515–518, 1995.

[159] T. Valentine. Upside-down faces: a review of the effects of inversion upon face recognition. *British Journal of Psychology*, 79:471–491, 1988.

[160] C. van Petten. Words and sentences: event-related brain potential measures. *Psychophysiology*, 32:511–525, 1995.

[161] R. Vandenberghe, C. Price, R. Wise, O. Josephs, and R.S.J. Frackowiak. Functional anatomy of a common semantic system for words and pictures. *Nature*, 383:254–256, 1996.

[162] E.F. Vonesh and V.M. Chinchilli, editors. *Linear and nonlinear models for the analysis of repeated measurements*, volume 154 of *Statistics: textbooks and monographs*. Marcel Dekker, Inc. New York, Basel, Hong Kong, 1996.

[163] R. Wayland, D. Bromley, D. Pickett, and A. Passamante. Recognizing determinism in a time series. *Physical Review Letters*, 70:580–582, 1993.

[164] World Health Organization. *The ICD-10 classification of mental and behavioural disorders: diagnostic criteria for research*. World Health Organization, Geneva, 1994.

Abbreviations/Keywords

α-band	: fundamental spectral component of neural activity; 8 to 13 Hz
β-band	13 to 30 Hz
θ-band	4 to 7 Hz
γ-band	*higher frequency components of neural activity*; here: operationally defined as 20 to 45 Hz
$\Delta t \times \Delta f$	: uncertainty product in time and frequency associated with spectral transforms; $= \frac{1}{4\pi}$ for Gabor transforms
Φ	: unknown mapping symbolising the process of measurement
$\mathcal{R}^n$	: n-dimensional Euclidean space
ϱ	: Spearman's rank correlation coefficient
A	: image of an animal
A	: angular measure
A*number*	: denotes an autistic subject
AAFT	: amplitude-adjusted Fourier transform
ANOVA	: analysis-of-variance
autism	: a developmental disorder affecting behaviour
autistic subject	: here: high-functioning individual diagnosed as autistic
B	: image of a motor-bike
B	: number of bootstrap replications
behavioural response	: either reaction time or task performance score
bootstrap	: (epoch) re-sampling method for estimating the standard error of a measure
Bruce and Young model	: influential neuropsychological model describing the stages of identification and recognition of face information
C	: denotes terminal word congruity and the associated neural responses
cloze	: psycholinguistics: to complete a pattern (altered from *close*). Here: related to the likelihood of a word to be a terminal word of a sentence

	(usually called cloze-probability)
congruity	: refers to the property of a terminal word being related in meaning to the preceding sentence
D	: image of a dot pattern
D	: refers to an epoch which is classified as stationary and deterministic
DAQ	: data acquisition
deterministic	: here: indicating a process without a stochastic content
DF	: degrees of freedom
dimensional image	: image of a vector under the operation of incrementing the embedding dimension
DISSIM	: baseline independent measure of the difference between evoked signal powers at time t
EBD	: embedding dimension
ECD	: equivalent current dipole
EEG	: electroencephalography
EOG	: electro-oculogram
epoch	: stretch of brain signals time-locked to an external stimulus
evoked response	: signal obtained from several epochs by averaging time-slice by time-slice; here: synonymous with event-related response
evoked component	: any clearly identifiable peak (possibly extended) of an evoked response
F	: image of a face (adult or boy)
F	: frequency (lower case f also used)
face processing	: neural mechanisms related to the perception of face information
face specificity	: distinction of face responses from responses to other objects according to a given measure
fMRI	: functional magnetic resonance imaging
FNN	: false nearest neighbours method
FT1	: face task 1 (identification of image class)
FT2	: face task 2 (identification of identity)
FT3	: face task 3 (identification of emotion)

FPT	: face pre-stimulus task (identification of image class)
Gabor spectrogram	: time-frequency map (or matrix) obtained from a signal by Gabor transform
GDS-X	: Gabor density function for calculating sections of spectrograms; X can be T (time), F (frequency), or A (angular alignment)
gof	: goodness-of-fit
gradiometer	: detector (pick-up coil) for measuring spatial first derivatives of the magnetic field
HSD	: Tukey's honestly significant difference
HUT	: Helsinki University of Technology
I	: denotes terminal word incongruity and the associated neural responses
I+/I-	: condition where γ-band phase-locking is significant following I-stimuli (C-stimuli)
image	: grey-scale bitmap presented as a visual stimulus
IRP	: integrated regional power
ISI	: inter-stimulus interval
ISOTRAK	: 3D positioning system
K	: parameter of the Gabor transform determining the resolution in time and frequency
language processing	: here: neural mechanisms related to the perception of word and sentence information
L	: embedding lag
LPC	: late positive evoked component (mainly EEG)
LOT	: left occipito-temporal channel group
LT	: language task; terminal word (in)congruity
M	: image of a mug
MCG	: magnetocardiography
MEG	: magnetoencephalography
MRI	: magnetic resonance imaging
N1	: evoked component commonly seen in many EEG and MEG paradigms
N400	: late evoked component, specifically related to the

	processing of semantic information (mainly EEG)
Neuromag-122	: magnetoencephalographic facility at HUT
NF	: image of a non-face object
NIRP	: normalised integrated regional power
normal subject	: control subject without any known neuropathological history
oscillatory dynamics	: here: γ-band activity well localised in time
OVLP	: measure of overlap between points in a Gabor spectrogram
P	: a measure of power
p	: probability (error of type I)
P2	: evoked component commonly seen in many EEG and MEG paradigms
P300	: cognitive evoked component (EEG and MEG)
PAN	: head co-ordinate system (pre-auricular + nasion)
PET	: positron emission tomography
phase-locked	: characterising γ-band activity phase-locked to the stimulus (upon repetition)
pre-stimulus state	: 'hypothetical' characterisation of an epoch before stimulus arrival
PSS	: pre-stimulus state
R	: refers to an epoch which is either classified as non-stationary or non-deterministic
rCBF	: regional cerebral blood flow
response	: mainly: brain signals related to a stimulus; also: behavioural response
ROI	: region of interest
ROT	: right occipito-temporal channel group
RP	: regional power
RT	: reaction time
rotated gradient	: arrow plot visualising the reading from two orthogonal gradiometers
S*number*	: denotes a normal subject
$S^{\mathcal{C}}$	: signal detected by a given gradiometer (channel)
$S^{\mathcal{D}}$	: 2-vector composed of the signals measured at a given

	detector site
SID	: script-based image display system
signal power	: square of the signal amplitude
SNR	: signal-to-noise ratio
spontaneous activity	: here: synonymous with raw or unprocessed activity
ST	: measure of stationarity (based on the trace of the covariance matrix)
stationary	: indicating convergence of autocorrelation
SQUID	: superconducting quantum interference device
surrogate data	: replacement data sharing certain (generic) features with the original signals; used for hypothesis testing
SY	: measure of synchronous γ-band activity
synchronous activity	: same as phase-locked activity
T	: time
T-*measure*	: T-test associated with a given measure, e.g. P, SY
time image	: image of a (embedded) vector in reconstructed space under time evolution
TRE	: translation error associated with an epoch (TRE is bounded from below for signals with a stochastic content
W	: image of a word
Z-TRE	: z-score associated with the TRE measure